A LASER LIGHT SCATTERING STUDY OF TRANSPORT AND CRITICAL PHENOMENA

Thesis by

Erdoğan Güları

In Partial Fulfillment of the Requirements

for the Degree of

Doctor of Philosophy

California Institute of Technology

Pasadena, California

1973

(submitted May 17, 1973)

ACKNOWLEDGEMENTS

I am grateful to my advisor, Professor C. J. Pings, for his interest and guidance throughout the course of the investigation and also for giving me freedom with research and helping me to find a job.

Special thanks go to H. H. Reamer and the personnel of the Chemical Engineering Shop without whose help most of this work could not have been done, and to Dr. R. L. Schmidt for initiating the project, and to R. J. Brown for sharing the frustrations caused by the spectrometer and his help, and to Dr. A. F. Collings for helpful discussions, and to D. Powers for doing the GC analyses.

I am also thankful to the Morrisons and the rest of the group for making life a bit more pleasant, and to the people who preserved the National Parks for enabling us to see the Mother Nature at her best.

During my graduate studies I received financial assistance in the form of a Graduate Teaching Assistantship and a Graduate Research Assistantship from Caltech, an Earle C. Anthony Fellowship, and Graduate Reseach Assistantships from Air Force Office of Scientific Research, National Science Foundation, Standard Oil of California, Procter and Gamble, and Atlantic Richfield Company.

Finally I would like to thank my parents for their encouragement and my wife, Esin, who worked twice as hard as I did, doing housework and research simultaneously, for her understanding.

ABSTRACT

The intensity and Rayleigh linewidth have been measured as a function of temperature and scattering angle for light scattered by concentration fluctuations near the critical point of the binary liquid system 2,6-lutidine-water.

From the intensity data it is found that $\gamma = 1.26 \pm 0.02$ and $\nu = 0.61 \pm 0.07$. From the linewidth data the mutual diffusion coefficients were calculated as a function of temperature. It is found that the diffusion coefficient decreases as the critical point is approached. The behavior of the linewidth as a function of $k\xi$ was compared with the Kawasaki theory without the nonlocal viscosity and vertex corrections. General agreement with some systematic deviations is observed.

The shear viscosity anomaly in the same system was also studied in detail by measuring the shear viscosities as a function of temperature near the critical point. Results of analyses indicate that the viscosity is at most weakly divergent, with an exponent $\phi \simeq \pm 0.001$.

Light scattering techniques have been employed to measure the mutual diffusion coefficient D as a function of concentration in ten binary mixtures and the thermal diffusivity χ in nine pure liquids and one binary mixture. The diffusion coefficient was also measured at one or two

concentrations for four binary mixtures. The values obtained are in excellent agreement with the available literature data determined by more classical methods. Under most circumstances light scattering is found to offer a fast and accurate way of determining χ and D.

The turbidty τ and the decay rate Γ of the density fluctuations have been measured as a function of temperature on the critical isochore of ethane near the critical point.

From the turbidity data absolute values of isothermal compressibilities and correlation lengths were calculated. The isothermal compressibility K_T and the correlation length ξ are found to behave as:

$$K_T = 1.24\pm0.11\times10^{-3}(\Delta T/T_c)^{-1.225\pm0.02}\ \text{atm}^{-1}$$

$$\xi = 1.64\pm0.20\ (\Delta T/T_c)^{-0.644\pm0.02}\ \text{Å}.$$

From the Γ data thermal diffusivities, thermal conductivities and excess thermal conductivities were calculated as a function of temperature. It is found that the thermal diffusivity does not exhibit a simple power law behavior whereas the excess thermal conductivity does with an exponent of $\psi = 0.605\pm0.02$. The singular part of the decay rate Γ^s, was compared with the Kawasaki expression with the nonlocal viscosity correction. It is observed that the nonlocal viscosity correction together with the vertex

and the correlation function corrections improve the agreement between the theory and the experiment.

The results for the isothermal compressibility, the thermal conductivity and the excess thermal conductivity are in very good agreement with the available literature data.

TABLE OF CONTENTS

LIST OF FIGURES

I. INTRODUCTION

A. Laser Light Scattering in the Study of Transport and Critical Phenomena

Dense phases present an almost insoluble theoretical problem, thus one has to rely heavily on experiments to obtain microscopic and macroscopic information. X-ray scattering, neutron scattering, light scattering, ultrasonics, nmr and esr are but a few of the techniques used in studying dense fluids.

Light scattering in itself is quite diverse. The present work only covers the use of quantitative measurements of the intensity and the spectrum of the scattered light in the study of transport and critical phenomena. Einstein[1] was the first one to relate the intensity of the light scattered by a fluid to the macroscopic properties of the fluid such as the isothermal compressibility and the dielectric constant. His treatment was later extended by Ornstein and Zernike[2] to account for the anomalous increase in the intensity as the critical point is approached. It was further shown that[3,4] the frequency spectrum of the scattered light contained transport coefficient information. However, until the development of gas lasers and the optical beating spectroscopy techniques in the 1960's it was not possible to make quantitative measurements of the spectrum of the scattered light

to obtain the transport coefficient information. This was due to the fact that the needed resolution, between $1/10^7$ and $1/10^{14}$, simply was not available from the ordinary light sources and the spectrometers.

Light scattering is an especially useful tool near the critical point for two reasons: Light is scattered strongly as the critical point is approached, giving a good signal to noise ratio, and no macroscopic gradients are needed. As a result in the recent years light scattering has been used very extensively in studying critical phenomena.

Compared to the fluids near their critical points and to the suspensions of macromolecules, liquids such as benzene or liquid mixtures at room temperatures scatter light by a factor of 10^3 to 10^5 times less. Due to this small signal, use of light scattering to determine the transport coefficients χ, the thermal diffusivity and D, the mass diffusivity, has been very limited and inconclusive as to the applicability of the method. In this work we have remedied this by showing that the data obtained by light scattering is as good as any of the results obtained by the more classical techniques.

B. Critical Phenomena[5,6]

Formally a "critical point" is defined as the point where the first derivatives of the thermodynamic potential remain "continuous" while only the higher order derivatives such as compressibility, specific heat or susceptibility are divergent or change discontinuously.

As the critical point is approached the microscopic fluctuations in density, energy, concentration etc. increase and can effectively reach macroscopic magnitudes. Correspondingly the related second thermodynamic derivatives become very large or tend to infinity. Currently there is a lot of both theoretical and experimental interest in the study of critical phenomena. Most of the interest stems from the fact that within experimental error almost all of the systems studied behave similarly near their critical points. The interest is mostly towards determination of asymptotic laws governing the approach to the critical point. These laws are characterized by the critical exponents.

A critical point exponent describes the behavior, near the critical point, of a general function $F(\varepsilon)$, with $\varepsilon = |T-T_c|/T_c$. It is defined by,

$$\lambda = \lim_{\varepsilon \to 0} [\log F(\varepsilon)/\log \varepsilon] \qquad (1)$$

The limit denoted by λ is called the critical exponent

for the function $F(\varepsilon)$. In short this is written as $F(\varepsilon) \simeq A\varepsilon^{\lambda}$. This notation does not imply $F(\varepsilon) = A\varepsilon^{\lambda}$; although the converse is true. In general the function $F(\varepsilon)$ has the form:

$$F(\varepsilon) = A\varepsilon^{\lambda}(1 + B\varepsilon^{x} + C\varepsilon^{y} + \cdots), \quad (x, y \geq 0) \tag{2}$$

Sufficiently near the critical point the leading term dominates the behavior of the function and thus the critical exponent λ can easily be determined from a log-log plot. Obviously the complete functional form provides more information but is not easy to determine. A second reason for the interest in the critical exponents is that there exists a large number of relations among them. Some of these relations arise from fundamental thermodynamic and statistical mechanical considerations and some are based on less general assumptions.

II. THEORY

A. Intensity of the Scattered Light

Einstein[1] showed that the light is scattered by a dense medium due to the local fluctuations in the dielectric constant ε'. His original treatment did not include the time dependence of the fluctuations and the correlations between the scattering volume elements. Using the equations of electricity and magnetism he derived the result:

$$I = G\sin^2\phi \int\int \exp(i\bar{k}\cdot(\bar{r}_1-\bar{r}_2)) \langle \Delta\varepsilon'(\bar{r}_1)\Delta\varepsilon'(\bar{r}_2)\rangle d\bar{r}_1 d\bar{r}_2 \quad (3)$$

where

$$G \equiv (I_o k_o^4)/(16\pi^2 R^2)$$

I is the scattered intensity, I_o is the incoming intensity, k_o is the wave number of the incoming light, ϕ is the angle between the direction of polarization of the incoming light and the plane of scattering, R is the distance from the scattering volume to the detector, $\bar{r}$ is the vector from the origin to the scattering element, and $\bar{k}$ is the change in the wave vector of the scattered light defined by:

$$k = \frac{4\pi n}{\lambda} \sin(\theta/2) \quad (4)$$

where λ is the wavelength of the incident light in vacuum, θ is the scattering angle and n is the refractive index of the medium.

The fluctuations in the dielectric constant can be expressed in terms of the fluctuations in a complete set of local variables. Thus one can in principle derive an explicit expression for the intensity of the scattered light in terms of measurable thermodynamic quantities. However, we will only deal with two special cases here: a pure fluid near its critical point and a binary mixture near its critical solution point. In a pure fluid the fluctuations in the dielectric constant can be considered to be the result of fluctuations in density and temperature which are statistically independent variables[7].

$$\Delta\varepsilon'(\rho,T) = (\partial\varepsilon'/\partial\rho)_T\Delta\rho + (\partial\varepsilon'/\partial T)_\rho\Delta T \tag{5}$$

Close to the critical point:

$$(\partial\varepsilon'/\partial\rho)_T\Delta\rho >> (\partial\varepsilon'/\partial T)_\rho\Delta T \tag{6}$$

(note that this approximation is very good for most pure liquids even away from the critical point, see Ref. (7) pages 35-36.)

We then have

$$\Delta\varepsilon'(\rho,T) = (\partial\varepsilon'/\partial\rho)_T\Delta\rho \tag{7}$$

substituting this into Eq. (3) we obtain

$$I = G\sin^2\phi(\partial\varepsilon'/\partial\rho)_T^2\int\int\exp(i\bar{k}\cdot(\bar{r}_1-\bar{r}_2))\langle\Delta\rho(\bar{r}_1)\Delta\rho(\bar{r}_2)\rangle d\bar{r}_1 d\bar{r}_2. \tag{8}$$

If we further define $\Delta\rho_k$ to be the Fourier transform of

$\Delta\rho(\bar{r})$ given by,

$$\Delta\rho_k = \int \exp(i\bar{k}\cdot\bar{r})\,\Delta\rho(\bar{r})\,d\bar{r}. \tag{9}$$

Eq. (8) can then be written as

$$I = G \sin^2\phi\,(\partial\varepsilon'/\partial\rho)_T^2 \langle|\Delta\rho_k|^2\rangle. \tag{10}$$

Assuming that there are no correlations between the fluctuations in different volumes,

$$\langle|\Delta\rho_k|^2\rangle = \langle|\Delta\rho|^2\rangle \tag{11}$$

where $\Delta\rho$ is the thermodynamic or k=0 limit. From thermodynamic fluctuation theory[7] we have,

$$\langle|\Delta\rho|^2\rangle = K_T BT, \text{ per unit volume} \tag{12}$$

B is the Boltzmann constant, K_T is the isothermal compressibility and T is the absolute temperature. Substituting Eq. (12) into Eq. (10) we obtain,

$$I = G \sin^2\phi\,(\rho\partial\varepsilon'/\partial\rho)_T^2 K_T BT. \tag{13}$$

In the above derivation it was assumed that no correlations existed between the different scattering volumes, which is true away from the critical point but not near the critical point, where the density fluctuations reach almost macroscopic dimensions. Ornstein and Zernike[2] remedied this problem; in their treatment the correlation function is dominated by the long range tail given by,

$$<\Delta\rho(\bar{r}_1)\Delta\rho(\bar{r}_2)> \propto (1/r)\exp(-r/\xi) \tag{14}$$

where $r=|\bar{r}_1-\bar{r}_2|$ and ξ is the two particle correlation length. Using this correlation function Ornstein and Zernike (shortened to OZ from here on) obtained:

$$<|\Delta\rho_k|^2> \propto (1+k^2\xi^2)^{-1}\xi^2. \tag{15}$$

The constant of proportionality can be determined by comparing the k=0 limit of Eq. (15) with Eq. (12) to get:

$$<|\Delta\rho_k|^2> = (K_T BT\rho^2)(1+k^2\xi^2)^{-1}. \tag{16}$$

Also from this comparison we see that OZ-theory predicts $K_T \sim \xi^2$, or using the corresponding critical exponents we have $\gamma=2\nu$. Finally for the intensity of light scattered by density fluctuations in a pure fluid, close to the critical point, we have

$$I = G \sin^2\phi(\rho\partial\varepsilon'/\partial\rho)_T^2 K_T BT(1+k^2\xi^2)^{-1} \tag{17}$$

or

$$I(k,\xi) = I(0,\xi)(1+k^2\xi^2)^{-1}. \tag{18}$$

For a binary mixture near its critical point we assume that the fluctuations in the dielectric constant are mainly due to the fluctuations in the local concentration, i.e.

$$\Delta\varepsilon' = (\partial\varepsilon'/\partial C)_{T,P}\Delta C \tag{19}$$

C is the concentration. Again using the thermodynamic fluctuation theory to determine the thermodynamic limit[8]

$$<|\Delta C|^2> = BT/(\partial\mu'/\partial C)_{P,T}. \tag{20}$$

Including the OZ correction together with the proportionality constant we obtain for the intensity of scattered intensity from a binary mixture near its critical temperature,

$$I = G \sin^2\phi(\partial\varepsilon'/\partial C)^2_{T,P}BT(\partial\mu'/\partial C)^{-1}_{T,P}(1+k^2\xi^2)^{-1} \tag{21}$$

We would like to point out that $\mu'$is a specially defined chemical potential[9] and if one replaces μ' by μ the chemical potential of one of the components Eq. (21) becomes[10]:

$$I = G \sin^2\phi(\partial\varepsilon'/\partial C)^2C(C-1)BT(\rho(\partial\mu/\partial C)_{P,T})^{-1}(1+k^2\xi^2)^{-1}. \tag{22}$$

Equations (21) and (22) can be rewritten as:

$$I(k,\xi) = I(0,\xi)(1+k^2\xi^2)^{-1}. \tag{23}$$

Equations (17) and (21) were derived for the absolute scattered intensity. If we are only interested in the relative intensities, they reduce to

$$I(k,\xi) = AK_T \sin^2\phi/(1+k^2\xi^2) \tag{24}$$

for a pure fluid and

$$I(k,\xi) = A'(\partial\mu/\partial C)^{-1}_{T,P}\sin^2\phi/(1+k^2\xi^2) \tag{25}$$

for a binary mixture.

According to Eqs. (24) and (25) a plot of the inverse scattered intensity versus k^2 (called an OZ plot) will be a straight line with the slope being proportional to the correlation length squared and the intercepts being proportional to K_T^{-1} and $(\partial\mu/\partial C)_{T,P}$ respectively. Both K_T^{-1} and $(\partial\mu/\partial C)_{T,P}$ are predicted to have the asymptotic temperature dependence ε^{γ} ($\varepsilon=|T-T_c|/T_c$). Thus the intercepts of the OZ plots will be proportional to ε^{γ} and the slopes will be proportional to $\varepsilon^{\gamma}\xi^2$, but the OZ theory yields $\gamma=2\nu$, where ν is the critical exponent associated with the correlation length $\xi\sim\varepsilon^{-\nu}$. Therefore the slopes should be independent of temperature if the OZ theory is valid.

Eqs. (24) and (25) can be integrated over all angles to obtain the following expressions for the turbidity τ:

$$\tau = AK_T F(\alpha) \tag{26}$$

$$\tau = A'(\partial\mu/\partial C)^{-1}_{T,P} F(\alpha) \tag{27}$$

where $\alpha = 2(k_o\xi)^2$ and $F(\alpha)$ is given by,

$$F(\alpha) = [(2\alpha^2+2\alpha+1)/\alpha^3]\ln(1+2\alpha) - 2(1+\alpha)/\alpha^2. \tag{28}$$

In most cases measurement of the turbidity is simpler than measurement of the intensity as function of the scattering angle. Thus one can obtain the same information from turbidity measurements using Eqs. (26) and (27).

It has been suggested[12] that in the immediate neighborhood of the critical point OZ plots show a downward curvature, indicating deviations from the OZ theory. Previous to these experimental findings Fisher[13] had proposed that the OZ correlation function should be replaced by the more general function:

$$<\Delta\rho(\bar{r}_1)\Delta\rho(\bar{r}_2)>\propto(1/r^{1+\bar{\eta}})\exp(-r/\xi)(1+Q(r/\xi)) \qquad (29)$$

where $\bar{\eta}<<1$.

For $k\xi>>1$ his result may be expressed as:

$$I(k,\xi) = I(0,\xi)[1+k^2\xi^2]^{(\bar{\eta}/2)-1} \qquad (30)$$

This form does indeed predict a downward curvature very close to the critical point. Experimentally it is quite difficult to distinguish between Eqs. (23) and (30) due to the fact that $\bar{\eta}<<1$. Fisher's analysis also predicts that for $k\xi<<1$ the slopes of OZ plots will be temperature dependent.

P. Calmettes and coworkers[14] have integrated Eq. (30) to obtain τ. Their $F(\alpha)$ is as follows:

$$F(\alpha) = \frac{[(1+2\alpha)^{\bar{\eta}/2}-1]\{1+\alpha[2-\frac{\bar{\eta}}{2}+\alpha^2(2+\frac{\bar{\eta}}{2}+\frac{\bar{\eta}^2}{4})]-\bar{\eta}\alpha(1+\alpha)\}}{\alpha^3\,\frac{\bar{\eta}}{2}(1+\frac{\bar{\eta}}{2})(2+\frac{\bar{\eta}}{2})} \quad (31)$$

Experimentally one usually assumes that the OZ theory is valid and $\bar{\eta}$ is deduced from the relation between the critical exponents γ, ν, and $\bar{\eta}$:

$$\gamma \leq (2-\bar{\eta})\nu \ . \quad (32)$$

Numerical studies on model systems indicate that $\bar{\eta} \simeq 0.06$.

B. The Spectrum of the Scattered Light

In the previous section we were only interested in the intensity of the scattered light. If we also want to find out about the spectrum of the scattered light the complete expression for the intensity would be:

$$I(\bar{k},\omega) = G \sin^2\phi S(\bar{k},\omega) \tag{33}$$

where $S(\bar{k},\omega)$ is the generalized structure factor which contains the information about the fluctuations and ω is the change in the angular frequency of the scattered light. $S(\bar{k},\omega)$ is defined by Van Hove to be the space and time Fourier transform of the two body autocorrelation function of the fluctuations in the medium[15]:

$$S(\bar{k},\omega)=\int\int\int \exp\{[i\bar{k}\cdot(\bar{r}_1-\bar{r}_2)+i\omega t]\}\langle\Delta\varepsilon'(\bar{r}_1,t)\Delta\varepsilon'(\bar{r}_2,0)\rangle \, d\bar{r}_1 d\bar{r}_2 dt. \tag{34}$$

One can obtain an explicit expression for $S(\bar{k},\omega)$ either by using molecular theory of scattering or by using linearized hydrodynamics. Using hydrodynamic theory is the easier approach. We will illustrate it for a binary mixture. To keep the algebra simple we will assume that the concentration fluctuations are the main source of scattering,

$$\Delta\varepsilon' = (\partial\varepsilon'/\partial C)_{T,P}\Delta C \tag{35}$$

Substituting Eq. (35) into Eq. (34) and performing the space Fourier transforms we obtain,

$$S(\bar{k},\omega) = \int \exp(i\omega t) \langle \Delta C_k(t) \Delta C_{-k}(0) \rangle dt. \tag{36}$$

To evaluate the time integral we have to know the time dependence of the concentration fluctuations. We can get the time dependence by solving the diffusion equation for ΔC.

In a binary liquid the solute particle current $\bar{J}$ is given by the phenomenological equation

$$\bar{J} = -L\bar{\nabla}\mu = -L(\partial\mu/\partial C)_{T,P}\bar{\nabla}C \tag{37}$$

where L is the Onsager kinetic coefficient for diffusion, μ is the solute chemical potential. The solute particle flow must also satisfy the continuity equation

$$\bar{\nabla}\cdot\bar{J} + \partial C/\partial t = 0 \quad . \tag{38}$$

Combining Eqs. (37) and (38) yields the diffusion equation:

$$\partial C/\partial t = D\nabla^2 C \tag{39}$$

where $D=L(\partial\mu/\partial C)_{T,P}$ is the mutual diffusion coefficient (also called the mass diffusivity). The concentration fluctuation ΔC must also satisfy the diffusion equation:

$$\partial \Delta C/\partial t = D\nabla^2(\Delta C). \tag{40}$$

Taking the Fourier transform of both sides we have

$$\partial \Delta C_k/\partial t = -Dk^2(\Delta C_k) \quad . \tag{41}$$

Solving (41) yields,

$$\Delta C_k(t) = \Delta C_k(0)\exp(-Dk^2 t) \quad . \tag{42}$$

Substituting into (36) and evaluating gives:

$$S(k,\omega) = <|\Delta C_k|^2>\{2Dk^2/[(Dk^2)^2 + \omega^2]\} \tag{43}$$

which is a Lorentzian centered about the frequency of the incident light. The width of the Lorentzian 2Γ is $2Dk^2$. Thus by measuring the linewidth one can get the diffusion coefficient of the solute.

Using the hydrodynamic approach Mountain[16] has obtained the following results:

$$S(k,\omega) \overset{cen}{=} <|\Delta \rho_k|^2>[(C_p - C_v)/C_p](2\chi k^2)/[(\chi k^2)^2 + \omega^2] \tag{44}$$

for a pure fluid and,

$$S(k,\omega) \overset{cen}{=} (\partial \varepsilon'/\partial C)^2_{P,T}[BT/(\partial \mu/\partial C)_{P,T}]\{2Dk^2/[(Dk^2)^2+\omega^2]\}$$
$$+(\partial \varepsilon'/\partial T)^2_{C,P}[BT/C_p]^2\{2\chi k^2/[(\chi k^2)^2+\omega^2]\} \tag{45}$$

for a binary mixture with $\chi >> D$.

In the above equations C_p is the heat capacity at constant pressure, C_v is the heat capacity at constant volume,

χ is the thermal diffusivity ($\chi = \lambda_T/\rho C_p$, λ_T is the thermal conductivity).

The above expressions were derived using the linearized hydrodynamic equations which are valid when the size of the fluctuations are much smaller than the wavelength of the light (i.e. $k\xi<<1$). Thus they apply only away from the critical point. As the critical point is approached the fluctuations in density and concentration increase in size and are no longer small compared to the wavelength of the light and they are also correlated, as we have seen in the previous section.

M. Fixman[17] was the first one who tried to modify the hydrodynamic equations so that they would be applicable close to the critical point. His result for the linewidth was (from here on all the equations will be written only for a pure fluid; the equivalent formulas for a binary mixture can be obtained by replacing χ with D) :

$$\Gamma = \chi k^2(1+k^2\xi^2) \quad . \tag{46}$$

Experimentally it was found that this expression was valid up to $k\xi\simeq 1$, or in the "nonlocal hydrodynamics" region.

According to the dynamical scaling theory approach developed by Ferrell et al[18] and Halperin and Hohenberg[19] the k and ξ dependence of a transport property

are connected. The main assumption of dynamical scaling is that the decay rate of the fluctuations, Γ, can be described by a homogenous function of k and $1/\xi$, that is

$$\Gamma = \phi(k,1/\xi) = k^z\phi(1,1/k\xi) = \xi^{-z}\phi(k\xi,1) \qquad (47)$$

In the hydrodynamic region, $k\xi<<1$, $\Gamma=\chi k^2$. Comparing this with Eq. (47) we see that $\chi=\xi^{2-z}$. From a mode-mode coupling analysis of transport Kadanoff and Swift[20] predicted that in the hydrodynamic regime χ should be inversely proportional to the correlation length, indicating that z=3 in Eq. (47). Using this value of z in Eq. (47) we obtain $\Gamma=k^3\phi(1,0)$ for $k\xi>>1$. Thus the dynamical scaling theory predicts that in the critical region the linewidth should be independent of ξ or temperature.

Kawasaki[21] developed the mode-mode coupling theory further and obtained an explicit expression for the function ϕ. His result is

$$\Gamma = (BT/16\eta^*)(2k^2/\pi)[x+x^3+(1-x^4)\tan^{-1}(1/x)] \qquad (48)$$

where $x=1/k\xi$. The parameter η^* was defined as the high frequency limit of shear viscosity and was treated as a constant. For $k\xi<<1$ Eq. (48) reduces to $\Gamma=(BTk^2/6\pi\eta^*\xi)$; comparison with the hydrodynamic theory result gives $\Gamma=BT/6\pi\eta^*\xi$. Ferrel[22] has also obtained Eq. (48) by using decoupled mode theory and his derivation is much simpler.

Ferrel's basic assumption is that the density and the velocity fluctuations are statistically independent. In the result for χ if we replace χ by D we see that it is exactly the same as the Stokes-Einstein relationship for the diffusion coefficient of spherical solute particles with radius ξ in a solvent of viscosity η^*.

Kawasaki function (Eq. (48)) represents the behavior of the linewidth Γ quite well in general, but systematic deviations from it have been observed[23,24] and the definition of the parameter η^* has been questionable from the start due to the fact that the experimental shear viscosity shows a weak anomaly as the critical point is approached[25,26]. The ambiguity of η^* has been removed by Kawasaki and Lo[27] by relating η^* to the experimentally measured shear viscosity $\eta^*=\eta(k=0,T)/f(k\xi)$. The function $f(k\xi)$ is given numerically in Ref. (27). Lo and Kawasaki[28] have also obtained the first order vertex corrections to Eq. (48) in the case of a binary mixture. Both of the mentioned improvements are in the direction of increasing the agreement between the theory and the experiment.

Recently it was pointed out that the Kawasaki linewidth expression was based on the validity of the OZ correlation function form, and thus may need corrections. Numerical correction factors for more general correlation

functions have been obtained by Swinney and coworkers[29]. Chang et al[24] have obtained the following expression using the correlation function proposed by Fisher.

$$\Gamma/k^3 = \frac{(BT/8\pi\eta^*)[(1+x^2)/x^3]\{x+[2+\bar{\eta}+\frac{(x^2-1)(1-\bar{\eta})^2}{\bar{\eta}}]\tan(\bar{\eta}\tan^{-1}x)\}}{(1+\bar{\eta})(1+\frac{\bar{\eta}}{2})[x-\tan(\bar{\eta}\tan^{-1}x)]}$$

with $x=k\xi$. (49)

For $\bar{\eta}=0$ Eq. (49) reduces to Eq. (48).

Finally it was shown that the Kawasaki linewidth expression applies only to the singular part of the linewidth and one has to subtract off the normal part before making any comparisons between the theory and the experiment[24,29,30].

C. Light-Beating Spectroscopy

There are several excellent review articles covering this subject in detail (B. Chu[31], Cummins and Swinney[32] and Benedek[33]). Here we will only discuss the technique very briefly to show how one obtains the optical spectrum from the photo current spectrum.

The power spectrum $P_i(\omega)$ of the current is given by the Wiener-Khintchine theorem:

$$P_i(\omega) = (1/\pi)\int \exp(i\omega\bar{\tau}) C_i(\bar{\tau}) d\bar{\tau} \qquad (50)$$

where $C_i(\bar{\tau}) = \langle i(t) i(t+\bar{\tau})\rangle$ is the current autocorrelation function, $i(t)$ is given by $i(t)=e\sigma E^*(t)E(t)$, e is the electronic charge, σ is a suitably defined quantum efficiency and $E^*(t)E(t)=I(t)$ is the instantaneous intensity. Taking the discrete nature of the photocurrent into account we obtain the following for $C_i(\bar{\tau})$[32]:

$$C_i(\bar{\tau}) = e\langle i\rangle\delta(\bar{\tau}) + \langle i\rangle^2 g^{(2)}(\bar{\tau}) \qquad (51)$$

where $g^{(2)}(\bar{\tau})$ is the normalized second order correlation function defined by:

$$g^{(2)}(\bar{\tau}) = \langle E^*(t)E(t)E^*(t+\bar{\tau})E(t+\bar{\tau})\rangle / \langle E^*E\rangle^2 . \qquad (52)$$

From here on the treatment depends on whether we use homodyne detection, only scattered light falling on the phototube, or heterodyne detection, both scattered and

unscattered light falling on the phototube.

a. Homodyne detection

The field of monochromatic light scattered by a fluid or a solution of macromolecules is a Gaussian random process and it is characterized by an autocorrelation function

$$C_E(\bar{\tau}) = \langle E^*(t)E(t+\bar{\tau})\rangle = \langle I\rangle g^{(1)}(\bar{\tau}) \tag{53}$$

where $g^{(1)}(\bar{\tau})$ is defined as the first order normalized correlation function. For a random Gaussian field $g^{(2)}(\bar{\tau})$ can be expressed in terms of $g^{(1)}(\bar{\tau})$ (References (34) and (35)) :

$$g^{(2)}(\bar{\tau}) = 1 + |g^{(1)}(\bar{\tau})|^2. \tag{54}$$

The normalized correlation functions we are concerned with in this study are of the form,

$$g^{(1)}(\bar{\tau}) = \exp(-i\omega_o\bar{\tau})\exp(-\Gamma|\bar{\tau}|) \tag{55}$$

corresponding to a Lorentzian optical spectra given by:

$$\begin{aligned} I(\omega) &= (\langle I\rangle/2\pi)\int \exp(i\omega\bar{\tau})\exp(-\Gamma|\bar{\tau}|)d\bar{\tau} \\ &= \langle I\rangle(\Gamma/\pi)/(\Gamma^2+\omega^2) \ . \end{aligned} \tag{56}$$

The photocurrent spectrum associated with this field is found from Eqs. (50), (51) and (54) to be

$$P_i(\omega) = e\langle i\rangle/\pi + \langle i\rangle^2\delta'(\omega) + \frac{2\langle i\rangle^2(2\Gamma/\pi)}{(2\Gamma)^2+\omega^2} \tag{57}$$

We see that the photocurrent spectrum consists of three components, the first term is the shot noise term, the second is the dc term that is normally blocked out in analyzing the spectrum and the third term is a Lorentzian with a width twice that of the optical spectrum.

b. Heterodyne spectroscopy

Completely general treatment of the heterodyning case is quite complex and difficult. We will assume that the intensity of the local oscillator is much larger than the intensity of the scattered light, a condition that is met in this study, then the current autocorrelation function given in Eq. (51) simplifies considerably. For the autocorrelation functions of the local oscillator and the scattered field we have:

$$\langle i_s(t)\rangle = e\sigma\langle E_s^*(t)E_s(t)\rangle \ , \tag{58}$$

$$\langle i_{Lo}(t)\rangle = e\sigma\langle E_{Lo}^*(t)E_{Lo}(t)\rangle = e\sigma|E_{Lo}|^2 \tag{59}$$

where E_s is the field under study and

$E_{Lo}(t) = E_{Lo}^0\exp(-i\omega_{Lo}t)$ is the local oscillator field.

Since $\langle I_{Lo}\rangle >> \langle I_s\rangle$ we can expand $C_i(\bar{\tau})$ using

$$E(t) = E_s(t) + E_{Lo}^0\exp(-i\omega_{Lo}t) \ , \tag{60}$$

to obtain[32]

$$C_i(\bar{\tau}) = ei_{Lo}\delta(\bar{\tau}) + i_{Lo}^2 + i_{Lo}\langle i_s\rangle\{\exp(i\omega_{Lo}\bar{\tau})g_s^{(1)}(\bar{\tau}) + \exp(-i\omega_{Lo}\bar{\tau})g_s^{*(1)}(\bar{\tau})\}. \quad (61)$$

Using the above current autocorrelation function in the Wiener-Khintchine theorem, Eq. (50) yields the photocurrent spectrum.

$$P_i(\omega) = (ei_{Lo})/(2\pi) + i_{Lo}^2\delta(\omega) + \frac{i_{Lo}\langle i_s\rangle}{2\pi}\int\exp(i\omega\bar{\tau})[\exp(i\omega_{Lo}\bar{\tau})g_s^{(1)}(\bar{\tau}) + \exp(-i\omega_{Lo}\bar{\tau})g_s^{*(1)}(\bar{\tau})]d\bar{\tau}. \quad (62)$$

Substituting in $g_s^{(1)}(\bar{\tau}) = \exp(-i\omega_o\bar{\tau})\exp(-\Gamma|\bar{\tau}|)$ we obtain for the photocurrent spectrum:

$$P_i(\omega) = ei_{Lo}/\pi + i_{Lo}^2\delta'(\omega) + \frac{2i_{Lo}\langle i_s\rangle(\Gamma/\pi)}{[\omega-|\omega_o-\omega_{Lo}|]^2+\Gamma^2} \quad (63)$$

For unscattered light coming from the same laser $\omega_{Lo}=\omega_o$, which is the case in this study, Eq. (63) reduces to

$$P_i(\omega) = ei_{Lo}/\pi + i_{Lo}^2\delta'(\omega) + \frac{2i_{Lo}\langle i_s\rangle(\Gamma/\pi)}{(\omega^2+\Gamma^2)} \quad (64)$$

The first term is the shot noise term, the second is the dc component and the third is a Lorentzian identical in shape to the optical spectrum.

c. Discussion

In the above simplified treatment we have assumed that:

1. Only one coherence area was involved in the detection process, ($A_{coh}=2\lambda^2/\Omega$, Ω is the solid angle the source subtends at the detector.).
2. The incoming light provides a pure monochromatic field.
3. The measurements are done over sufficiently long periods of time to obtain the ensemble averages.

Without going into the details the effects of deviations from the above assumptions are as follows: If the signal does not come from one coherence area, the ratio of the signal term to the shot noise term is less than the theorethical maximum. Experimentally it is possible to maximize the signal to shot noise ratio by varying the pinhole sizes, which define the scattering volume and the scattering angle, changing the distances between the pinholes and the detector and the sample and by focusing the incident light to decrease the scattering volume. The incoming light is never perfectly monochromatic even for lasers operating in single mode. In this study we have used a Coherent Radiation Model 52A Argon Ion Laser in multimode operation. Cummins and Swinney[32] extend the treatment given above to multimode lasers and show that the result obtained for a monochromatic source also hold for a multimode laser without any modifications. All of the results given above were in terms of <i> the

ensemble average of the photocurrent. Experimentally if one uses a swept filter spectrum analyzer, the time is quite finite and thus there are fluctuations in the detected photocurrent. The fluctuations in the photocurrent are not a problem in the case of correlators, which determine the current autocorrelation function, and with real time spectrum analyzers. With correlators and real time spectrum analyzers it is possible to average the signal over very long periods of time and approach the ensemble averages very closely.

III

LIGHT SCATTERING AND SHEAR VISCOSITY STUDIES OF THE BINARY SYSTEM 2,6-LUTIDINE WATER IN THE CRITICAL REGION*

Erdoğan Güları, A. F. Collings, R. L. Schmidt†, and C. J. Pings
Division of Chemistry and Chemical Engineering
California Institute of Technology
Pasadena, California 91109

(Journal article complete with figures and references, published in J. Chem. Phys. 56, 6169(1972). For raw data see Tables II to IX.)

Abstract

Measurements have been made at the critical mixing composition of the system 2,6-lutidine-water for a (T_c-T) range of 0.001°-7.5°C for the intensity and Rayleigh linewidth and of 0.007°-27.4°C for the shear viscosity. We find that

$$I_c^{-1}(0) \propto (\varepsilon)^{(1.26\pm0.02)}$$

$$\xi_s = (2.0\pm0.2)(\varepsilon)^{-(0.61\pm0.08)} \text{ Å}$$

$$D = (0.290\pm0.020)(\varepsilon)^{(0.554\pm0.015)}\times10^{-5} \text{ cm}^2/\text{sec}$$

$$\xi_\Gamma = (2.92\pm0.19)(\varepsilon)^{-(0.567\pm0.015)} \text{ Å}$$

where $\varepsilon=(T_c-T)/T_c$, $I_c(0)$ is the intensity extrapolated to zero angle, ξ_s the correlation length from intensity measurements, D the mutual diffusion coefficient, and ξ_Γ the correlation length obtained from fitting the Kawasaki equation to linewidth measurements with the above value of D. We find that the Ornstein-Zernike-Debye theory is valid for $(T_c-T)>0.03$°C and the Kawasaki mode-mode coupling theory gives a good overall description of the behavior of the linewidth of the Rayleigh line. The Kadonoff-Swift-Kawasaki result $\gamma-\psi=\nu$ seems to be valid with $\nu=\nu_s=\nu_\Gamma$. We also find that the excess shear viscosity does not exhibit a simple power law dependence on (T_c-T) as the critical temperature is approached.

INTRODUCTION

In recent years there has been considerable interest in critical phenomena, both theoretical and experimental. Critical exponents have been obtained for single component and binary liquid systems. One of the shortcomings of the previous experiments has been the fact that each experimenter obtained only one or two critical exponents. To obtain a complete set of critical exponents one has to go to three or four sources, for which experimental results might differ considerably due to different sample purities, experimental techniques, and temperature calibration and control. This is especially true in the case of binary systems where due to different amounts of impurities present, thermodynamic properties such as the critical temperature can change significantly. In this paper we report results near the lower consolute point of the system 2,6-lutidine-water for the exponents γ, $\gamma-\psi$, ψ, ν_s, and ν_Γ determined by light scattering techniques and for the exponent ϕ determined by shear viscosity measurements.

BRIEF THEORY

Detailed theories of critical phenomena have been developed[1-4]. Here we will only outline the results of these developments with the necessary equations for data analysis.

A. Intensity

Einstein[1] was the first to derive an expression for the intensity of scattered light in terms of density and concentration fluctuations. His theory was later extended by Ornstein and Zernike[2] and by Debye[3] (referred to as the OZD theory) to include the long range correlation effects. According to the Debye theory, the relative scattered intensity due to concentration fluctuations in a binary critical mixture can be approximated by the relation

$$I_c(K) \propto \left(\frac{c}{n}\frac{\partial n}{\partial c}\right)^2 \frac{T/T_c}{(T/T_c)-1+K^2\ell^2/6} \qquad (1)$$

in which c denotes the concentration, n the refractive index of the mixture, T_c the critical mixing temperature, ℓ the Debye interaction parameter[3], and K is the wave vector given by

$$K = \frac{4\pi n}{\lambda}\sin(\theta/2) \qquad (2)$$

λ = wavelength of the light

θ = scattering angle

n = refractive index of the medium

Fisher[5] proposed:

$$\frac{I_c(K)}{I_c(0)} = \xi_s^{\bar{\eta}-2}/[\xi_s^{-2} + K^2]^{1-\bar{\eta}/2} \qquad (3)$$

where ξ_s is a temperature-dependent correlation length (the subscript s indicates that it is obtained from scattered intensity measurements) and $\bar{\eta}$ is a small number whose magnitude indicates the degree of deviation from the OZD theory.

Using the "scaling law" concept we can represent the asymptotic temperature dependence by

$$I^{-1}(0) \propto \varepsilon^{\gamma} \qquad (4)$$

$$\xi_s = \xi_{s_o} \varepsilon^{-\nu_s} \qquad (5)$$

where $\varepsilon = \frac{T-T_c}{T_c}$. From Eq. (3) we find that γ, $\bar{\eta}$, and ν_s are related by

$$\gamma = (2-\bar{\eta})\nu_s \qquad (6)$$

B. Frequency Spectrum

Expressions for the central part of the frequency spectrum (Rayleigh line) of scattered light have been derived at three levels of complexity:

1) Linearized hydrodynamics: The dynamics of density and concentration fluctuations are described by the linearized equations of hydrodynamics giving the following expression for the Rayleigh line[6]:

$$S(K,\omega) = \left(\frac{\partial \varepsilon}{\partial c}\right)^2 \left(\frac{k_B T}{(\partial \mu/\partial c)_{p,T}}\right)\left(\frac{2DK^2}{(DK^2)^2+\omega^2}\right) +$$

$$\left(\frac{\partial \varepsilon}{\partial T}\right)_{c,p}\left(\frac{k_B T}{c_p}\right)^2 \left(\frac{2\chi K^2}{(\chi K^2)^2+\omega^2}\right) \qquad (7)$$

Here D is the mutual diffusion coefficient, ε the dielectric constant, k_B the Boltzmann constant, μ the chemical potential, χ the thermal diffusivity, c_p the heat capacity of the mixture at constant pressure, and ω the change in frequency from the incident frequency.

For many binary solutions and solutions of macromolecules the second part of Eq. (7) is negligible compared to the first part, and the Rayleigh line is a single Lorentzian with a halfwidth Γ given by

$$\Gamma = DK^2 \qquad (8)$$

Since correlation effects were neglected, Eq. (8) is only valid away from the critical point (i.e., for $K\xi_\Gamma << 1$).

2) Nonlocal hydrodynamics: As the critical point is approached, the increasing range of correlations destroys the local nature of hydrodynamics. Fixman[7] modified the hydrodynamic equations to include the effect of the long range correlations. Solutions of Fixman's equation lead to a Lorentzian whose linewidth is described by[8]

$$\Gamma = DK^2(1 + \xi_\Gamma^2 K^2) \qquad (9)$$

ξ_Γ is a temperature dependent correlation length and the subscript indicates that it is determined from linewidth

measurements. Far from the critical point, $K\xi_\Gamma << 1$, and Eq. (8) is recovered.

3) Mode-mode coupling: Recently Kawasaki[4] has carried out a detailed theory of mode-mode coupling of fluctuations in fluids and has derived the following closed expression for the Rayleigh linewidth which applies to all values of $K\xi_\Gamma$:

$$\Gamma = \frac{k_B T}{16\eta^*} \frac{2K^3}{\pi} \{(K\xi_\Gamma)^{-1} + (K\xi_\Gamma)^{-3} + (1-(K\xi_\Gamma)^{-4}) \tan^{-1}(K\xi_\Gamma)\} \quad (10)$$

η^* is the high frequency part of shear viscosity and is a constant. For $K\xi_\Gamma << 1$, Eq. (10) reduces to Eq. (8), with D given by $D=k_B T/6\pi\eta^*\xi_\Gamma$. For $K\xi_\Gamma \lesssim 1$ we obtain

$$\Gamma = DK^2(1 + \frac{3}{5} K^2\xi_\Gamma^2) \quad (11)$$

which is identical to Eq. (9) except for the factor 3/5. In the limit $K\xi_\Gamma >> 1$, Eq. (10) becomes

$$\Gamma = AK^3 \quad (12)$$

where A is given by

$$A \equiv \frac{k_B T}{16\eta^*} = \frac{3}{8} \pi D\xi_\Gamma \quad (13)$$

Ferrell[9] has developed an alternative derivation of Eq. (10).

Using the "scaling law" approach, the mutual diffusion coefficient and the correlation length ξ_Γ are predicted to have the asymptotic temperature dependence:

$$D = D_o \varepsilon^{\gamma-\psi} \quad (14)$$

$$\xi_\Gamma = \xi_o \varepsilon^{-\nu_\Gamma} \tag{15}$$

Since η^* is a constant in the Kawasaki theory, $\gamma - \psi = \nu_\Gamma$. Kadanoff and Swift[10] predict the same result from a mode-mode coupling analysis of transport coefficients in the critical region.

C. Viscosity

The temperature dependence of the viscosity of nearly all pure and multi-component liquids can be adequately represented over a limited range of temperature by the Arrhenius equation:

$$\log \eta = A + \frac{B}{T} \tag{16}$$

A and B are constants independent of temperature.

Attempts have been made to separate the viscosity of binary systems near the critical point into an anomalous part $\Delta\eta$ and a normal part η_{cl}:[11]

$$\eta = \Delta\eta + \eta_{cl} \tag{17}$$

In particular, these efforts have concentrated on determining a critical exponent ϕ for the viscosity at the critical concentration defined by

$$\Delta\eta = H\varepsilon^{\phi} + \ldots \tag{18}$$

Attempts have also been made to analyze the relative anomalous viscosity in the form[12]

$$\frac{\Delta\eta}{\eta_{cl}} = H'\varepsilon^{\phi} + \ldots. \tag{19}$$

Debye, Chu and Woermann[13] and also Woermann and

Sarholz[14] noted that the viscosity of several binary liquid systems near the critical temperature can be represented by an empirical equation of the form

$$\eta = (e^{A+B\varepsilon})(\varepsilon^{\phi}) \tag{20}$$

This equation has the same asymptotic behavior as Eq. (19) thus presenting an alternative way of determining the critical exponent ϕ.

Some of the recent theories predict finite viscosities at the critical point[4,10,15]. For this purpose a generalization of Eq. (18) is

$$\Delta\eta = \frac{H''}{\phi} (\varepsilon^{\phi}-1) + G \tag{21}$$

Fisher[16] pointed out that Eq. (21) corresponds to a cusp for $0<\phi<1$, a power law divergence for $\phi<0$ and a logarithmic divergence for $\phi=0$.

EXPERIMENTAL

A. Materials

"Baker" grade 2,6-lutidine was dried over anhydrous calcium sulfate. The dry lutidine was distilled under dry nitrogen using a fractionation column. A high reflux to distillate rate was used and only the center cut representing a boiling point range of 0.2°C was kept. Distilled water was filtered through a 25 mμ millipore filter to remove any dust and was degassed under vacuum. The purity of the lutidine was checked by gas chromatography using a 3/16" diameter column of length 15' packed with Carbowax 20M adsorbed on 80/100 Chromosorb P. No impurity peaks were observed with a detection threshold of 0.02%.

A stock solution of mole fraction 0.0658 lutidine was prepared by weight and mixed under nitrogen. After making allowances for handling and evaporation, the overall accuracy of the composition was approximately 0.1%.

B. Light Scattering Spectrometer

A schematic drawing of the spectrometer is shown in Fig. 1. A triangular optical rail was mounted on a Micro-Inch microscope base to obtain a highly flexible and accurate optical turntable. The cell could be moved in X,Y,Z directions with an accuracy of 0.02 mm or better, and the scattering angles could be read to within one minute of arc.

A thin vertical wire at the center of an empty scattering cell was used as a reference for alignment. The final accuracy of the alignment was approximately equal to the thickness of the reference wire, 0.08 mm. For intensity measurements two slits 25 mm apart were used to define the scattering angle. For linewidth measurements two pinholes 30 cm apart were used to define the scattering volume. The laser and the optics were mounted on a heavy machinist's table which was isolated from the floor by neoprene rubber pads.

A filtered fluorescin solution (0.6 mg/100 ml) was used to calibrate the spectrometer for intensity measurements. The observed scattered intensity was constant to within 1% over an angular range of 50°-120° and to within 5% over 20°-140°. With a 30 mm O.D. cell the corrected intensity was constant to better than 1% from 20° to 150°.

The output intensity of the laser was stabilized to ±0.2% by a feedback circuit. As a second check the intensity of the main beam was measured using a silicon-diode detector.

C. Temperature Control and Measurement

The primary temperature controlling device was a P. M. Tamson Viscometer bath with a control of ±0.002°C. Critical temperatures of the light scattering samples were determined by suspending the cells in a large, water-

filled test tube which in turn was submerged in the bath. The temperature fluctuations within the sample were estimated to be less than ±0.0005°C. The critical temperature was checked both before and after scattering measurements.

The temperature of the light scattering cell during intensity and linewidth measurements was controlled by inserting the cell in a brass block. A helical water channel was cut in the outer rim of the block which was sealed in an insulating jacket of lucite. The viewing slit was sealed with saran-wrap. Water from the viscometer bath was circulated through the brass block. In this way the temperature of the sample could be regulated to ±0.001°C for several hours. Typical long term drifts did not exceed 0.005°C/day. The temperature of the room was also controlled to ±0.2°C during measurements. Careful observations were made which confirmed that negligible heating effects were produced by irradiating the cells with the laser.

A platinum resistance thermometer (Electric Thermometer Inc., Type 6-20) was used in all the temperature measurements. This had previously been calibrated against an N.B.S. certified Leeds and Northrup platinum resistance thermometer. The resistance of the thermometer was measured using a L & N Guarded Potentiometer (Catalog No. 7550) and a Hewlett Packard 419A D.C. Null Voltmeter.

An N.B.S. certified 100Ω L & N standard resistor was used as a reference. Both the standard resistor and the thermometer were of N.B.S. approved design. The resolution of the circuit was better than 0.0005°C.

D. Light Scattering Measurements

Before any measurements were taken, the laser and the other electronics were allowed to warm up for at least four hours. During this time the sample came to thermal equilibrium for the first large temperature change.

Three sizes of sample cells made from precision bore nmr tubing by Wilmad Glass Company were used: 15 mm O.D. (13.5 I.D.), 10 mm O.D. (9.1 mm I.D.), and 5 mm O.D. (4.5 mm I.D.). For intensity measurements only the 10 mm O.D. cell was used.

Intensity measurements were taken at 10° intervals from 30° to 50° and 110° to 130°. From 50° to 110° data were taken at 5° intervals. The measured intensity usually reached its final value within 10 minutes of a temperature change. However, at least 45 minutes of equilibration time was allowed between measurements.

Frequency spectra were taken over an angular range 25° to 120°. At least three spectra were taken at each value of ΔT and θ; in this way the statistical uncertainties in the halfwidths were decreased. Only the 10 mm and 5 mm cells were used for small ΔT measurements which were

made only at $\theta=98°$ with the smaller cell. Comparative data with the 15 mm and 10 mm cells indicated no observable effect of multiple scattering on the measured linewidths.

Turbidity measurements were made with the same spectrometer with a square sample cell and the detector placed at 0° angle. The transmitted light intensity at a large ΔT (14°C below T_c) was used as a reference intensity I_o. The intensities at smaller ΔT values were related to turbidity α by the relation

$$I_t = I_o \exp(-\alpha d) \qquad (22)$$

where d is the distance through which light is transmitted in the fluid.

E. Viscosity Measurements

A modified size 50 Canon-Fenske viscometer, mounted conventionally in the water bath was used to measure viscosities. Times were measured by a Lab-Chron (Model 1402) timer which could be read to a tenth of a second.

To prevent shifting of composition and T_c due to evaporation, the viscometer was not open to the atmosphere. Before putting in a new sample the viscometer was evacuated and then was allowed to saturate with the vapors from a large stock solution which was kept at the same temperature as the viscometer. Dry air was bled in until atmospheric pressure was reached. The sample was introduced into the viscometer with a 10 ml syringe.

The viscometer was calibrated and used according to NBS Monogram 55. Run times were of the order of 700 seconds and the reproducibility in repeated runs was never worse than 0.1%.

F. Data Treatment

For the intensity data we have considered the following correction factors: (1) Volume, (2) Attenuation, (3) Dust and stray light, and (4) Multiple scattering.

Volume corrections are necessary because the phototube "sees" different volumes at different angles of observation[17]. The scattered intensity after volume correction is $I=I_p \sin\theta$ where I_p is the measured intensity.

Attenuation correction: The incident intensity I_o of the light beam is decreased to I_t, the transmitted intensity, after it has travelled a distance d through the medium: $I_t = I_o \exp(-\alpha d)$, where α is the turbidity coefficient. For a cylindrical cell $d=2R$, R is the inner redius of the scattering cell.

Dust and stray light were corrected for by determining the excess scattered intensity I_{ex} at a large ΔT value (13°C) and subtracting from the observed intensities ($\Delta T \leq 6$°C). The excess scattered intensity after attenuation correction is $I_{ex}(\theta) \exp(-2\alpha R)$.[18]

The value of the scattered intensity after volume,

attenuation, dust and stray light corrections is[18]

$$I(\theta) = (I_p(\theta) - I_{ex}(\theta) \exp(-2\alpha R)) \sin\theta \exp(2\alpha R) \qquad (23)$$

The lutidine-water system is highly turbid; to eliminate multiple scattering one has to go to smaller path lengths as ΔT is decreased. We could not go to a 5 mm scattering cell due to serious reflection problems. As a result we did not make intensity measurements for ΔT values less than 0.017°C.

The Lorentzian spectra obtained for linewidth studies were computer-fitted using a Marquardt least squares algorithm[19] to obtain the halfwidths. The reproducibility between repeated measurements was better than 5%.

The measured kinematic viscosities were converted to dynamic viscosities using our own density data. Density measurements were made by suspending a calibrated pycnometer in the water bath. The reproducibility of the densities was never worse than 0.01%. The overall absolute accuracy of the viscosity values is better than 0.3%.

RESULTS

A. Intensity Measurements

Solving Eqs. (1) and (3) for $I_c^{-1}(K)$ at a constant temperature T, we get

$$\text{from Eq. (1)} \quad I_c^{-1} = A + BK^2 = A + B'\sin^2\theta/2 \tag{24}$$

$$\text{from Eq. (2)} \quad I_c^{-1} = I_c^{-1}(0)[1+\xi_s^2 K^2]^{1-\bar{\eta}/2} \tag{25}$$

where A and B' are temperature dependent constants. If OZD theory holds, a plot of reciprocal intensity versus $\sin^2\theta/2$ should be a straight line as shown in Fig. 2.

The downward curvatures in an OZD plot of small angles and large values of ΔT were caused by excess scattering due to dust and stray light. Eventually the excess scattered intensity became small compared to the scattered intensity due to concentration fluctuations and the downward curvature disappeared.

The upward curvatures at large angles have been observed virtually in all binary liquid mixtures in strongly opalescent regions[18] and have been attributed to multiple scattering[20-22].

We also observed small upward curvatures at small angles for small ΔT values ($\Delta T<0.1°C$). The curvature was significant compared to experimental uncertainties for $\Delta T=0.017°C$ data set. We believe this was also due to multiple scattering rather than being a real deviation from the OZD theory. We did not use this set of data in our

curve fittings. Thus we conclude that within experimental error, Eq. (24) holds for our data and $\bar{\eta} \simeq 0$ in Eq. (25).

Taking $\bar{\eta} = 0$ we fitted our data to Eq. (25) using least squares to get a value of $I_c^{-1}(0)$ and ξ_s^2 for each temperature. ΔT dependences were determined using Eqs. (4) and (5). Our results are $\gamma = 1.260 \pm 0.020$, $\xi_o = 2.00 \pm 0.20$ Å and $\nu_s = 0.61 \pm 0.08$. We have plotted on a log-log scale $I_c^{-1}(0)$ vs. ΔT in Fig. 3 and ξ_s vs. ΔT in Fig. 4. We tried to eliminate the effects of multiple scattering in ξ_s by rejecting the data below 0.1°C.

B. Linewidth Measurements

Hydrodynamic region ($K\xi_\Gamma << 1$): Our 45 data points for which $K\xi_\Gamma \leq 0.15$ (as determined in the following paragraphs) accurately establishes the K^2 angle dependence. We determined D the mutual diffusion coefficient by finding the limiting value of Γ/K^2 as $K^2 \to 0$ for each temperature. A least squares fit of Eq. (14) to our data yielded $D_o = (0.290 \pm 0.020) \times 10^{-5}$ cm^2/sec and $\gamma - \psi = 0.554 \pm 0.015$. A log-log plot of D vs. ΔT is shown in Fig. 5.

Nonlocal hydrodynamics region ($K\xi_\Gamma \leq 1$): Using our data we find that small deviations from hydrodynamic behavior are accurately described by Fixman's equation (Eq. (9)). We also find that it is quite hard to get reasonable statistical accuracy for the parameters ξ_{Γ_o} and ν_Γ. We think this is due to the high correlation between

the four parameters in Eq. (9). A least squares fit to our 100 points in the range $K\xi_\Gamma \leq 1$ gave: $D_o=(0.24\pm0.02)\times10^{-5}$ cm^2/sec, $\gamma-\psi = 0.53\pm0.02$, $\xi_{\Gamma_o}=0.4\pm0.6$ Å and $\nu_\Gamma=0.7\pm0.2$. Using D_o and $\gamma-\psi$ values obtained from the diffusion coefficient changes ξ_{Γ_o} and ν_Γ values slightly but does not decrease the statistical uncertainties significantly.

Critical region ($K\xi_\Gamma >> 1$): We find that very near the critical point the linewidth exhibits the predicted temperature independent K^3 behavior (Eq. (12)).

We also made a least squares analysis of the data for all regions using the complete Kawasaki expression (Eq. (10)). Without fixing any parameters, we obtained the following "best fit" values from our 123 data points, which cover a ΔT range of 0.001°C to 7.5°C:

$$\xi_{\Gamma_o} = 3.0\pm0.2 \text{ Å}$$
$$\nu_\Gamma = 0.541\pm0.015$$
$$\eta^* = 2.87\pm0.24 \text{ centipoises}$$

Using the relationship

$$A = \frac{k_B T}{16\eta^*} = \frac{3}{8}\pi D\xi_\Gamma$$

we get

$$A = 9.2\pm0.8\times10^{-14} \text{ cm}^3/\text{sec}$$
$$D_o = 0.260\pm0.020\times10^{-5} \text{ cm}^2/\text{sec}$$

The Kawasaki equation with these values for the parameters

is shown in Fig. 6 along with the experimental data. The data in the region $0.2<K\xi_\Gamma<1.0$ show a small systematic departure from the Kawasaki theory as has been observed in other investigations[23,24].

As opposed to allowing all three parameters to vary independently. the Kawasaki expression can also be fitted to the linewidth data with ξ_{Γ_o} and ν_Γ as adjustable parameters and $D_o = 0.290\times10^{-5}cm^2/sec$, the experimental value obtained in the procedure previously described. With no significant change in the quality of the fit, we obtained the following values: $\xi_{\Gamma_o} = 2.92\pm0.19$ Å and $\nu_\Gamma=0.567\pm0.015$. As a second method the fit was made replacing η^* with experimental shear viscosity data yielding $\xi_{\Gamma_o} = 3.50\pm0.24$ Å and $\nu_\Gamma = 0.570\pm0.013$.

The use of experimental viscosities eliminated the slight systematic deviations around $K\xi = 1$ but introduced systematic deviations of the order of 1% in the ranges $K\xi << 1$ and $K\xi >> 1$.

We feel that the values of ξ_{Γ_o} and ν_Γ obtained by fixing D_o are the most meaningful results to report for the fit of the Kawasaki theory to linewidth data.

C. Viscosity Measurements

Compared to the well known divergences of $I_c^{-1}(0)$, and D, the behavior of shear viscosity in binary mixtures is not very well established due both to a lack of good

data and theory. Much of the ambiguity is due to different methods of subtracting off the "normal" part of the shear viscosity. To gain some insight into the problem we used two different equations to represent the "normal" behavior.

Assuming that the Arrhenius equation, Eq. (16), gives an adequate description of the "normal" part of the viscosity, from the first three data points we obtain

$$\eta = 2.703\ 10^{-5} \exp[\frac{3386}{K^\circ}] \text{ centipoises}$$

However, using this equation we obtained significant excess viscosities for ΔT values as large as 18°C. We think this was due to the inadequacy of the Arrhenius equation. Since the lutidine-water system at the critical concentration is 94 mole percent water, we felt that the "normal" behavior would be dominated by water. Therefore as a second method we used the equation

$$\log_{10}\frac{\eta_T}{\eta_{T_o}} = \frac{A(T_o-T) + B(T_o-T)^2}{C + T} \qquad (26)$$

where $\eta_{T_o} = 4.9923$ centipoises

$T_o = 6.089°C$

$A = 1.848 \pm 0.017$

$B = 0.002077 \pm 0.000059$

$C = 86.233 \pm 0.949$

The parameters A, B and C were determined by a least squares analysis of the first 7 data points assuming that

no excess viscosity existed for $\Delta T > 14.4°C$. Equation (26) has been successfully used to represent the behavior of the viscosity of water which also shows large systematic deviations from the simple Arrhenius equation[25,26]. Experimental data along with the two equations used are shown in Fig. 7 for large ΔT values. Figure 8 shows the experimental data for small values of ΔT.

The "excess" viscosities obtained using both methods of characterizing normal behavior are shown in Fig. 9. We have fitted Eq. (21) to both sets of data to obtain the following sets of parameters:

a) From excess viscosities determined by using the Arrhenius equation,

$H'' = -0.0950 \pm 0.0023$ centipoises

$G = -0.179 \pm 0.012$ "

$\phi = -0.0017 \pm 0.0028$

b) Fom excess viscosities determined by using Eq. (26),

$H'' = -0.0759 \pm 0.0013$ centipoises

$G = -0.268 \pm 0.0085$ "

$\phi = -0.00049 \pm 0.00045$

We have also determined the exponent ϕ for the excess viscosity without first subtracting off the "normal" part. Expressing the total viscosity by

$$\eta = \Delta\eta + \eta_{cl}(T)$$

using Eq. (21) for $\Delta\eta$ and either Eq. (16) or Eq. (26) for

$\eta_{cl}(T)$, we obtained the following values for the exponents:

$$\phi = -0.00065 \pm 0.00014 \text{ (from Eq. (17))}$$

$$\phi = +0.00238 \pm 0.00022 \text{ (from Eq. (26))}$$

The quality of the fits in both cases was excellent with the standard deviation being 0.0202 for the first method and 0.0114 for the second method.

When we used Eq. (20) to analyze the total shear viscosity we obtained

$$A = 0.408 \pm 0.017$$

$$B = 11.68 \pm 0.38$$

$$\phi = -0.0507 \pm 0.0046$$

The quality of the fit was not very good and there were systematic deviations of about 2%. Limiting the fit of data to $\Delta T < 8°C$ improved the quality of fit slightly, yielding $\phi = -0.0407 \pm 0.0022$. The values of dynamic viscosities are given in Table I as a function of ΔT.

The errors quoted are what we believe to be the real errors and not the standard deviations obtained from unweighted least squares fittings.

DISCUSSION

We have determined the critical composition and tem perature of the lower consolute system 2,6-lutidine-water to be $X_L = 0.0658$, $T_c = 33.37_2 \pm 0.01°C$, compared to the previously reported values of $X_L = 0.065 \pm 0.001$, $T_c = 33.57°C$[27], $X_L = 0.067$, $T_c = 33.93 \pm 0.005°C$[28], $X_L = 0.0665$, $T_c = 34.06°C$[29], and $X_L = 0.0632$, $T_c = 33.927°C$[30]. We would like to note that we could reproduce the T_c of Ref. (27) just by duplicating the conditions (air saturation) under which it was measured.

Our light scattering results for the exponents γ, $\gamma-\psi$, ψ, ν_s, and ν_Γ are shown in Table II along with measurements on other simple fluids and on binary mixtures.

As can be seen from Table II, our results agree quite well with other single component and binary systems. Our $(\gamma-\psi)$ value seems to be slightly low compared to the rest. However, if we subtract the ψ value of 0.674 for CO_2 obtained by Murthy and Simon[31] from the γ value of 1.219 for CO_2 obtained by Lunacek[32], we obtain a $(\gamma-\psi)$ value of 0.545 for CO_2 which is in excellent agreement with our result. Recently it has been suggested that the $(\gamma-\psi)$ values should be corrected for the background effects. When correction is made for the nonsingular contribution to thermal conductivity the exponent $(\gamma-\psi)$ drops from 0.73 to 0.62 for CO_2[11]. The same suggestion has also been

made for the binary mixtures where the Onsager coefficient for diffusion is claimed to have a nonsingular part[34].

We have not made any corrections for the background term whose existence has not been proven for any binary system by independent experiments. Sengers and coworkers[34] obtain a positive background correction due to the fact that their ν_Γ obtained from Kawasaki expression is larger than ν_s obtained from intensity measurements. We have $\nu_s > \nu_\Gamma$ which would indicate a negative background correction.

From intensity data we find that within experimental error $\gamma=2\nu_s$ and $\bar{\eta} = 0$. Mode-mode coupling theories[4,10] predict that $\gamma-\psi = \nu_\Gamma$. Our values of $(\gamma-\psi) = 0.554\pm0.015$ and $\nu_\Gamma = 0.567\pm0.015$ seem to verify this. There has been some question about the equality of the correlation lengths determined from intensity and linewidth measurements. Our results from intensity data $\xi_{s_o} = 2.0\pm0.2$ Å, $\nu_s = 0.61\pm0.08$ compare favorably with values of $\xi_{\Gamma_o} = 2.92\pm0.19$ Å, $\nu_\Gamma = 0.567\pm0.015$ from linewidth measurements. Values of ν_Γ and ν_s reported for the isobutyric acid + water system by B. Chu[33] seem to indicate a significant difference between ν_s and ν_Γ but error bars are not quoted.

We find that the overall behavior of the linewidth of the Rayleigh line is quite well described by the Kawasaki theory, even though small systematic deviations

exist for $K\xi \simeq 1$. These are removed of we replace the viscosity in the Kawasaki expression with the experimental shear viscosities. This approach may not be valid since the viscosity in the theory is $\eta^*(K,\xi)$ at large K values[4] rather than $\eta(0,\xi)$. However, Kawasaki states that it is possible to identify the high frequency viscosity $\eta^*(K,\xi)$ with the experimental viscosity $\eta(0,\xi)$. The use of experimental viscosities brings the correlation length exponent closer to the one determined from intensity measurements. A similar observation has been made for the system 3-methyl pentane-nitroethane[34]. We could not make an independent check on the theory using correlation lengths determined from intensity measurements as has been done by Sengers ans co-workers[34] as the correlation lengths from our intensity measurements do not cover a sufficiently large ΔT range.

The high frequency viscosity η^* obtained from a least squares fit of the linewidth data varying all three parameters independently is 2.87±0.20 cps. When the experimental D_o is employed and ξ_{Γ_o} and ν_Γ are varied, η^* is found to be 2.65±0.20.cps. These values can be compared with an estimate of 2.62 cps which is obtained by extrapolating the experimental shear vescosity data under the assumption that the critical viscosity is nondivergent.

As is seen from our values for the viscosity exponent

ϕ, the lutidine-water system exhibits basically the same type of viscosity anomaly that has been observed for upper consolute systems[13,14,35]. However, due to hydrogen bonding the temperature dependence of viscosity away from the critical point is more complex than that represented by a simple Arrhenius equation[27].

Although the magnitude of the excess shear viscosity and the rate of increase depend on the method of subtraction of the normal part, the changes in the exponents obtained from measurements close to the critical temperature are not significant as is seen in Fig. 9. Our exponents for the "excess" shear viscosity are much smaller than most of the values reported in Table III, which leads us to believe that the excess shear viscosity is at most logarithmically divergent or exhibits a very strong cusp at the critical point. Of the four methods of analysis used, three predicted very small negative exponents and and one a very small positive exponent. In all four fittings the last experimental point was lower than the predicted values. This difference is larger than the experimental uncertainty, which might indicate a trend toward a finite viscosity. Similar rounding off has been observed previously[35]. However, we feel that on the basis of the data it is not possible to distinguish between a logarithmic divergence and a strong cusp. One thing is evident

from our data; the viscosity anomaly is not a strong one as has been suggested by the data of Barber and Champion[36] and Woermann and Sarholz[14], or by the mean field theories given in Table II. We think that the method of defining the "normal" part is responsible for the sharp rise in the excess viscosity for large ΔT values as is demonstrated in Fig. 9. Significant excess viscosities exist for ΔT values as large as 10°C and one has to be careful in defining what are normal and what are excess contributions to momentum transport.

ACKNOWLEDGMENTS

We would like to thank Dr. V. P. Gutschick for thermodynamic data on the L-W system, and Dale Powers for assistance with the chromatography check of the lutidine. We are grateful to Ronald J. Brown and Hollis Reamer for their many suggestions on experimental technique and data analysis. George Griffith and his staff are due thanks for expert advice on design and construction of sections of the apparatus.

REFERENCES

* Research sponsored by Directorate of Chemical Science, AFOSR(SRC)-OAR, USAF Grant No. AFOSR 68-1382.

† Present adress: Department of Chemistry, Lousiana State University, New Orleans, La. 70122.

1. A. Einstein, Ann. Phys. 33, 1275 (1910).

2. L.S.Ornstein and F. Zernike, Proc. Roy. Acad. Sci. (Amsterdam) 17, 793 (1914); 18, 1318 (1916); 19, 1520 (1917); Phys. Z. 19, 134 (1918); 27, 761 (1926).

3. P. Debye, (a) in Non-Crystalline Solids, edited by V. D. Frechette (Wiley, New York, 1960); (b) in Electromagnetic Scattering, edited by M. Kerker (MacMillan, New York, 1963).

4. K. Kawasaki, Phys. Letters 30A, 325 (1969); Phys. Rev. A1, 1750 (1970), Ann. Phys. 61, 1 (1970).

5. M. E. Fisher, J. Math. Phys. 5, 944 (1964).

6. R. D. Mountain and J. M. Deutch, J. Chem. Phys. 50, 1103 (1969).

7. M. Fixman, J. Chem. Phys. 33, 1357 (1960).

8. W. D. Bothch, dissertation, University of Oregon, 1963 (unpublished), p. 63.

9. R. A. Ferrell, University of Maryland Preprints, Tech. Report No. 70-097.

10. L. P. Kadanoff and J. Swift, Phys. Rev. 166, 89 (1968).

11. Section II, Viscosity part is a substantial recaputi-

lation of that given by, J. V. Sengers, University of Maryland Preprints, Tech. Report No. 71-074.

12. J. H. Simmons, A. Napolitana, and P. B. Macedo, J. Chem. Phys. 53, 1165 (1970).
13. P. Debye, B. Chu, and D. Woermann, J. Polymer Sci. A1, 249 (1963).
14. D. Woermann and W. Sarholz, Ber. Bunsenges Physik. Chem. 69, 319 (1965).
15. J. Swift, Phys. Rev. 173, 257 (1968).
16. M. E. Fisher cited in ref. 11.
17. B. Chu, J. Chem. Phys. 41, 226 (1964).
18. W. P. Kao and B. Chu, J. Chem. Phys. 50, 3986 (1969).
19. D. W. Marquardt, J. Soc. Industrial & Appl. Math. 11, 431 (1963).
20. B. Chu, Natl. Bur. Std. Misc. Publ. 273, 123 (1966).
21. B. Chu, J. Chem. Phys. 42, 426, 3742 (1965).
22. B. Chu, J. Chem. Phys. 42, 2293 (1965).
23. D. L. Henry, H. L. Swinney, and H. Z. Cummins, Phys. Rev. Letters 25, 1170 (1970).
24. P. Berge, P. Calmettes, C. Laj, M. Tournaire, and B. Volochine, Phys. Rev. Letters 22, 1123 (1970).
25. J. F. Swindells, Handbook of Chemistry and Physics, edited by C. D. Hodgeman (Chemical Rubber Co., Akron, Ohio, 1969) 50th edition.
26. L. Korson, W. Drost-Hansen, and F. J. Millero (private communication).

27. V. P. Gutschick and C. J. Pings, J. Chem. Phys. 55, 3845 (1971).

28. R. Pancirov and H. Brumberger, J. Am. Chem. Soc. 86, 3562 (1964).

29. J. D. Cox and E. F. G. Herrington, Trans. Faraday Soc. 52, 926 (1956).

30. A. W. Loven and O. K. Rice, Trans. Faraday Soc. 59, 2723 (1963).

31. M. L. R. Murthy and H. A. Simon, Phys. Rev. A2, 1458 (1970).

32. J. H. Lunacek and D. S. Canell, Phys. Rev. Letters 17, 841 (1971).

33. B. Chu and F. J. Schoenes, Phys. Rev. Letters 21, 6 (1968); B. Chu, F. J. Schoenes, and W. P. Kao, J. Am. Chem. Soc. 90, 3042 (1968).

34. R. F. Chang, P. H. Keyes, J. V. Sengers, and C. O. Alley, Phys. Rev. Letters. 27, 1706 (1971).

35. A. Stein, J. C. Allegra, and G. F. Allen, J. Chem. Phys. 55, 4265 (1971).

36. T. Barber and J. V. Champion, Phys. Letters A29, 622 (1969).

TABLE I

SHEAR VISCOSITIES AS A FUNCTION OF ΔT

$T_c = 33.372°C$

$\Delta T°C$	η (centipoises)	$\Delta T°C$	η (centipoises)
27.420	4.992	0.231	2.221
23.714	4.240	0.197	2.232
20.550	3.726	0.160	2.251
18.341	3.423	0.129	2.267
17.112	3.273	0.106	2.290
14.938	3.027	0.080	2.309
14.372	2.971	0.063	2.336
12.454	2.788	0.038	2.377
11.154	2.675	0.025	2.404
10.501	2.625	0.017	2.439
10.217	2.599	0.013	2.453
9.392	2.535	0.007	2.470
8.484	2.471	-0.008	2.403*
7.335	2.394		
6.375	2.332		
5.385	2.275		
4.414	2.224		
3.935	2.203		
3.441	2.177		
2.473	2.149		
1.650	2.132		
1.008	2.136		
0.646	2.156		
0.443	2.180		
0.313	2.205		
0.276	2.219		
0.257	2.224		

*The average viscosity for the two phases during separation

TABLE II

SUMMARY OF CRITICAL EXPONENTS FOR A NUMBER OF SYSTEMS

System	Ref.	γ	$\gamma-\psi$	ψ	ν_s	ν_Γ
Xe	23		0.751±0.004			
Xe	a	1.26				
Xe	b	1.244 1.228			0.57±0.05	
SF_6	c		1.26±0.02			
CO_2	d		0.73±0.02			
CO_2	32	1.219±0.010			0.633±0.01	
CO_2	31			0.674±0.002		
Isobutyric acid-water	33	1.24±0.05	0.68±0.04	0.56	0.62	0.41
n-Hexane-nitrobenzene	e		0.66±0.02			0.70±0.10
Aniline-cyclohexane	24		0.61±0.07			0.588±0.06
Phenol-water	f	1.32±0.03	0.68±0.03	0.66±0.04		0.58±0.10
Polystyrene-cyclohexane	g		0.77			0.58
3-Methylpentane-nitroethane	35	1.231±0.04			0.616±0.013	
2,6-lutidine-water	This work	1.26±0.02	0.554±0.015	0.71±0.035	0.61±0.08	0.567±0.015

TABLE II(continued)

Ref.

a M. Vicentini-Missoni, J. M. H. Levelt Sengers, and M. S. Green, Phys. Rev. Letters 22, 389(1969)

b M. Giglio and G. B. Benedek, Phys. Rev. Letters 23, 1145(1969)

c G. B. Benedek, in Polarization Motiere et Rayonnement Livre de Jubile en L'honeur du Professeur A. Kastler (Presses Universitaire de France, Paris,1969)

d H. L. Swinney and H. Z. Cummins, Phys. Rev. 171, 152(1968)

e H. Chen and N. Polonsky-Ostrowsky, Opt. Commun. 1, 64(1969)

f P. N. Pusey and W. I. Goldburg, Phys. Rev. Letters 23, 67(1969)

g N. Kuwahara, D. V. Fenby, M. Tamsky, and B. Chu, J. Chem. Phys. 55, 1140(1971)

TABLE III

SUMMARY OF VISCOSITY SINGULARITIES

System	Ref.	Exponent	Equation
Iso-octane-perfluoro-heptane	13,14	-0.07	a
Phenol-water	13,14	-0.05	a
Isobutyric acid-water	13,14	-0.05	a
Isobutyric acid-water	45	+0.12	b^1
Hexane-nitrobenzene	14	-0.04	a
Cyclohexane-aniline	14	-0.04	a
Cyclohexane-aniline	42	0(log)	d
3-Methylpentane-nitroethane	43	-0.04	a
3-Methylpentane-nitroethane	44	0.005±0.014	b^1
2,6-Lutidine-water	This work	-0.050±0.002	a
		-0.0017±0.0028	c^1
		-0.0005±0.0004	c^2
		-0.00065±0.00014	b^2
		0.00238±0.00022	b^3
THEORETICAL PREDICTIONS			
Mean Field Theories			
Fixman	47	$\eta \sim \varepsilon^{-1/2}$	
Deutsch, Mountain and Zwanzig	48	$\eta \sim \varepsilon^{-1/2}$	
Kawasaki	49	finite	
Scaling Theories			
Kadanoff and Swift	10,15	$\eta \sim \ln\varepsilon$ or finite	
Kawasaki	4	finite	

TABLE III (continued)

Equation		
a		$\eta = e^{A+B\varepsilon}e^{\phi}$
b		$\eta = \frac{A}{\phi}(\varepsilon^{\phi}-1) + \eta_{cl}(T) + D$
where	1	$\eta_{cl}(T) = B\varepsilon + C$
	2	$\eta_{cl}(T) = B\varepsilon^{C/T}$
	3	$\eta_{cl}(T) = B \exp \frac{C\Delta T + E\Delta T^2}{F + \Delta T}$
c		$\Delta\eta = \eta - \eta_{cl}(T) = \frac{A}{\phi}(\varepsilon^{\phi}-1) + B$
where	1	$\eta_{cl}(T)$ defined by Eq. (16)
	2	$\eta_{cl}(T)$ defined by Eq. (26)
d		$\Delta\eta = -A\ln(\varepsilon) + B$

FIGURE CAPTIONS

Fig. 1. A schematic of the light scattering spectrometer

Fig. 2. Plot of reciprocal scattered intensity in arbitrary units vs. $\sin^2(\theta/2)$. Only a representative seven of the twenty isotherms studied are shown here.

Fig. 3. Log-log plot of $I(0)^{-1}$ vs. ΔT. The solid line is given by $\log I(0)^{-1} = -0.218+1.260\varepsilon$. Run 1 ●; Run 2 o. The lowest ΔT point was not employed in the least squares fit.

Fig. 4. Log-log plot of the correlation lengths from intensity measurements vs. ΔT. The solid line is given by $\xi = 2.0\varepsilon^{-0.61}$ Å.

Fig. 5. Log-log plot of the mutual diffusion coefficient D vs. ΔT. The solid line is given by $D = 0.290\varepsilon^{0.554}\times10^{-5}$ cm^2/sec.

Fig. 6. Log-log plot of Γ/K^3 vs. $(K\xi_\Gamma)^{-1}$ for the ΔT range 0.001° - 7.5°C. The solid line is given by the Kawasaki linewidth expression with the parameters $\eta^*=2.87$ cps, $\nu_\Gamma=0.541$, and $\xi_{\Gamma_o}=3.0$ Å.

Fig. 7. Plot of shear viscosity vs. T for large T values. ---- Eq. (16); ——— Eq. (26), using the parameters given in the text.

Fig. 8. Plot of shear viscosity vs. T for small ΔT values.

Fig. 9. Log-log plot of $\Delta\eta$ vs. ΔT for two representations of the "normal" viscosity. ● η_{cl} from Eq. (16); o η_{cl} from Eq. (26).

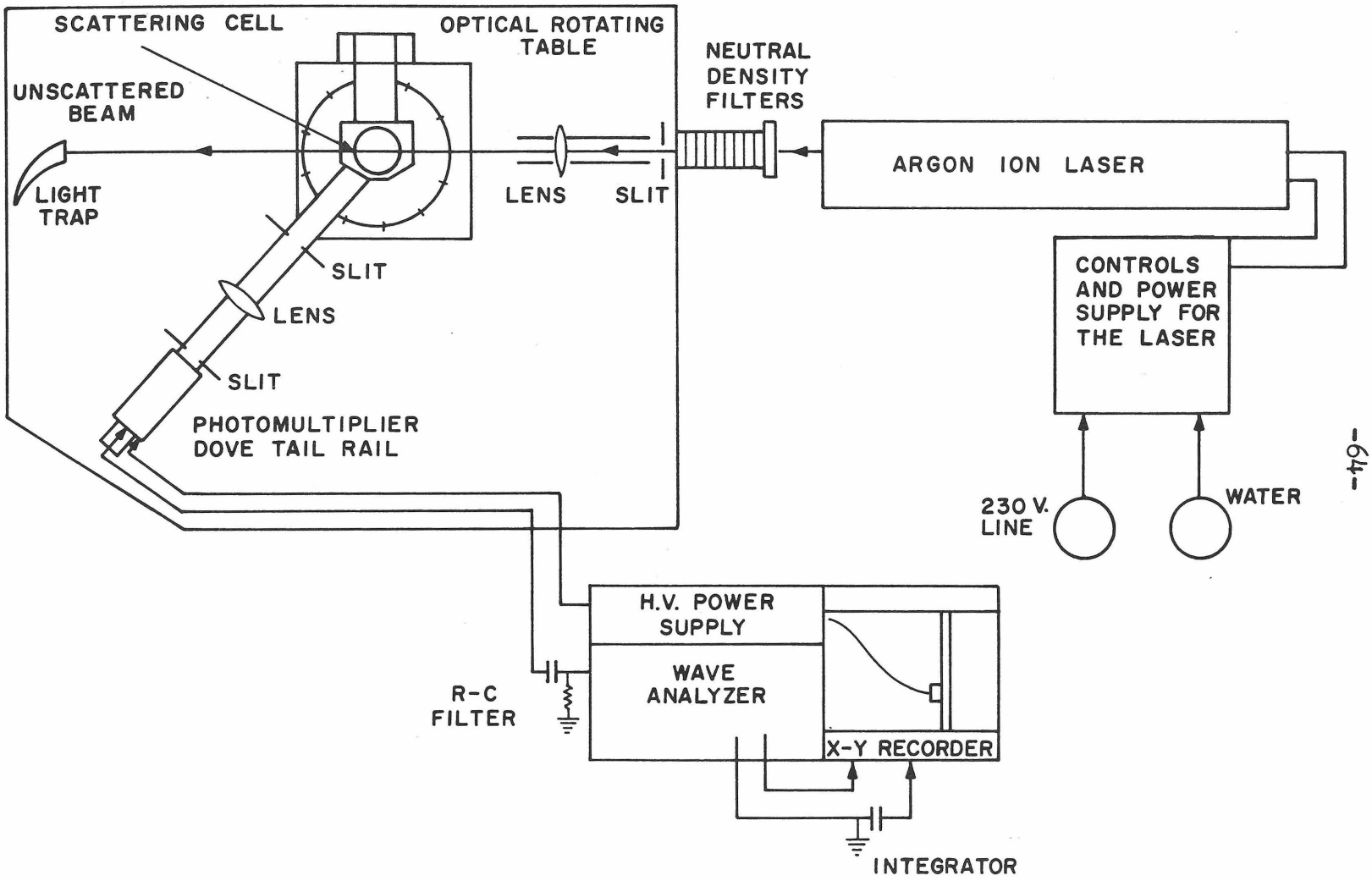
SCATTERING CELL
OPTICAL ROTATING TABLE
NEUTRAL DENSITY FILTERS
UNSCATTERED BEAM
ARGON ION LASER
LIGHT TRAP
LENS
SLIT
SLIT
LENS
SLIT
PHOTOMULTIPLIER DOVE TAIL RAIL
CONTROLS AND POWER SUPPLY FOR THE LASER
230 V. LINE
WATER
H.V. POWER SUPPLY
WAVE ANALYZER
X-Y RECORDER
R-C FILTER
INTEGRATOR

Figure 1.

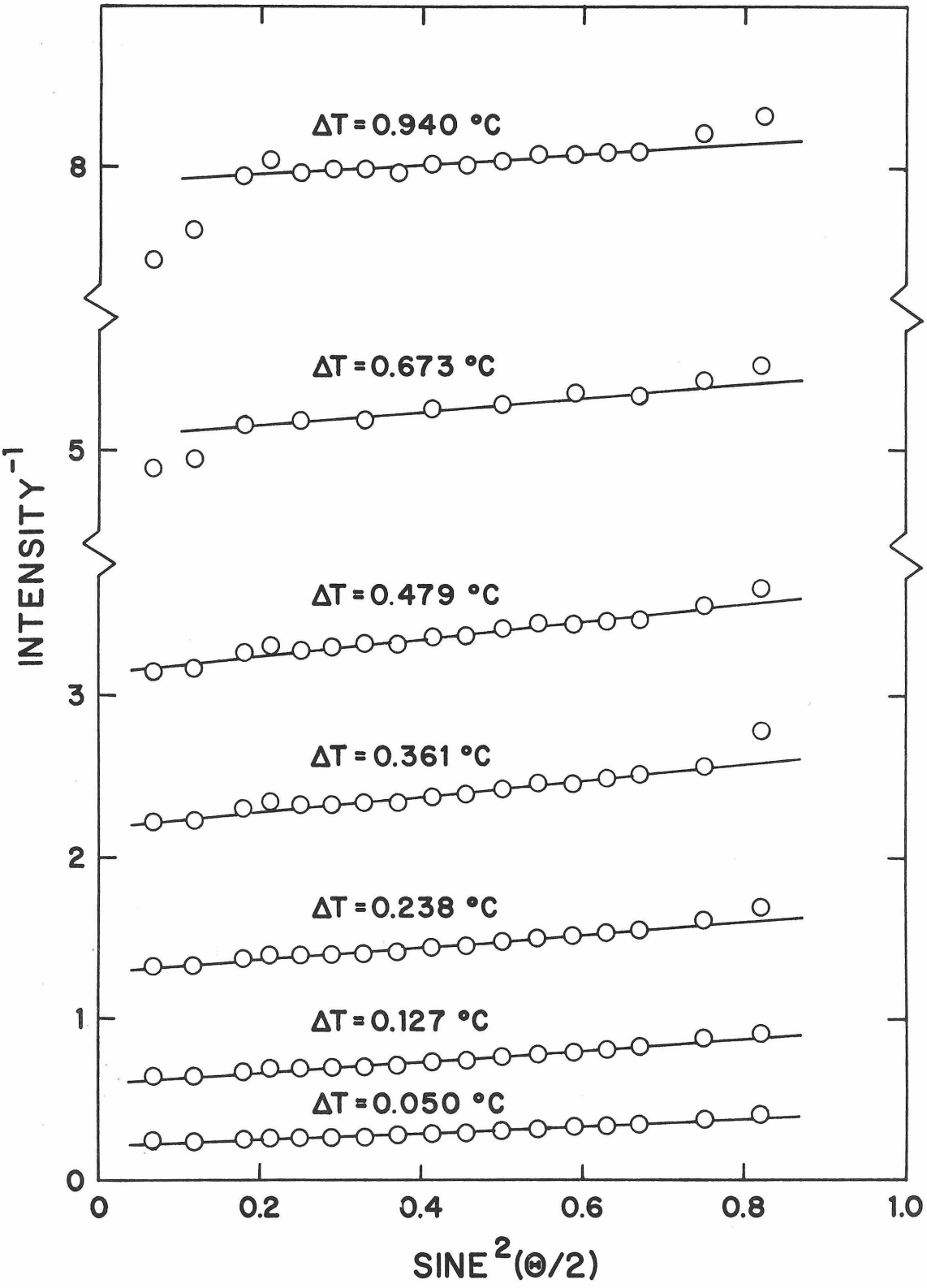
ΔT = 0.940 °C
ΔT = 0.673 °C
ΔT = 0.479 °C
ΔT = 0.361 °C
ΔT = 0.238 °C
ΔT = 0.127 °C
ΔT = 0.050 °C
INTENSITY^{-1}
SINE^2(Θ/2)
0
1
2
3
5
8
0.2
0.4
0.6
0.8
1.0

Figure 2.

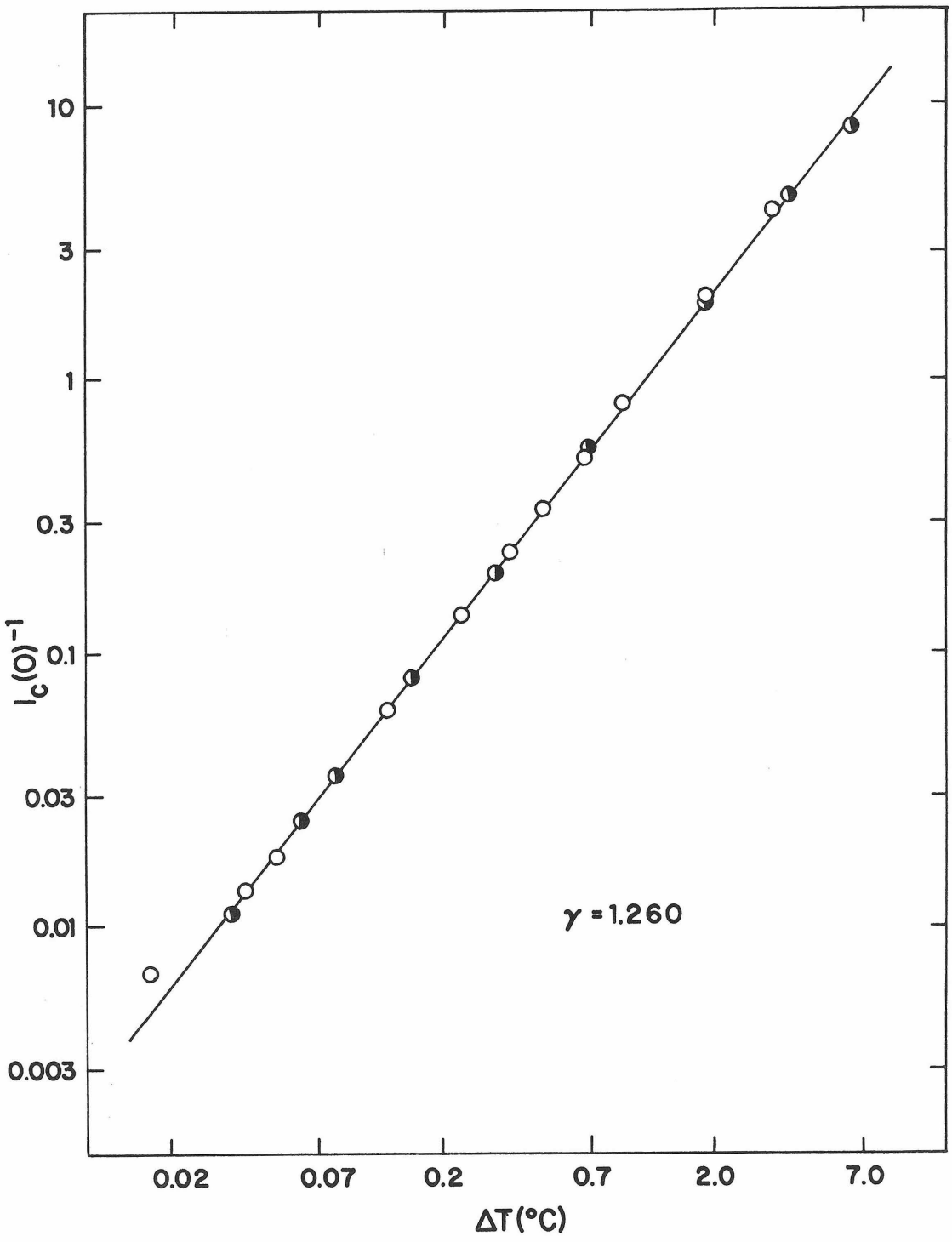

Figure 3.

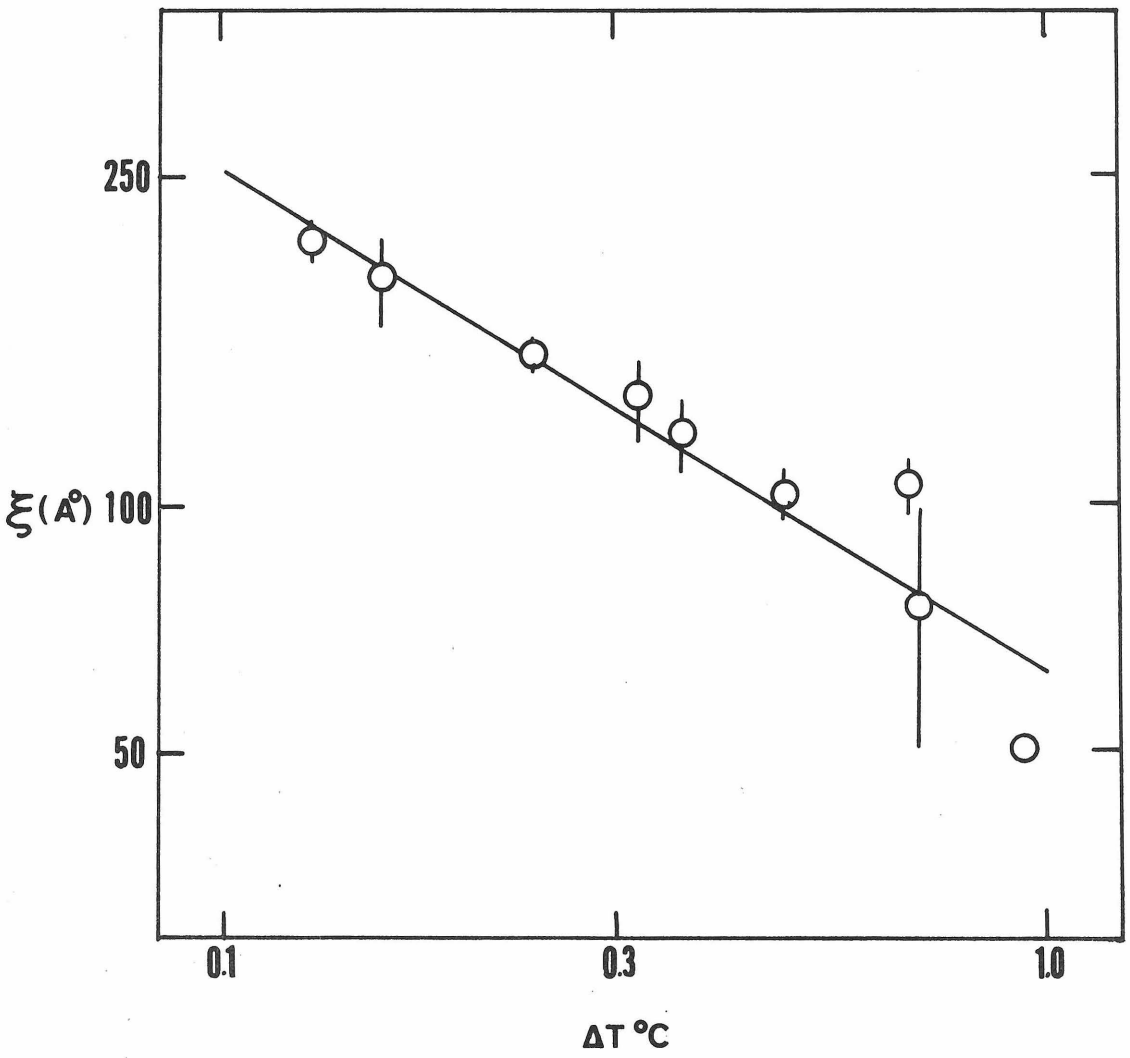

Figure 4.

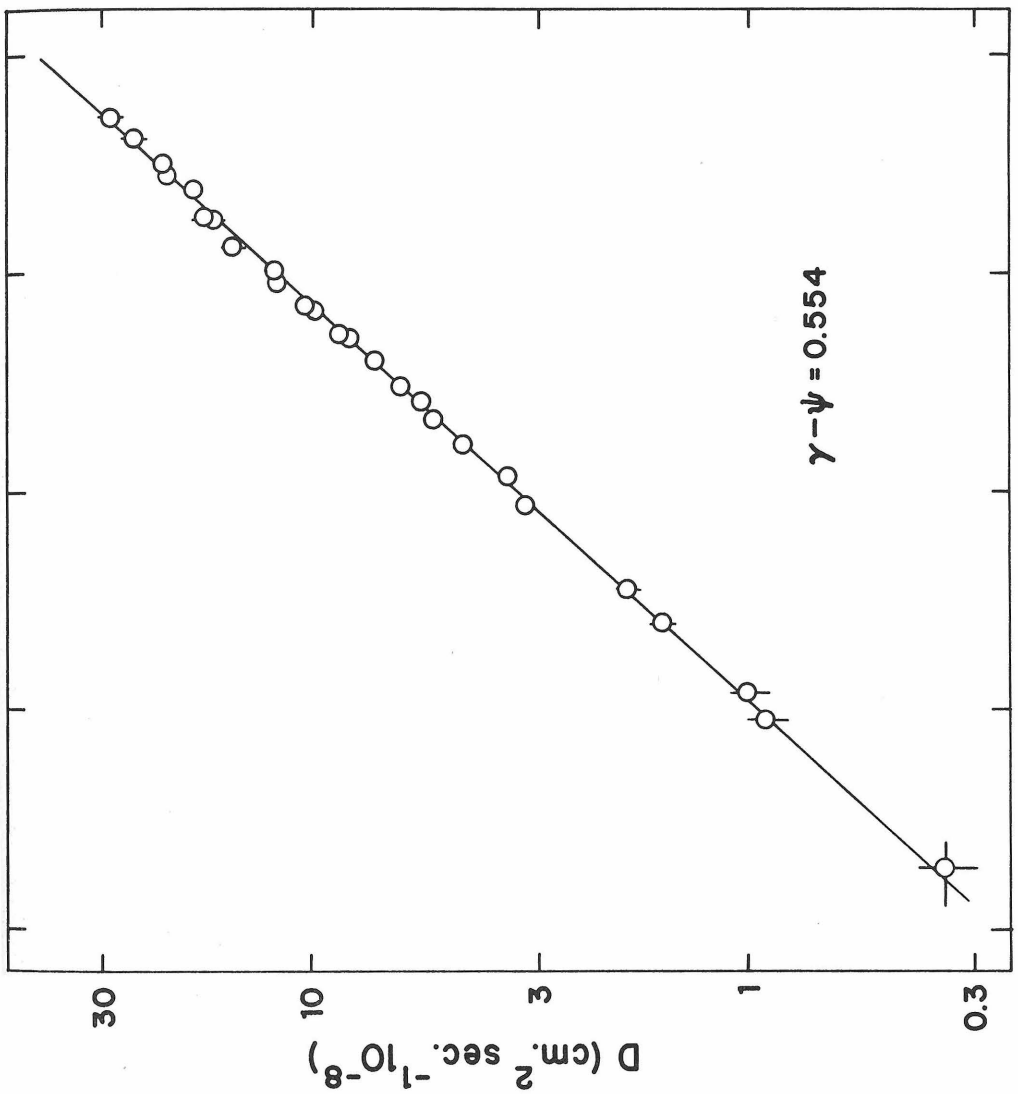

Figure 5.

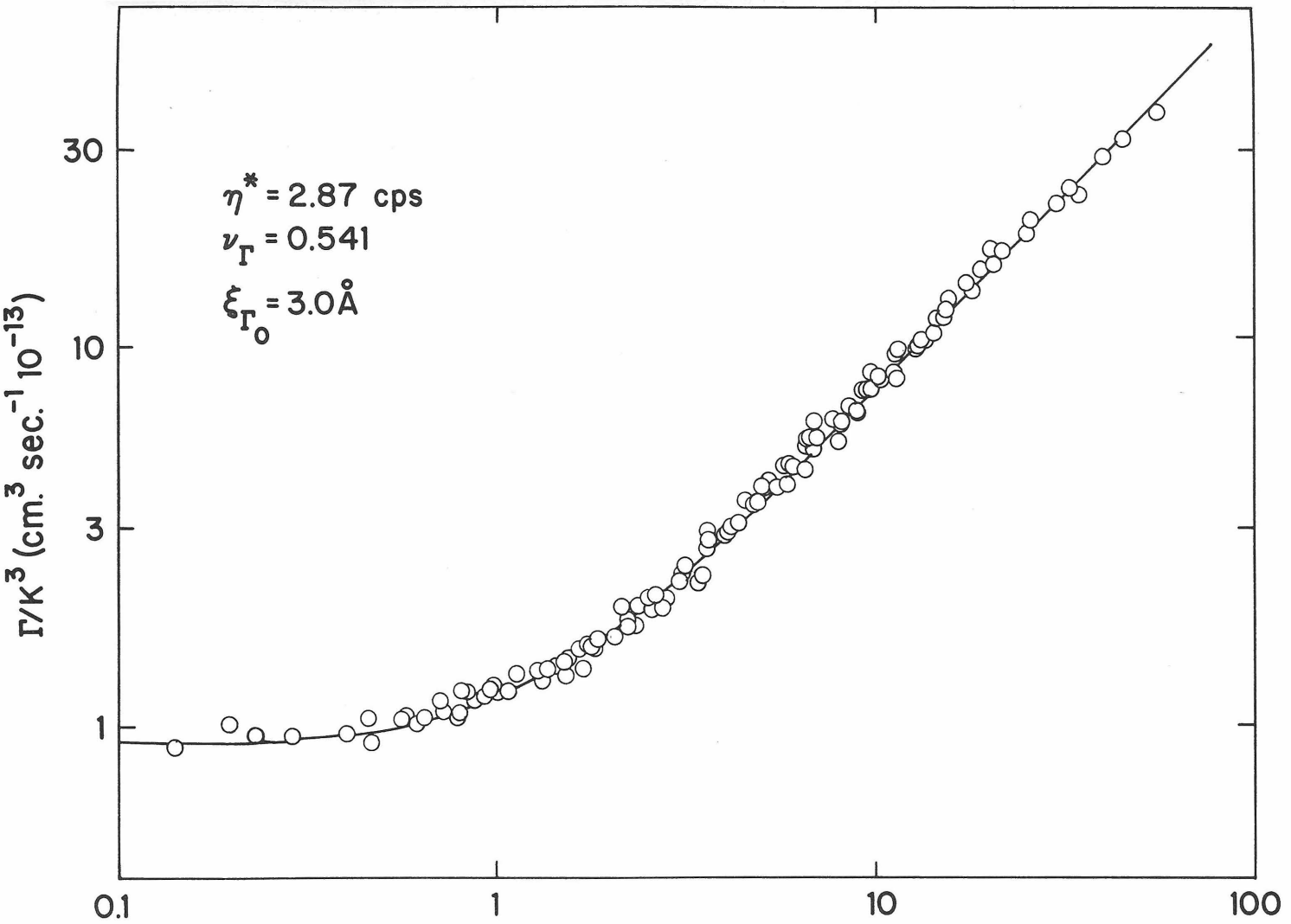
$\eta^* = 2.87$ cps
$\nu_\Gamma = 0.541$
$\xi_{\Gamma_o} = 3.0$Å
Γ/K^3 (cm.^{3} sec.$^{-1}$ 10^{-13})
30
10
3
1
0.1
1
10
100
$1/K\xi$

Figure 6.

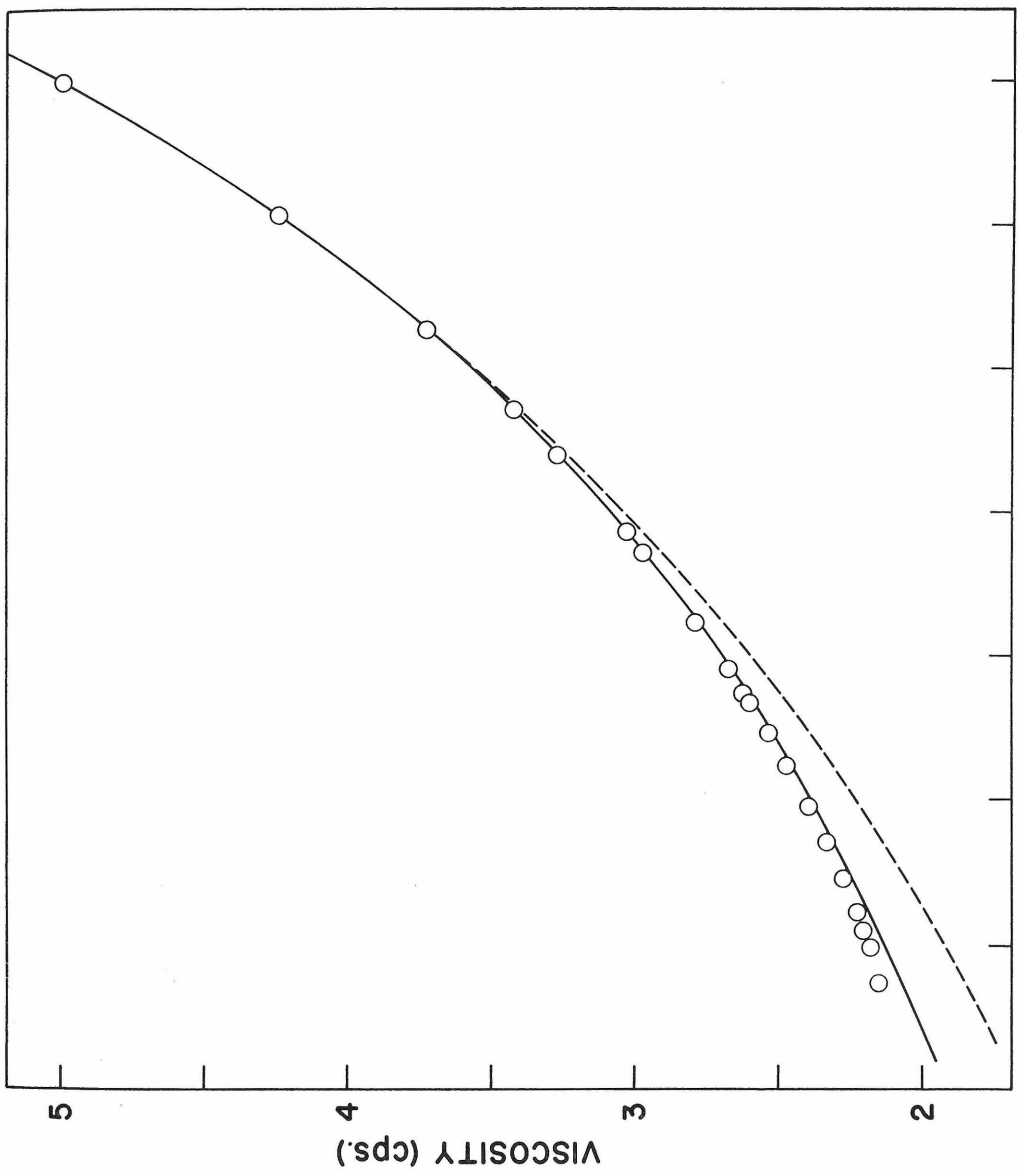

Figure 7.

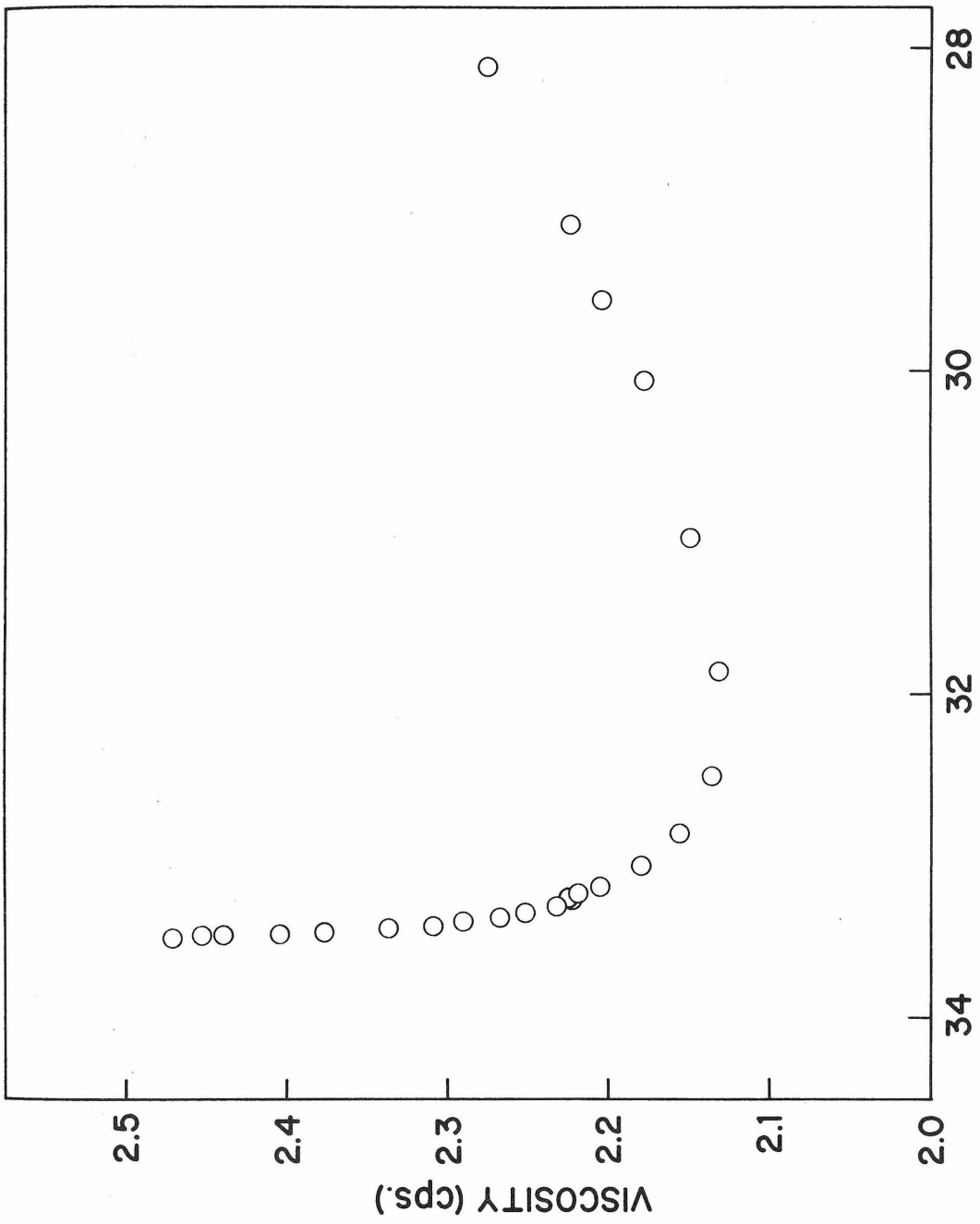

Figure 8.

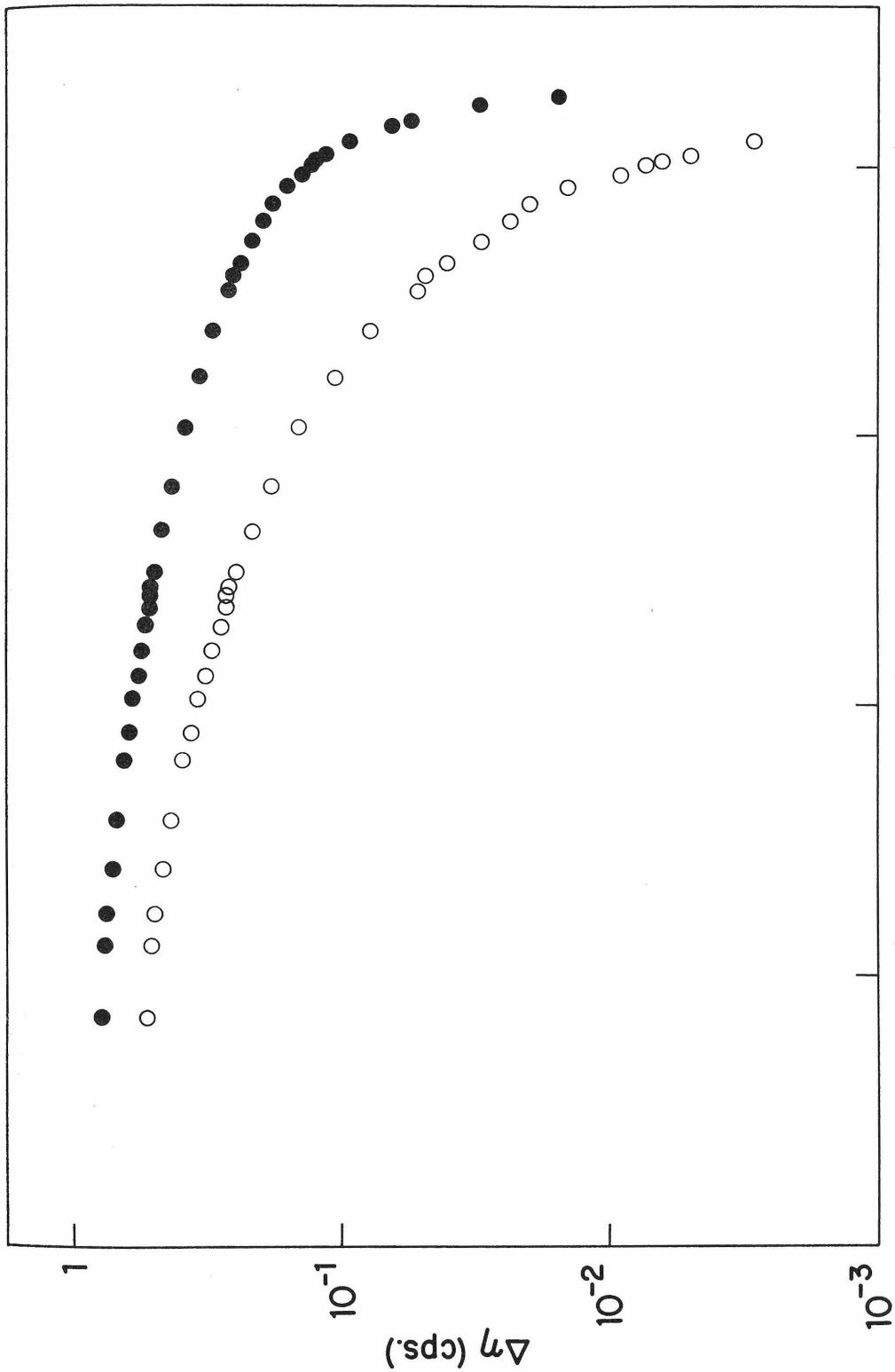

Figure 9.

IV

MEASUREMENT OF MUTUAL DIFFUSION COEFFICIENTS AND THERMAL DIFFUSIVITIES BY QUASI-ELASTIC LIGHT SCATTERING*

Erdoğan Güları, Ronald J. Brown, and C. J. Pings

Division of Chemistry and Chemical Engineering
California Institute of Technology
Pasadena, California 91109

(Draft for publication, complete with figures and references, will be submitted to AIChE Journal. The two values of thermal diffusivity for benzene-toluene mixtures were obtained by R. J. Brown who also did most of the editing. For extra data see Tables X to XXVI.)

*Research supported be the Directorate of Chemical Sciences, AFOSR-OAR, USAF Grant No. AFOSR-68-1382, by the Donald E. Baxter Foundation, and by the National Science Foundation under Grant No. GK-34045.

ABSTRACT

Quasi-elastic light scattering techniques have been employed to measure the mutual diffusion coefficient D_{AB} as a function of concentration in eight binary mixtures and the thermal diffusivity χ in nine pure liquids and two binary mixtures. The mass diffusivities obtained are accurate to typically 3% while thermal diffusivities are known to 5%; both types of values are in substantial agreement with the available bulk values. Under most circumstances light scattering is found to offer distinct advantages over the standard techniques for determining mass and thermal diffusivities.

SCOPE

Because both the mutual diffusion coefficient and the thermal diffusivity appear in transport equations, a knowledge of their values is of particular importance in many chemical engineering applications. However, there exists a relative scarcity of reliable mass and thermal diffusivity data. In recent years with the advances in laser technology, spectroscopic methods, and the theory of light scattering by fluids, quasi-elastic light scattering techniques have been successfully used to measure macromolecular diffusion coefficients and mass and thermal diffusivities for systems in the neighborhood of their critical point. In these cases light is scattered very strongly by the large entropy or concentration fluctuations. In contrast, normal mixtures and pure liquids scatter 10^4-10^5 times less — thus, there have been only a few attempts at determining D_{AB} and χ for these systems.

The objective of this study was to establish quasi-elastic light scattering as a convenient tool for the rapid and accurate determination of mass and thermal diffusivities. Mutual diffusion coefficients as a function of concentration are reported for eight systems. Extensive literature data exist for most of the mixtures studied. Thermal diffusivity measurements for nine pure liquids and two mixtures are also reported and compared to the values calculated from conven-

tional measurements of density, heat capacity, and thermal conductivity.

CONCLUSIONS AND SIGNIFICANCE

Using quasi-elastic light scattering, the thermal diffusivity χ and the binary mutual diffusion coefficient D_{AB} have been measured for a variety of pure liquids and binary mixtures. The resulting values are in close agreement with the available bulk values and are accurate to about 3% for mass diffusivities and 5% for thermal diffusivities. Because neither type of measurement is dependent on the imposition of a macroscopic gradient, many of the problems associated with conventional bulk measurements are eliminated.

Determinations require less than two hours for thermal diffusivities and thirty minutes for mass diffusivities, juxtaposed to the more time consuming classical approaches. On the basis of these experimental results, light scattering techniques can be used effectively to determine χ and D_{AB} for most liquid systems.

For almost half a century it has been known that the frequency spectra of light scattered from liquids by entropy and concentration fluctuations contain transport coefficient information (Mandel'shtam, 1926; Landau and Placzek, 1934). To resolve the extremely narrow lines predicted from the theory of the distributed spectra, the resolving power (ω_o/ω) of the spectrometer must approach 10^{14}. The best conventional spectroscopic method, the spherical Fabry-Perot interferometer, has a limiting resolution of $1:10^8$. Only with the advent of the laser as an intense, monochromatic light source, and the development of optical homodyne and heterodyne spectroscopy, has the study of the spectra from concentration and entropy fluctuations become possible. Cummins and Swinney (1969) and Chu (1970) have written extensive reviews of the optical-beating techniques.

The earliest quantitative spectral measurements were made on fluid systems near their critical point (Alpert, 1965; Ford and Benedek, 1965) and on macromolecular solutions (Dubin et al, 1967). In contrast to the now extensive use of quasi-elastic light scattering techniques to study critical phenomena and macromolecular dynamics there have been only a few attempts to measure transport coefficients in systems removed from their critical point. These efforts by Lastovka and Benedek (1966), Aref'ev et al (1967), Berge et al (1969, 1970), and Dubois et al (1970) demonstrated the feasibility of using light scattering techniques to determine transport coefficients. However, their limited results did not conclusively establish light scattering as a reliable

and efficient method for obtaining liquid diffusivities. The systems chosen were selected for their high degree of scattering, thus facilitating signal detection. The possibility of extending diffusivity determinations to other systems remained unclear. In three of five cases where binary mutual diffusion coefficients were measured, no conventionally determined data existed for comparison. The thermal diffusivities measured were not in agreement with bulk values calculated from literature data.

We present data which indicate that light scattering provides an accurate and convenient method of determining mutual diffusion coefficients for a large class of binary mixtures and thermal diffusivities for most pure liquids.

THEORY

Light is scattered by optical inhomogeneities. The physical reason for optical inhomogeneities in pure fluids is density fluctuations, which concomittantly produce fluctuations in the dielectric constant. In solutions, concentration fluctuations are an additional cause of fluctuations in the dielectric constant. These sources of time dependent optical inhomogeneities modulate the scattered light and produce the altered time dependence of the scattered electric field that contains information about the modes of fluctuation dissipation and hence the transport properties of the scattering medium.

Beginning with the expression from classical scattering theory for the scattered electric field (Landau and Lifshitz, 1960)

$$E_s(\underline{R},t) \sim e^{-i\omega_o t} \int_v \alpha(\underline{r},t) \exp\left[i(\underline{k}_o-\underline{k}_s)\ \underline{r}\ \right] d\underline{r} \qquad (1)$$

and performing a Fourier decomposition on fluctuations in the polarizability α, it is evident that only the Fourier component

$$\underline{K} = \underline{k}_s - \underline{k}_o \qquad (2)$$

of the fluctuation is responsible for the scattering seen at $\underline{R}$. The scattering wave vector

$$K = 2\left(\frac{2\pi n}{\lambda_o}\right) \sin\left(\frac{\theta}{2}\right) \qquad (3)$$

Recognizing that the polarizability is proportional to the dielectric constant ε , description of the scattered field reduces to the derivation of an expression for fluctuations in the dielectric constant $\delta\varepsilon(\underline{K},t)$.

Mandel'shtam (1926) and Landau and Placzek (1934) used thermodynamic fluctuation theory in conjunction with the macroscopic equations of heat conduction and mass diffusion to describe the time decay of fluctuations in the dielectric constant and the shape of the resulting distributed spectra. They reasoned that fluctuations in density can be expressed in terms of the independent thermodynamic variables, pressure and entropy, i.e., adiabatic and isobaric fluctuations. Modulation of light by adiabatic fluctuations of density physically represent local compressions and rarefactions of the fluid. Due to the elastic nature of the fluid, these fluctuations propagate throughout the sample and can be visualized as thermal elastic waves diffracted according to the Bragg condition. These waves result in the Brillouin peaks, which are not of further interest in this work.

Scattering from isobaric fluctuations in density is associated with temperature or entropy fluctuations. The dissipation of these fluctuations obeys the Fourier heat equation and is controlled by the thermal diffusivity. The component responsible for scattering is then

$$\delta T(\underline{K},t) = \delta T(\underline{K},0) \exp [-\chi K^2 t] \qquad (4)$$

Thus, fluctuations in temperature or entropy are exponentially decaying functions localized in space. An analogous situation

exists for the dissipation of concentration fluctuations in binary mixtures. The diffusion equation is obeyed, and its solution yields

$$\delta C(\underline{K},t) = \delta C(\underline{K},0) \exp [-D_{AB}K^2 t] \qquad (5)$$

Mountain (1966), Mountain and Deutch (1969), and Kadanoff and Martin (1963) have presented a more rigorous development in which the linearized equations of hydrodynamics were used to solve for the time dependence of concentration and density fluctuations. The results derived for a pure liquid are identical to those obtained from classical thermodynamic fluctuation theory; for binary mixtures, Mountain and Deutch observed a term resulting from the dynamics which does not appear from the thermodynamic theory (Miller, 1967). This additional term is a result of the coupling of temperature and concentration dissipation, i.e., the Dufour and Soret effects. Under the condition $\chi >> D_{AB}$, which obtains for the systems studied here, the formulae reduce to those developed from thermodynamic fluctuation theory and the experimental separation of the contributions from entropy and concentration fluctuations is possible.

The quantities of direct interest in quasi-elastic light scattering are the density-density correlation function $F(\underline{K},t)$ and its Fourier transform, the dynamic structure factor $S(\underline{K},\omega)$, which is the spectrum of the electric field.

For a pure fluid (Mountain, 1966)

$$F(\underline{K},t) = \langle \rho(-\underline{K})\rho(\underline{K},t)\rangle$$
$$\sim \langle |\delta\rho(\underline{K})|^2\rangle \left\{ \frac{C_p - C_v}{C_p} \exp\left[-\chi K^2 t\right] \right\} \tag{6}$$

and

$$S(\underline{K},\omega) \sim \langle |\delta\rho(\underline{K})|^2\rangle \left(\frac{C_p - C_v}{C_p}\right)\left(\frac{2\chi K^2}{(\chi K^2)^2 + \omega^2}\right) \tag{7}$$

For a binary mixture (Mountain and Deutch, 1969)

$$F(\underline{K},t) \sim \left(\frac{\partial \varepsilon}{\partial C}\right)^2_{P,T} \langle |\delta C(\underline{K})|^2\rangle \exp\left[-D_{AB}K^2 t\right]$$
$$+ \left(\frac{\delta \varepsilon}{\delta T}\right)^2_{P,C} \langle |\delta T(\underline{K})|^2\rangle \exp\left[-\chi K^2 t\right] \tag{8}$$

and

$$S(\underline{K},\omega) \sim \left(\frac{\delta \varepsilon}{\delta C}\right)^2_{P,T} \langle |\delta C(K)|^2\rangle \left\{ \frac{2D_{AB}K^2}{(D_{AB}K^2)^2 + \omega^2} \right\}$$
$$+ \left(\frac{\delta \varepsilon}{\delta T}\right)^2_{P,C} \langle |\delta T(K)|^2\rangle \left\{ \frac{2\chi K^2}{(\chi K^2)^2 + \omega^2} \right\} \tag{9}$$

subject to the condition $\chi >> D_{AB}$.

Equation (6) expresses the density correlation function in the real time domain as a decaying exponential with a decay time (the time required for the exponential to decay to e^{-1} of its initial value) of $(\chi K^2)^{-1}$. The corresponding spectrum in the frequency domain Eqn. (7) represents a Lorentzian with a half-width at half-height of $\chi K^2/2\pi$ Hz. Hence the thermal diffusion process may be characterized by either an exponential decay time or its conjugate half-width. Similarly, for a binary mixture

with concentration fluctuations the dominant source of scattering, the concentration correlation function Eqn. (8) is described by the decay time $(D_{AB}K^2)^{-1}$ or the corresponding half-width of Eqn. (9), $D_{AB}K^2/2\pi$. If temperature fluctuations should dominate, the characterization parameters are identical to those for a pure fluid.

The amplitude of the mass diffusivity term in Eqn. (9) is a function of the factors $(\delta\varepsilon/\delta C)_{P,T}$ and $<|\delta C|^2>$. The first term is dependent upon the difference between mass reduced polarizabilities of solute and solvent, as is evident from the Lorentz-Lorenz formula

$$\frac{\varepsilon-1}{\varepsilon+2} = \frac{4\pi}{3}\rho\left[C\frac{\alpha_1}{m_1} + (1-C)\frac{\alpha_2}{m_2}\right] \tag{10}$$

and its derivative

$$\left(\frac{\partial\varepsilon}{\partial C}\right)_{P,T} = \frac{4\pi}{3}\frac{(\varepsilon+2)^2}{3}\rho\left[\frac{\alpha_1}{m_1} - \frac{\alpha_2}{m_2} - \frac{3}{4\pi}\frac{\varepsilon-1}{\varepsilon+2}\left(\frac{1}{\rho_1} - \frac{1}{\rho_2}\right)\right] \tag{11}$$

where $\rho = [C/\rho_1+(1-C)/\rho_2]^{-1}$ is the mixture's density, α_1 is the molecular polarizability, and m_i is the molecular mass. It is evident that the amplitude of the concentration term in Eqn. (9) for a fixed composition is proportional to the difference between refractive indices of the two components. Experimentally one should expect reduced scattered intensities for solutions with comparable solute-solvent refractive indices, and a corresponding reduction in accuracy of the experimental results.

The mean square concentration fluctuation term can be expressed by

$$<|\delta C|^2>_{P,T} = k_B T\,(\partial\mu/\partial C)_{P,T}^{-1} \tag{12}$$

where μ is the chemical potential of solution, $(\partial\mu|\partial C)_{P,T}$ is a complex function of activities and molecular weights, but qualitatively as solute and solvent approach equal concentrations the term should increase in magnitude. Conversely, as the solution becomes more dilute in either component, the intensity of scattering should decrease and the accuracy of the associated data become poorer.

APPARATUS AND EXPERIMENTAL METHODS

A schematic diagram of the light scattering spectrometer used in this study is given in Figure 1. The laser, detection optics and sample were mounted on an NRC vibration isolation table to prevent extraneous vibrations from contributing to the time dependence of the scattered light. The incident light beam was the 4880 Å line of a Coherent Radiation 52A argon ion laser. Two pinholes with an angular acceptance of 0.2° defined the scattering volume, and the scattering angle was determined by triangulation to better than 0.06°. Heterodyne spectroscopy was employed, using a ten centimeter path length cylindrical cell with optical quality flat windows. Stray light from imperfections and dust on the windows acted as the local oscillator source. The detector, an EMI 9634QR phototube, carried the fluctuating photocurrent to a Saicor 43A Correlator. The autocorrelation function was collected until the significant part of the function began to fill the memory — ten minutes to two hours was required, depending upon the signal to noise ratio of the photocurrent. The four hundred point autocorrelation function was then transferred in digital form from the correlator to paper tape for subsequent computer analysis.

Sample chemicals of reagent grade were used without further purification. The binary mixtures were prepared volumetrically with an estimated accuracy of 0.5%. All samples were multiply filtered through a fine fritted glass filter to

remove dust. A Bausch and Laumb refractometer was used to measure refractive indices; values have been corrected to $\lambda = 4880$ Å. The samples were maintained at room temperature, which did not drift more than 1°C during the course of an experiment. Because D_{AB} and χ exhibit a weak temperature dependence (typically less than 0.5% per degree centigrade), we estimate the maximum error due to temperature control to be less than 1%.

Current autocorrelation techniques were employed instead of swept filter spectrum analysis because correlation makes more efficient use of the signal and is able to perform signal averaging on the correlation function, thus improving the statistical accuracy of the data. In the case of heterodyne spectroscopy, the photocurrent autocorrelation function is an exact replica of the density (electric field) autocorrelation function, hence

$$C_i(\tau) = \langle i(t)i(t+\tau)\rangle \sim F(\underline{K},t) \tag{13}$$

and the decay time of the current exponential contains the coefficient of interest. The points of the correlation function were fit to a single exponential using the Marquardt nonlinear least squares algorithm. The decay time for a pure liquid

$$\tau^{-1} = \chi K^2 \tag{14}$$

and the value of K^2 determine χ. Values of τ were collected over a range of scattering angles. For the binary mixtures two exponentials are observed. Because the magnitude of concentration fluctuations in binary mixtures is generally greater than from

temperature fluctuations, and because the decay time for thermal diffusivity is smaller than from mass diffusivity by approximately two orders of magnitude, the effect of thermal diffusion can be compressed into the initial part (approximately ten points) of the correlation function; these points are neglected in the fit to determine the mass diffusivity decay time

$$\tau^{-1} = D_{AB}K^2 \tag{15}$$

τ values for D_{AB} were collected as a function of concentration for a single scattering angle.

To measure thermal diffusivities for binary mixtures, one must in general perform a two exponential fit to the data. Under the special circumstances of similar refractive indices for solute and solvent, density fluctuations become the predominant source of scattering and the data may be analyzed solely in terms of thermal diffusion. The two binary systems studied, toluene-benzene and toluene-bromobenzene, satisfy the criterion of matched refractive indices and hence have been analysed in terms of Eqs. (6) and (14).

RESULTS AND DISCUSSION

Mutual diffusion coefficient measurements appear in Table I. Thermal diffusivity results are compared in Table II with the literature bulk values. Errors quoted in Table I are based on two standard deviations of the single exponential fit plus an estimate of possible systematic errors. Errors appearing in Table II result from two standard deviations of the data to a best straight line plus possible systematic errors. Mass diffusivity values range in accuracy from 12% for dilute mixtures to better than 1% for more equimolar solutions. The accuracy of χ values in all cases is better than 10% and is typically 5%. In Figures 2-7, mutual diffusion coefficients from this study are plotted as a function of concentration with comparative literature data. Figures 8-11 exhibit values of the inverse decay time of the Rayleigh line as a function of the square of the scattering wave vector for light scattered from concentration fluctuations (Figure 8) and entropy fluctuations (Figures 9-11). Each datum represents a single correlation function. Half-widths are related to the exponential decay time τ by

$$\Gamma = (2\pi\tau)^{-1} \tag{16}$$

where Γ represents the conjugate Lorentzian half-width of the spectrum (Eqs. 7 and 9), thus the vertical axis represents both the inverse decay time of the exponential correlation function and the half-width of the corresponding Lorentzian.

As seen from these plots, the linear dependence predicted from theory by Eqs. (14) and (15) is accurately obeyed. Least squares fitting with statistical weighting has been used to determine the best straight lines.

Figures 2 through 7 show that our mutual diffusion coefficients are in excellent agreement with the bulk values reported in the literature. Two other light scattering measurements of mass diffusivities are available for comparison — both are from the system carbon disulfide-acetone. Berge et al (1970) reported $D_{AB} = 2.32 \times 10^{-5}$ cm^2/sec at room temperature for a 10% by volume acetone mixture. Aref'ev et al (1967) reported $D_{AB} = 0.30 \pm 0.04 \times 10^{-5}$ cm^2/sec for a 10% by weight acetone mixture at room temperature. In comparison our values are $2.42 \pm 0.04 \times 10^{5}$ at 20.0°C for a 10% by volume mixture and $2.23 \pm 0.06 \times 10^{-5}$ at 18.5°C for a 10% by weight acetone in carbon disulfide solution. It is concluded that Aref'ev's value is questionable.

The agreement between our values of thermal diffusivity and the values calculated from bulk measurements of λ, ρ and C_p data are satisfactory, as is evident from Table II. Included in Table II are the only other light scattering determinations of thermal diffusivity. Our value of 1.10 $\pm$ 0.02 x 10^{-3} cm^2/sec for pure carbon disulfide is the same as Berge's value of 1.1 x 10^{-3} cm^2sec (Berge et al, 1970). Berge and Dubois (1969) also reported χ = 0.655 $\pm$ 0.070 x 10^{-3} cm^2/sec for benzene, which is low compared to our experimental value of χ = 0.940 $\pm$ 0.050 x 10^{-3} cm^2/sec and the bulk value of χ = 0.963 x 10^{-3} cm^2/sec. Lastovka and Benedek (1966) reported χ = 0.879 $\pm$ 0.025 x 10^{-3} cm^2/sec for toluene, which agrees with our value of 0.849 $\pm$ 0.038 x 10^{-3} cm^2/sec.

It should be noted that where possible the quoted literature values for thermal diffusivity are taken from Touloukian, volumes 3 and 6. These volumes contain a comprehensive study of all the available data on liquid thermal conductivity and heat capacity for selected substances; the recommended reference values cited for each liquid have been used in Table II. The variation in experimentally determined thermal conductivities is of interest. Some results for the same system differ by as much as 50%, and variations of 25% are not uncommon, thus reflecting the difficulties associated

with the conventional thermal conductivity measurements. The most significant problems are (1) conduction corrections — ensuring that all of the supplied energy is used to establish the observed temperature distribution in the liquid; (2) convection — differences in temperature cause density changes which in turn establish convection currents and influence heat transfer; and (3) radiation between the surfaces enclosing the liquid. All of these effects may lead to an elevated thermal conductivity. In contrast, quasi-elastic light scattering does not require the imposition of macroscopic temperature gradients, thus convection is not a serious source of error. Clearly light scattering does not suffer from the problems of radiation and conduction associated with classical methods.

The limitations inherent to classical diffusion measurements are not so serious, although large discrepancies exist between values obtained by different investigators on the same system. Johnson and Babb (1956) discuss the different conventional techniques for determining mass diffusivities as well as their limitations and the consistency of data taken by several investigators. The most important limitation of these techniques is the requirement of a macroscopic concentration gradient. As a result, one generally obtains an integral diffusion coefficient rather than the more meaningful differential coefficient. In addition, the popular diaphragm cell technique requires calibration and is subject to bulk flows (Board and Spalding, 1966); both can contribute

to errors in the measurements of D_{AB}. Quasi-elastic light scattering needs no macroscopic concentration gradients and is not subject to calibration errors or bulk flow. Scattering arises from microscopic fluctuations in concentration, hence the measured diffusion coefficient is of a differential form. Some techniques, such as the diaphragm cell, may require days of operation for a single point, while light scattering determinations take less than an hour. The most precise conventional techniques employ interferometric methods (Dunlop et al, 1972) for continuously analyzing the changes of concentration with distance and time in a cell. Analysis of the data requires involved mathematical analysis. These measurements are limited in the same way as light scattering — they require a difference in refractive index between sample and solvent. This is the most serious limitation of the light scattering technique. Determinations of D_{AB} improve in accuracy and precision with (1) increasing refractive index differences between the binary components, as is evident from the $(\partial\varepsilon/\partial C)_{P,T}$ factor of Eqn.(8), and (2) the approach to equal concentrations, which is expressed in the $<|\delta C|>^2$ factor of the same equation.

ACKNOWLEDGEMENTS:

It is a pleasure to acknowledge helpful discussions with Dr. R. D. Mountain, Dr. A. F. Collings, H. H. Reamer and Mrs. E. Gulari.

LITERATURE CITED

Alpert, S. S., Proceedings of the Conference on Phenomena in the Neighborhood of Critical Points, N.B.S., Misc. Publ. 273 (Washington, D. C.: National Bureau of Standards, 1965).

Anderson, D. K., J. R. Hall, and A. L. Babb, J. Phys. Chem. 62, 404(1958).

Aref'ev, I. M., B. D. Kopylovskii, D. Sh. Mash, and I. L. Fabelinski, J.E.T.P. Letters 5, 355(1967).

Berge, P., P. Calmettes, M. Dubois, and C. Laj, Phys. Rev. Letters 24, 89(1970).

Board, W. J., and S. C. Spalding, AIChE Journal 12, 349(1966)

Bridgman, P. W., Proc. Am. Acad. Arts. Sci. 59, 141(1923).

Burchard, J. K. and H. L. Toor, J. Phys. Chem. 66, 2015 (1962).

Caldwell, C. S. and A. L. Babb, J. Phys. Chem. 59, 1113 (1955).

Chu, B., Ann. Rev. Phys. Chem. 21, 145(1970).

Cummins, H. Z. and H. L. Swinney, Progr. Opt. B, (1969)

Dubin, S. B., J. H. Lunacek, and G. B. Benedek, Proc. Nat. Acad. Sci. U. S. 57, 1164(1967).

Dubois, M., P. Berge and C. Laj, Chem. Phys. Letters 6, 227(1970).

Dunlop, Peter J., Barry J. Steel, and J. E. Lane, "Experi-

mental Methods for Studying Diffusion in Liquids, Gases and Solids", in Physical Methods of Chemistry Part IV: Determination of Mass, Transport and Electrical Magnetic Properties, ed. Arnold Weissberger and Bryant W. Rossiter, Techniques of Chemistry, Vol. I, 3 vols., (New York, New York: Wiley-Interscience, 1972), pp. 205-349.

Ford, N. C. and G. B. Benedek, Phys. Rev. Letters 15, 649(1965).

Johnson, P. A. and A. L. Babb, Chem. Revs. 56, 387(1956).

Kadanoff, L. P. and P. C. Martin, Ann. Phys., N. Y. 24, 419(1963).

Landau, L. D. and E. M. Lifshitz, Electrodynamics of Contimuous Media (London: Pergammon Press, 1960), p. 377.

Landau, L. D. and G. Placzek, Physik, Z. Sovijetunion 5, 172(1934).

Lastovka, J. B. and G. B. Benedek, Phys. Rev. Letters, 17, 1039(1966).

Lemonde, Ann. Phys. (Paris) 9, 399(1938).

Mandel'shtam, L. I., Zh. Russ. Fiz. Khim. Obshchestva 58, 381(1926); Collected Works, Vol. I (Izd. Akad. Nauk. SSSR, 1957).

Miller, G. A., J. Phys. Chem. 71, 2305(1967).

Miller, L. and P. C. Carman, Trans. Faraday Soc. 55, 1831(1959).

Mountain, R. D., Revs. Mod. Phys. 38, 205(1966).

Mountain, R. D. and J. M. Deutch, J. Chem. Phys. 50, 1103(1969).

Riedel. L., Chem. Ing.-Techn. 13, 321(1951).

Shaw, R., J. Chem. Eng. Data 14, 461(1969).

Touloukian, Y. S., P. E. Liley, and S. C. Saxena, Thermal Conductivity, Nonmetallic Liquids and Gases, eds. Y. S. Touloukian and C. Y. Ho, Thermophysical Properties of Matter, the TPRC Data Series, 13 vols. (New York: IFI/Plenum, 1970-), vol. 3.

Touloukian, Y. S., and T. Makita, Specific Heat, Nonmetallic Liquids and Gases, eds. Y. S. Touloukian and C. Y. Ho, Thermophysical Properties of Matter, The TPRC Data Series, 13 vols. (New York: IFI/Plenum, 1970-), vol. 6.

NOTATION

C = concentration, grams/cm^3

C_p = specific heat at constant pressure, J/°K-molecule

C_v = specific heat at constant volume, J/°K-molecule

D_{AB} = binary diffusivity, cm^2/sec

$\underline{E}_s$ = scattered electromagnetic field

$F(\underline{K},t)$ = density-density autocorrelation function

$\underline{K}$ = scattering wave vector, cm^{-1}

k_B = Bottzmann's constant, 1.38×10^{-16} erg/deg.

$\underline{k}_o$ = incident wave vector, cm^{-1}

$\underline{k}_s$ = wave vector in direction of scattering, cm

M_i = molecular weight of ith species, gm/mole

m_i = mass of ith molecular species, gm

n = refractive index

$\underline{R}$ = observation wave vector, cm

$\underline{r}$ = position wave vector, cm

T = temperature, °K

t = time, sec

Greek Letters

α = polarizability, cm^3

Γ = half-width of Rayleigh line, Hz

δ = fluctuation about the mean of a physical quantity

ε = dielectric constant

θ = scattering angle, degrees

λ = thermal conductivity, J-cm/°K-sec

λ_o = wave length of light in vacuo, Å

μ = chemical potential, cal/mole

ν = frequency, sec^{-1}

ρ = mean density, molecules/cm^{-3}

τ = exponential decay time, sec

χ = thermal diffusivity, cm^2/sec

ω = difference between incident and scattered frequency, cycles/sec

ω_o = incident frequency of laser light, cycles/sec

Table I: Mutual diffusion coefficient data

Nitromethane-Benzene	T=20.0°C
Mole fraction nitromethane	D_{AB} x10^5cm2/sec.
0.155	1.99 ± .14
0.293	1.63 ± .10
0.415	1.48 ± .07
0.525	1.27 ± .02
0.624	1.29 ± .05
0.713	1.35 ± .03
0.794	1.42 ± .04
0.869	1.50 ± .04
0.939	1.56 ± .07
N-Hexane -Benzene	T=19.9°C
Mole fraction hexane	
0.0346	2.17 ± .09
0.0704	2.08 ± .10
0.146	2.11 ± .06
0.226	2.09 ± .04
0.312	2.29 ± .06
0.405	2.38 ± .05
0.506	2.57 ± .04
0.614	2.94 ± .05
0.732	3.23 ± .10
0.860	3.96 ± .21
Acetone-Benzene	T=19.9°C
Mole fraction acetone	
0.0241	2.39 ± .17
0.0598	2.34 ± .10

Table I: Continued

0.142	2.24 ± .07
0.232	2.21 ± .04
0.363	2.39 ± .04
0.487	2.53 ± .09
0.606	2.66 ± .04
0.720	2.92 ± .05
0.829	3.11 ± .09
0.930	3.27 ± .12
Methanol-Benzene	T=20.0°C
Mole fraction methanol	
0.0429	1.91 ± .10
0.104	1.27 ± .10
0.196	0.831± .024
0.279	0.730± .009
0.354	0.729± .006
0.485	0.791± .009
0.594	0.960± .014
0.687	1.18 ± .01
0.767	1.44 ± .01
0.837	1.68 ± .02
0.898	2.00 ± .04
0.952	2.08 ± .05
0.977	2.22 ± .19
Toluene-Bromobenzene	T=19.9°C
Mole fraction toluene	
0.124	1.13 ± .13
0.372	1.46 ± .07

Table I: Continued

0.622	1.56 ± .12	
0.798	1.74 ± .09	
Methyl alcohol-Butyl alcohol	T=19.5°C	
Mole fraction methanol		
0.361	0.518 ± .042	
0.601	0.814 ± .050	
0.772	1.04 ± .07	
0.900	1.14 ± .06	
Acetone-Carbon disulfide		
10% by vol. acetone	2.42 ± .04	T=20.0°C
10% by wt. acetone	2.23 ± .06	T=18.5°C
Carbon tetrachloride - Carbon disulfide	T = 18.6°C	
Mole fraction carbon tetrachloride		
0.0650	2.92 ± .12	
0.135	2.74 ± .10	
0.294	2.44 ± .05	
0.494	2.34 ± .04	
0.714	2.25 ± .09	
0.849	2.13 ± .09	
Ethanol-Benzene	T=18.6°C	
Mole fraction ethanol		
0.0736	1.16 ± .04	
0.144	1.00 ± .07	
0.279	0.857 ± .011	
0.501	0.891 ± .009	
0.694	1.17 ± .05	
0.858	1.52 ± .06	
0.932	1.62 ± .05	

TABLE II

THERMAL DIFFUSIVITIES OF PURE LIQUIDS AND BINARY MIXTURES

$\chi \times 10^3$ (cm^2/sec)

System	This study	T(°C)	Bulk Value* at 20°C
(pure liquids)			
Acetone	0.881±0.033	18.2	0.934 (Touloukian, vols. 3 & 6)
Benzene	0.956±0.040	19.5	0.963 (ibid.)
Bromobenzene	0.518±0.025	20.0	0.749 (Riedel, 1951; Shaw, 1969)
Carbon disulfide	1.10 ±0.04	19.3	1.29 (Bridgman, 1923; Shaw, 1969)
Carbon tetrachloride	0.719±0.016	20.0	0.771 (Touloukian, vols. 3 & 6)
Ethanol†	0.839±0.046	19.8	0.889 (ibid.)
n-Hexane	0.740±0.033	20.0	0.837 (ibid.)
Methanol†	1.16 ±0.10	18.2	1.035 (ibid.)
Toluene	0.849±0.039	19.0	0.922 (ibid.)
(binary mixtures)			
Toluene-bromobenzene			
12.5% by vol. toluene	0.649±0.025	19.9	
62.5%	0.688±0.039	19.9	
Toluene-benzene			
30.0% by vol. toluene	0.869±0.040	20.0	
50.0%	0.815±0.035	20.0	
70.0%	0.772±0.030	20.0	
90.0%	0.847±0.035	20.0	

	Other light scattering determinations		Reference
Benzene	0.655±0.070	∿ 20	(Berge, 1969)
Carbon disulfide	1.1	∿ 20	(Berge, 1970)
Toluene	0.879±0.025	20.0	(Lastovka & Benedek, 1966)

* In many cases it is possible to find C_p and λ combinations that give closer agreement with our thermal diffusivities.

† Single datum points were collected for methanol and ethanol.

FIGURE CAPTIONS

Figure (1) - A schematic drawing of the light scattering spectrometer used in this study.

Figure (2) - Mutual diffusion data for the nitromethane-benzene system: △ this work, T = 20.0±.2°C; ○ Miller and Corman (1959), T = 20.0°C.

Figure (3) - Mutual diffusion data for the acetone-benzene system: △ this work, T = 19.9±.2°C; ○ Anderson et al (1958), T = 25.15°C.

Figure (4) - Mutual diffusion data for the n-hexane-benzene system: △ this work, T = 19.9±.2°C; ○ Lemonde (1938), T = 5°C.

Figure (5) - Mutual diffusion data for the methanol-benzene system: △ this work, T = 20.0±.2°C; +, Caldwell and Babb (1955), T = 27.06°C, T = 11.0°C; ○ Lemonde (1938), T = 11°C.

Figure (6) - Mutual diffusion data for the ethanol - benzene system: △ this work, T = 18.6±.2°C; ⊗ Anderson et al (1958), T = 25.15°C; ○ Lemonde (1938), T = 15°C.

Figure (7) - Mutual diffusion data for the systems toluene-bromobenzene and methanol-butanol.
Toluene-bromobenzene: △ this work, T = 19.9±.2°C;
▲ Burchard and Toor (1962), T = 29.6±.03°C.
Methanol-butanol: □ this work, T = 19.5±.2°C.

Figure (8) - The inverse decay time $(2\pi\tau)^{-1}$ vs. K^2 due to concentration fluctuation in a 10% (vol.) acetone-carbon disulfide mixture. $(2\pi\tau)^{-1}$ for the exponential correlation function corresponds to the Lorentzian half-width Γ (in Hz) of the spectrum.

Figure (9) - Inverse decay time vs. K^2 for pure carbon disulfide.

Figure (10) - Inverse decay time vs. K^2 for pure carbon tetrachloride.

Figure (11) - Inverse decay time vs. K^2 from entropy fluctuations in a toluene-benzene mixture.

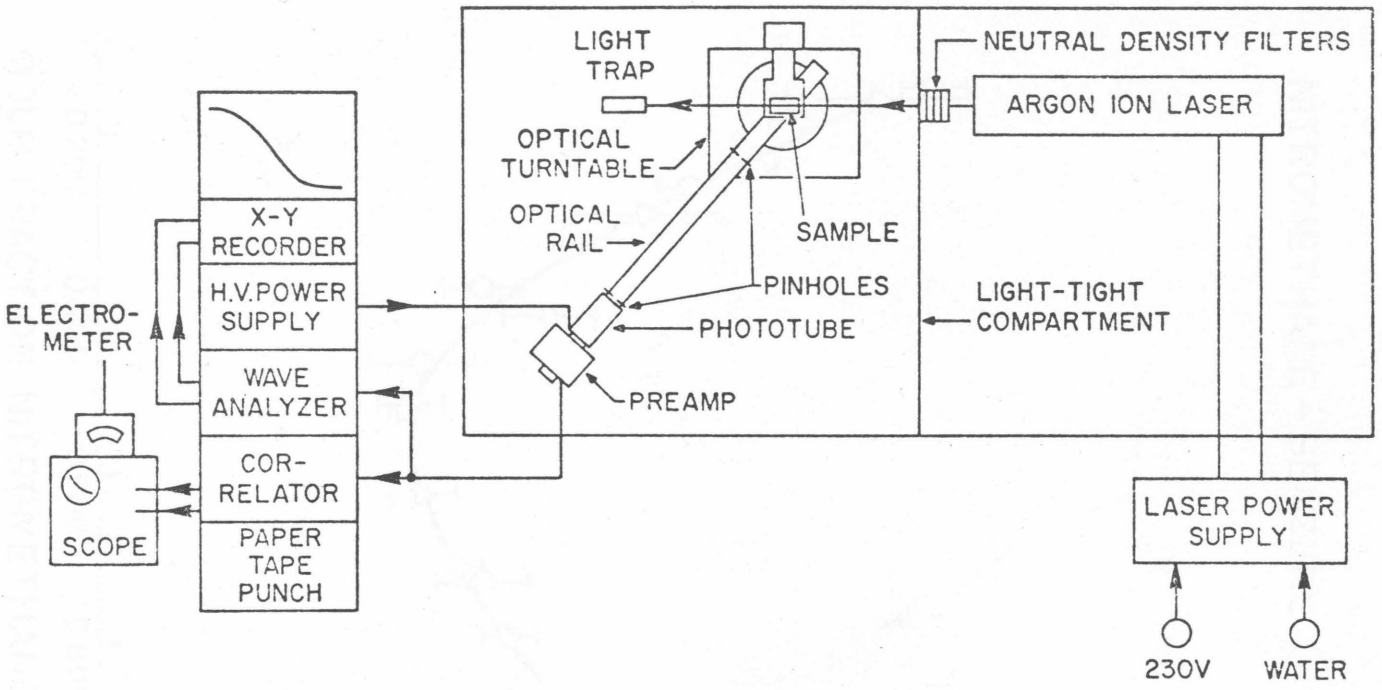
LIGHT TRAP
NEUTRAL DENSITY FILTERS
ARGON ION LASER
OPTICAL TURNTABLE
OPTICAL RAIL
SAMPLE
PINHOLES
PHOTOTUBE
PREAMP
LIGHT-TIGHT COMPARTMENT
X-Y RECORDER
H.V.POWER SUPPLY
WAVE ANALYZER
COR-RELATOR
PAPER TAPE PUNCH
ELECTRO-METER
SCOPE
LASER POWER SUPPLY
230V
WATER

Figure 1.

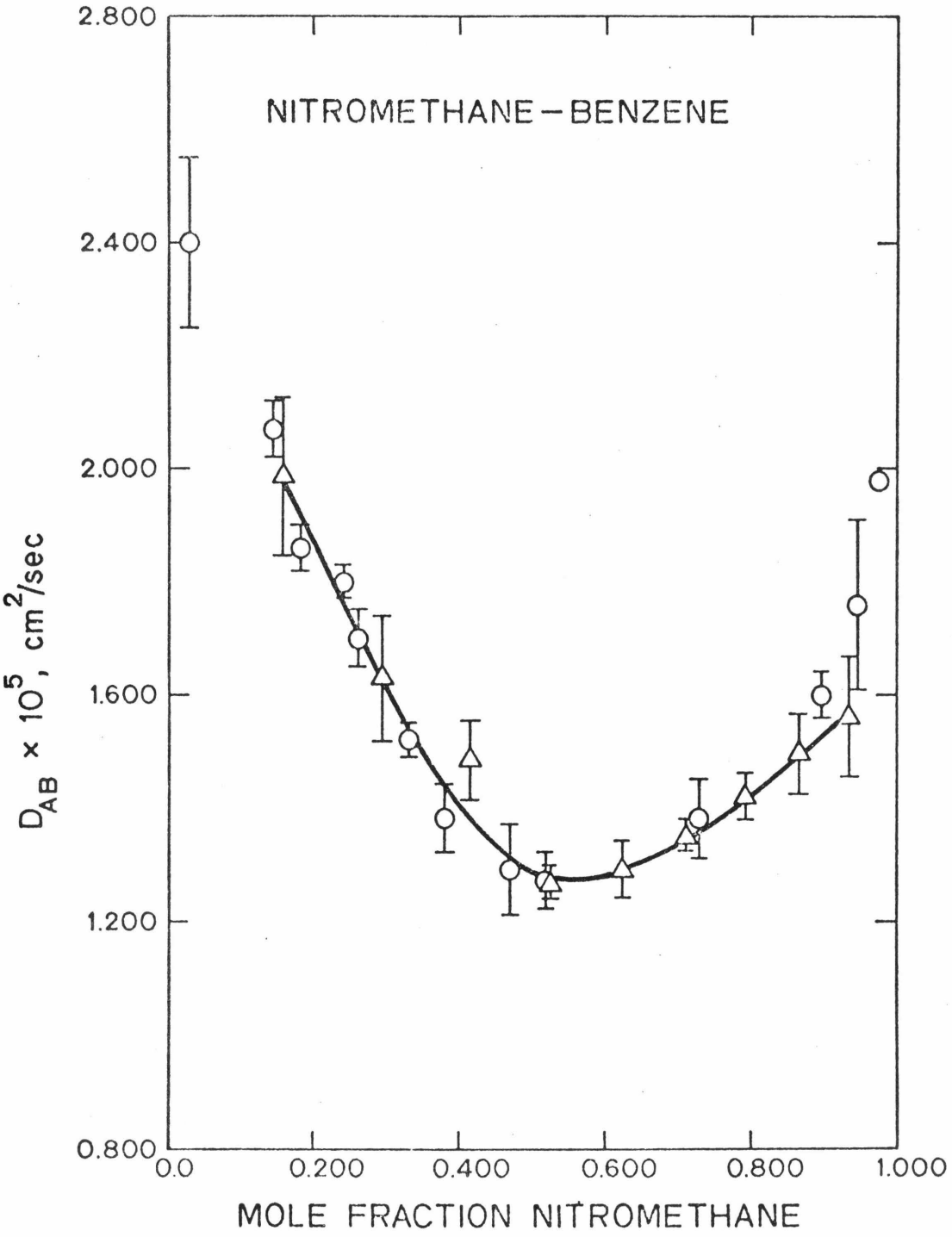
NITROMETHANE – BENZENE
2.800
2.400
2.000
1.600
1.200
0.800
$D_{AB} \times 10^5$, cm^2/sec
0.0
0.200
0.400
0.600
0.800
1.000
MOLE FRACTION NITROMETHANE

Figure 2.

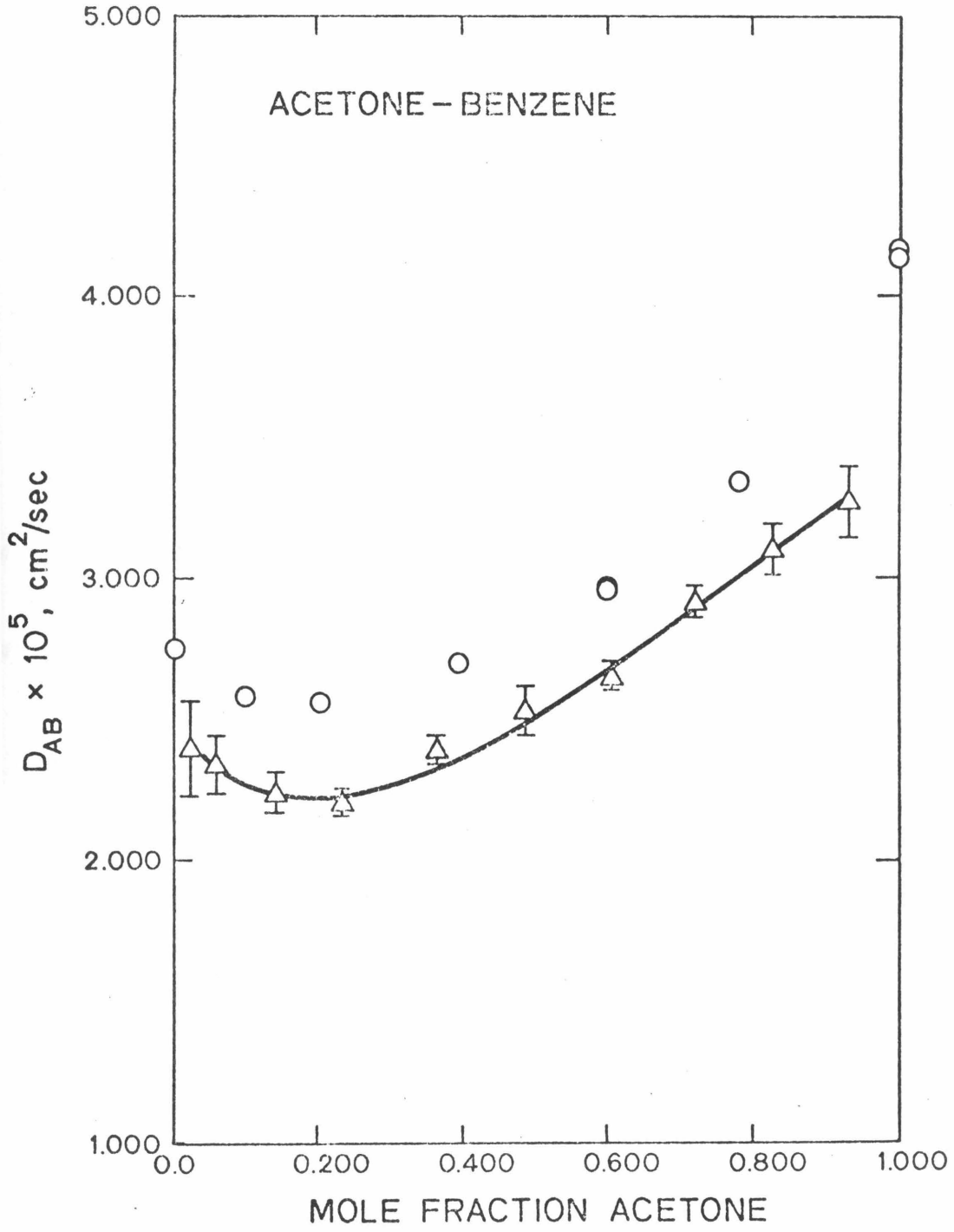
ACETONE – BENZENE
5.000
4.000
3.000
2.000
1.000
$D_{AB} \times 10^5$, cm^2/sec
0.0
0.200
0.400
0.600
0.800
1.000
MOLE FRACTION ACETONE

Figure 3.

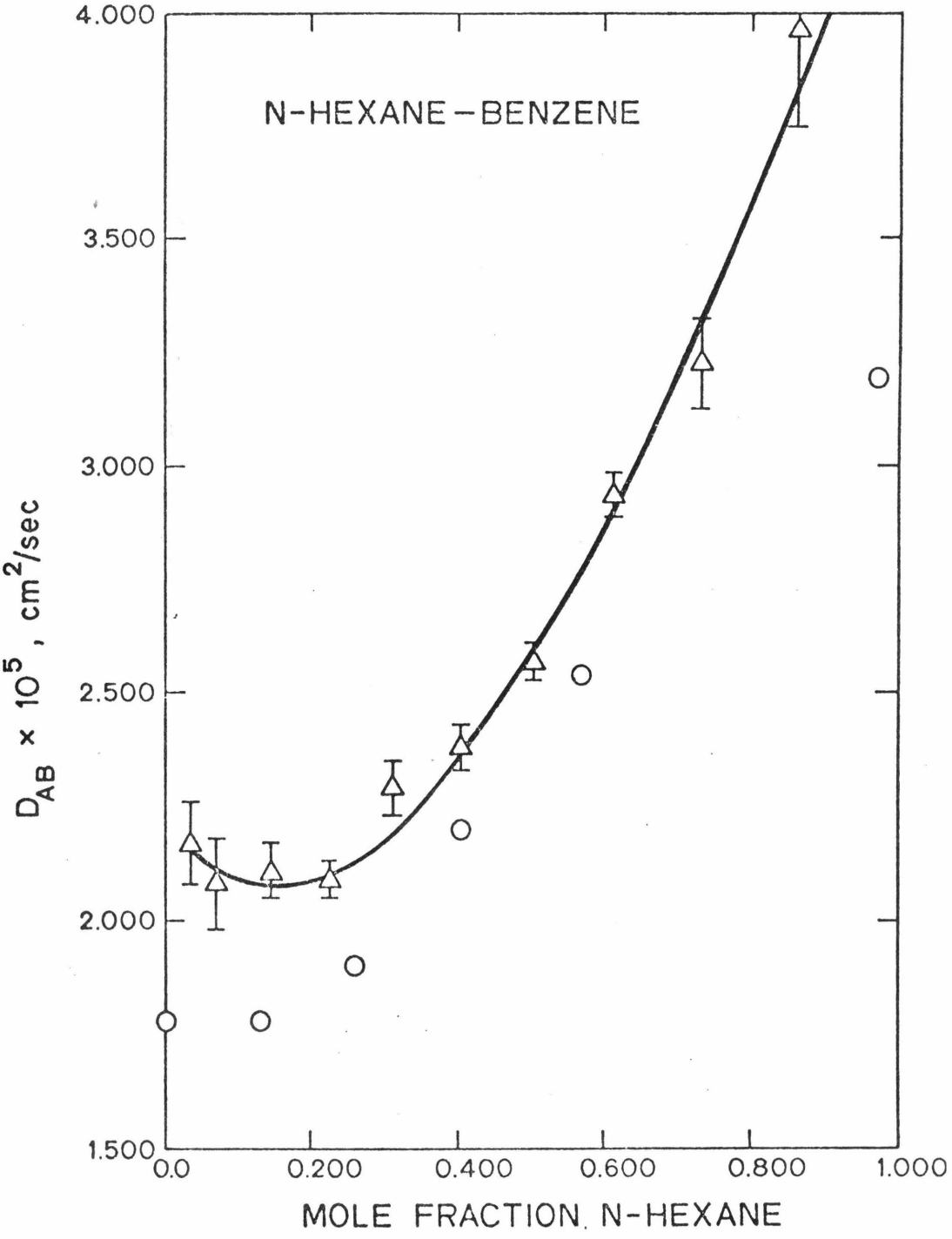
N-HEXANE – BENZENE
4.000
3.500
3.000
2.500
2.000
1.500
$D_{AB} \times 10^5$, cm^2/sec
0.0
0.200
0.400
0.600
0.800
1.000
MOLE FRACTION, N-HEXANE

Fifure 4.

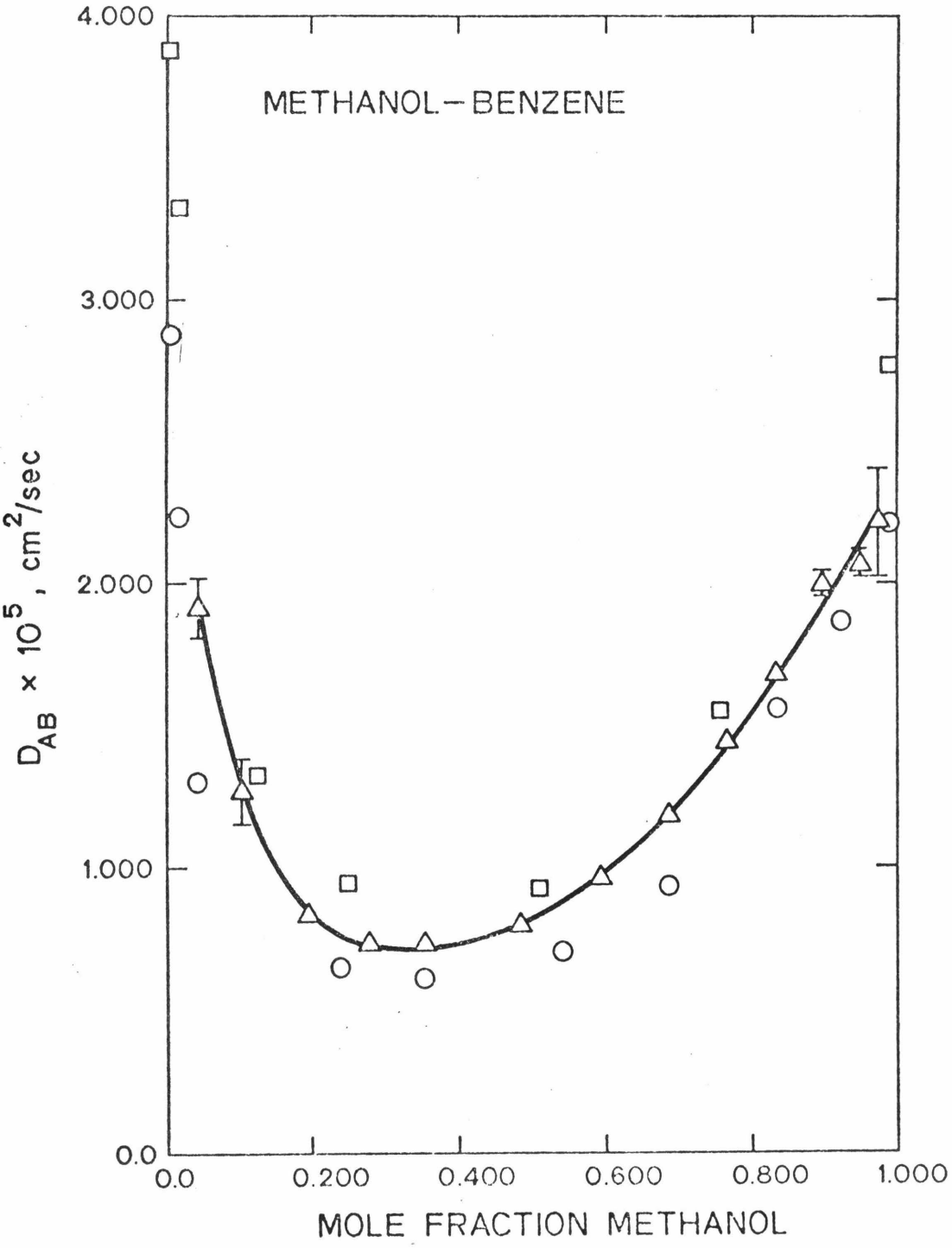
METHANOL–BENZENE
4.000
3.000
2.000
1.000
0.0
$D_{AB} \times 10^5$, cm^2/sec
0.0
0.200
0.400
0.600
0.800
1.000
MOLE FRACTION METHANOL

Figure 5.

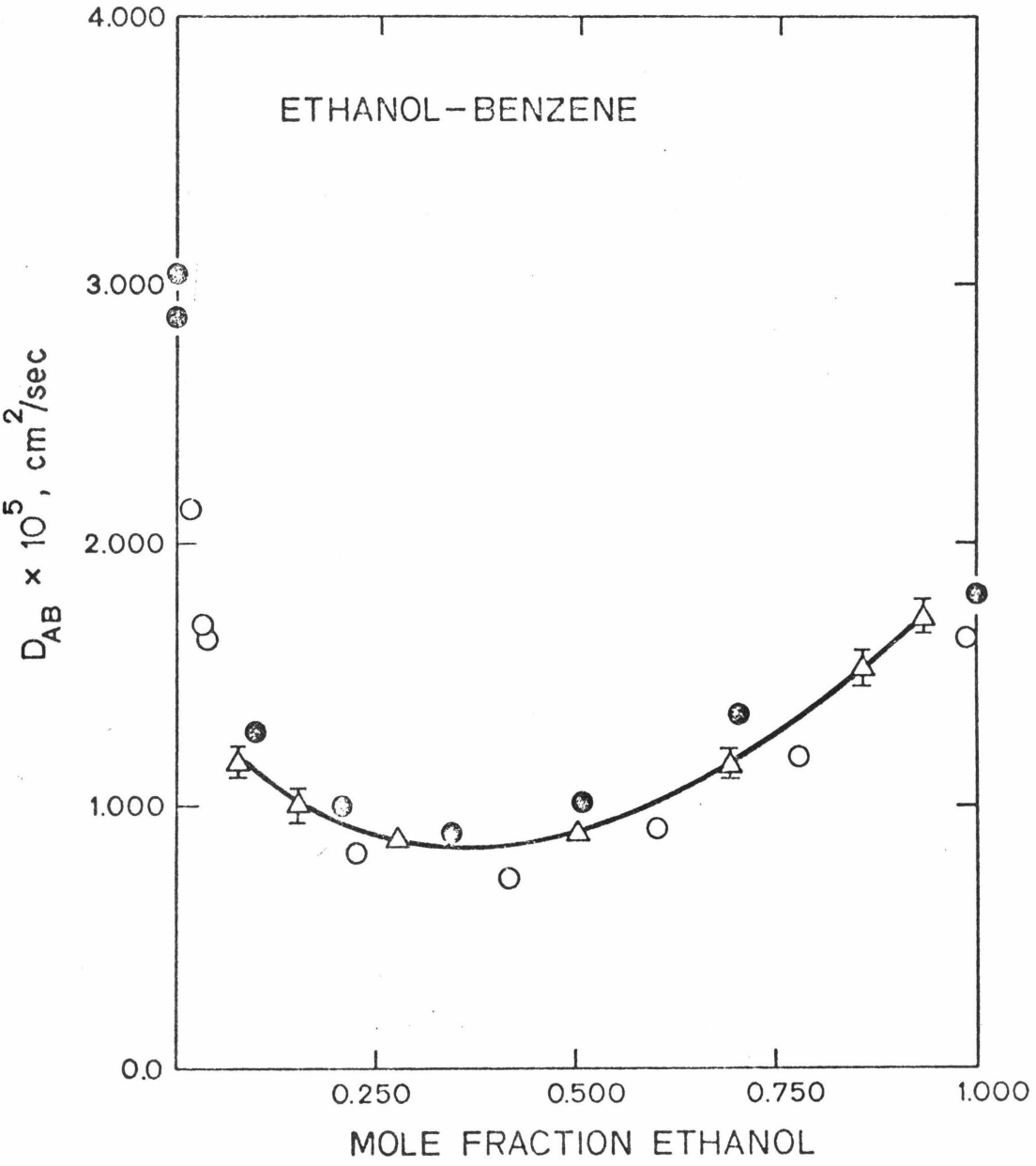
ETHANOL–BENZENE
4.000
3.000
2.000
1.000
0.0
$D_{AB} \times 10^5$, cm^2/sec
0.250
0.500
0.750
1.000
MOLE FRACTION ETHANOL

Figure 6.

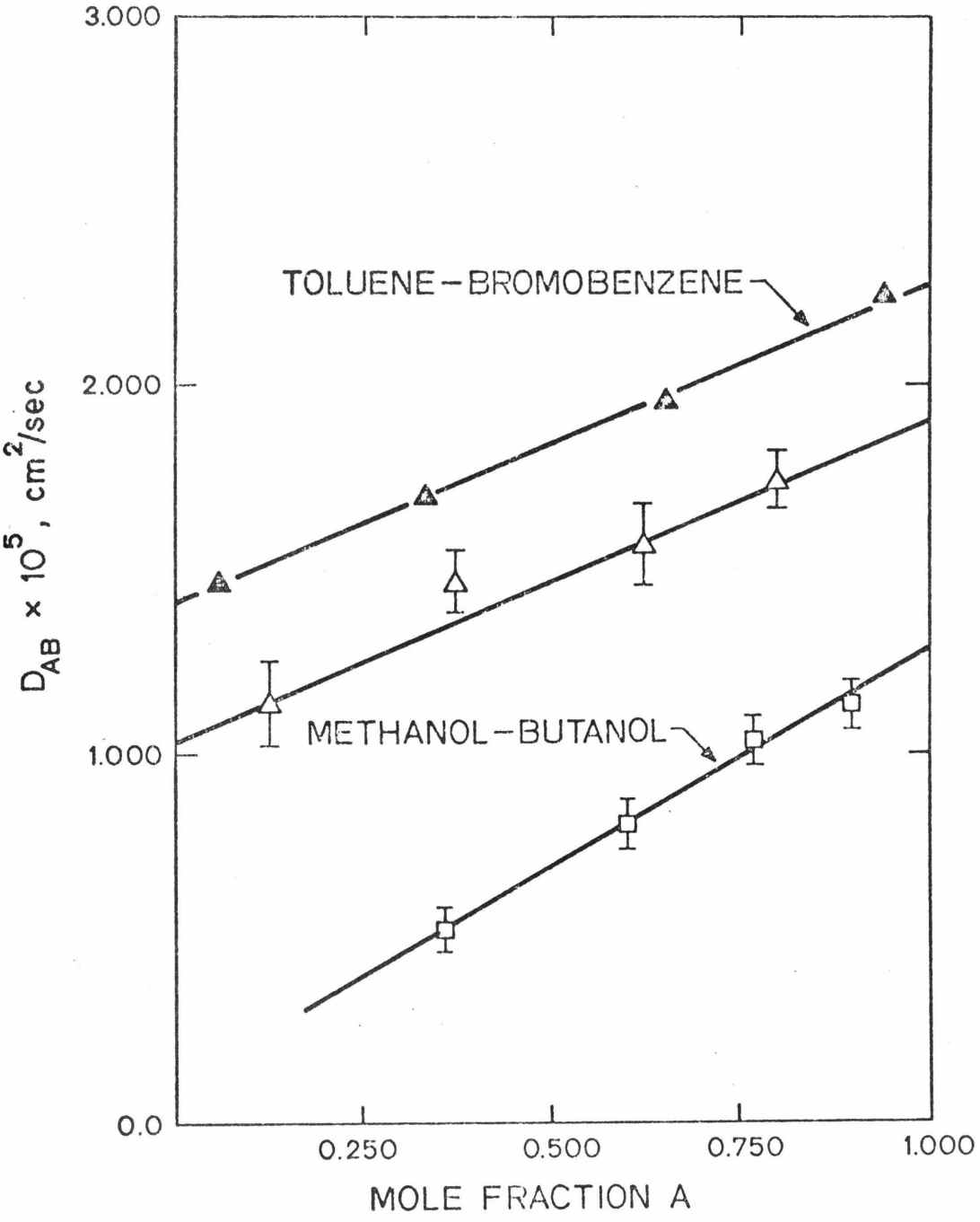
3.000
2.000
1.000
0.0
$D_{AB} \times 10^5$, cm^2/sec
TOLUENE–BROMOBENZENE
METHANOL–BUTANOL
0.250
0.500
0.750
1.000
MOLE FRACTION A

Figure 7.

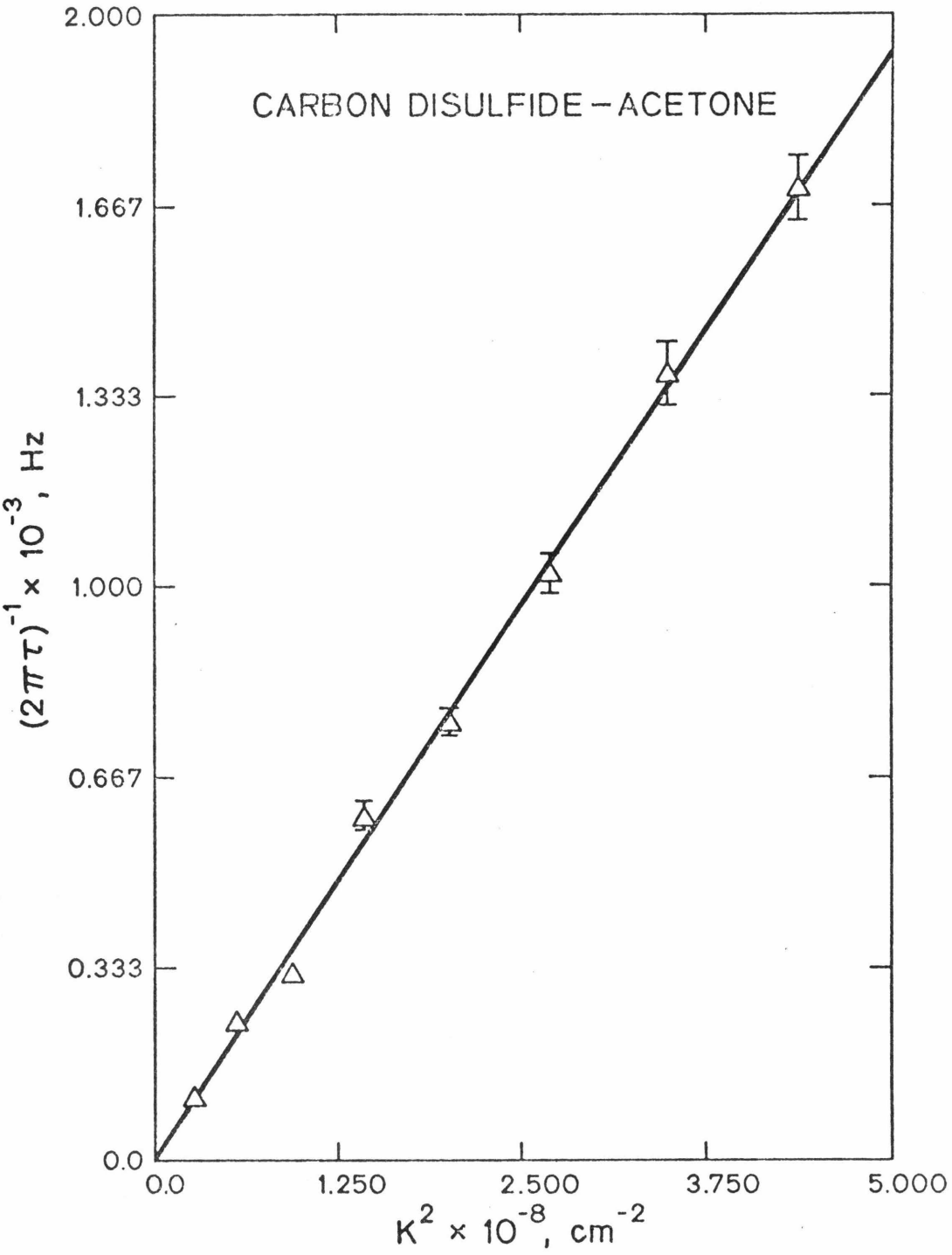
CARBON DISULFIDE – ACETONE
2.000
1.667
1.333
1.000
0.667
0.333
0.0
$(2\pi\tau)^{-1} \times 10^{-3}$, Hz
0.0
1.250
2.500
3.750
5.000
$K^2 \times 10^{-8}$, cm^{-2}

Figure 8.

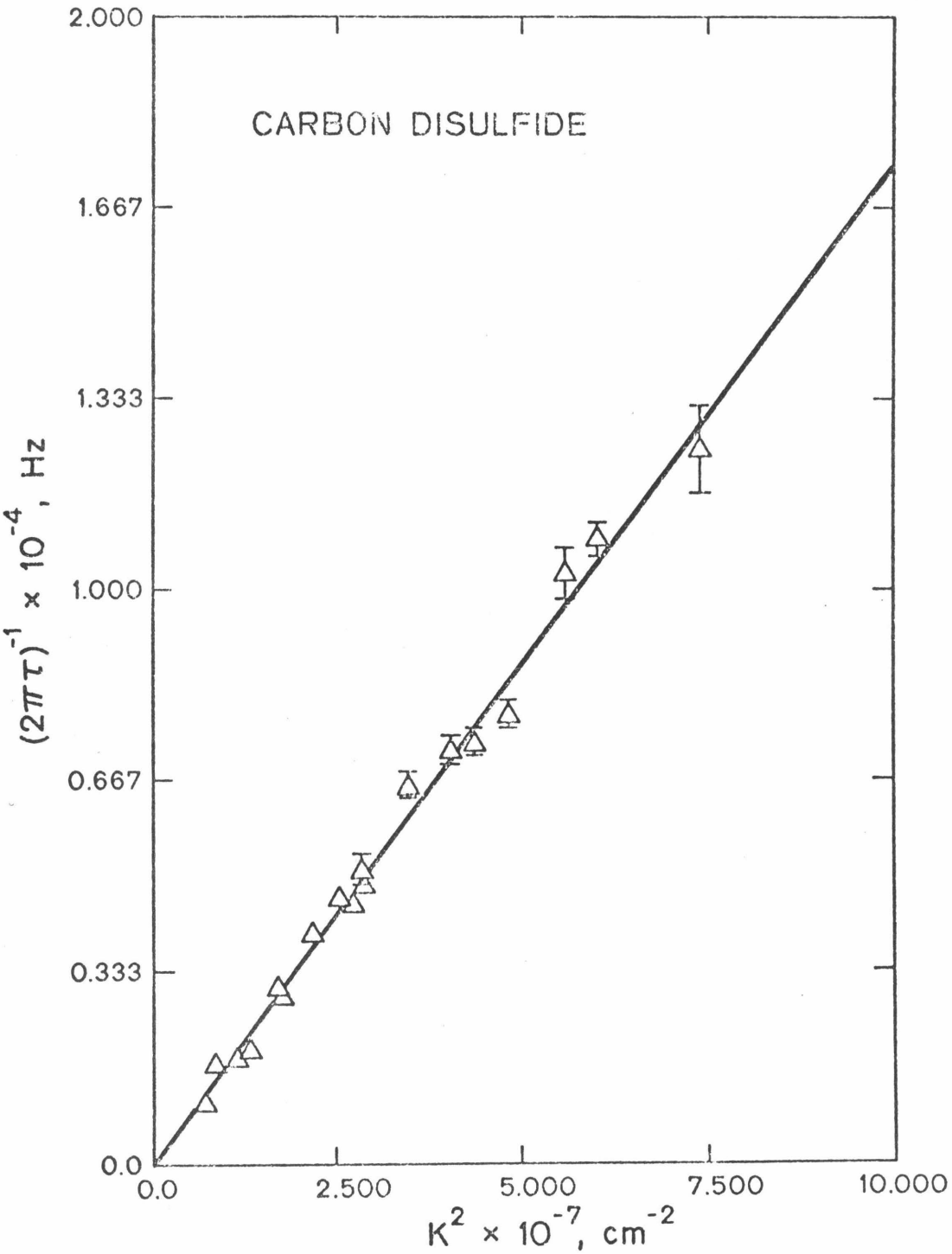
CARBON DISULFIDE
2.000
1.667
1.333
1.000
0.667
0.333
0.0
$(2\pi\tau)^{-1} \times 10^{-4}$, Hz
0.0
2.500
5.000
7.500
10.000
$K^2 \times 10^{-7}$, cm^{-2}

Figure 9.

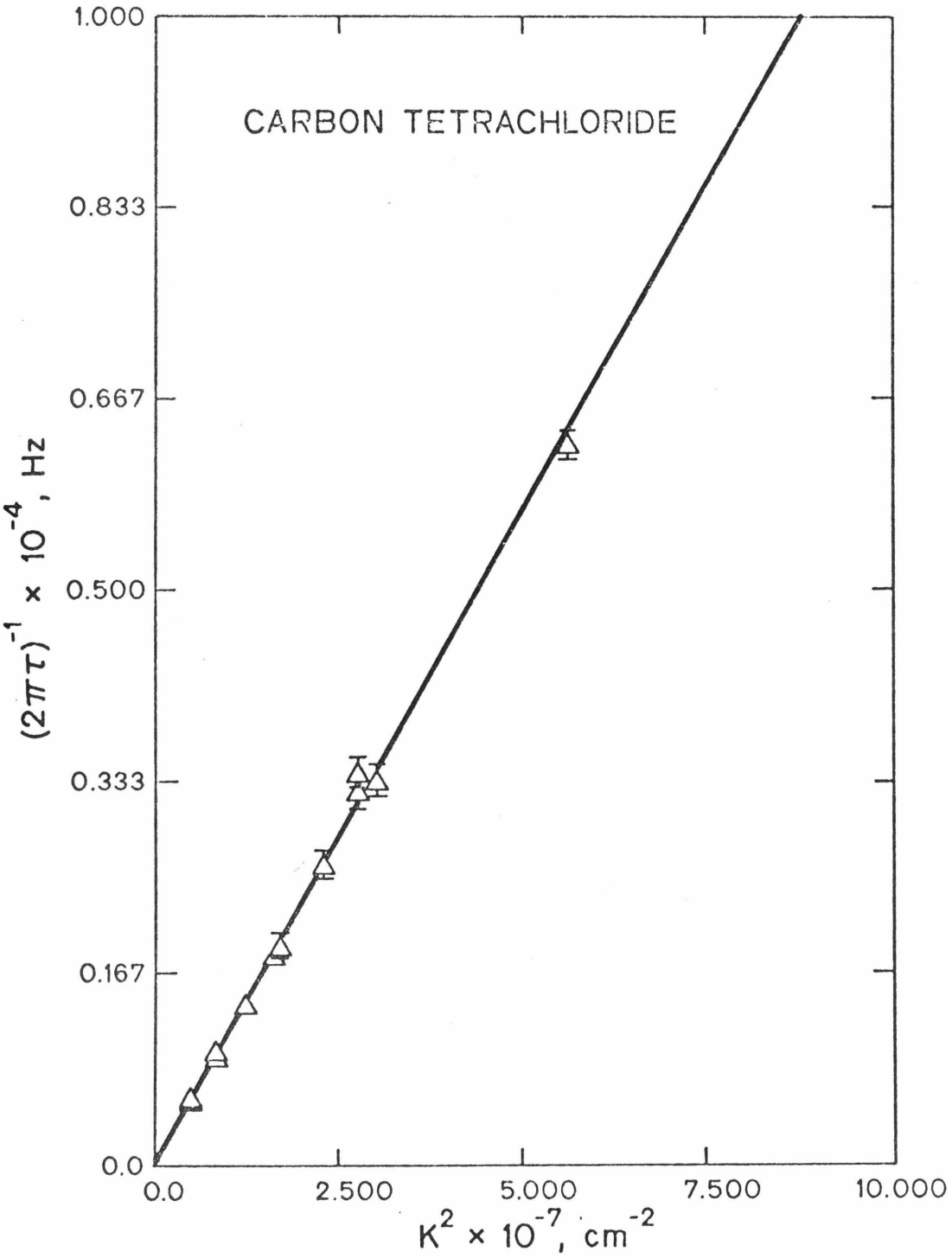
CARBON TETRACHLORIDE
1.000
0.833
0.667
0.500
0.333
0.167
0.0
$(2\pi\tau)^{-1} \times 10^{-4}$, Hz
0.0
2.500
5.000
7.500
10.000
$K^2 \times 10^{-7}$, cm^{-2}

Figure 10.

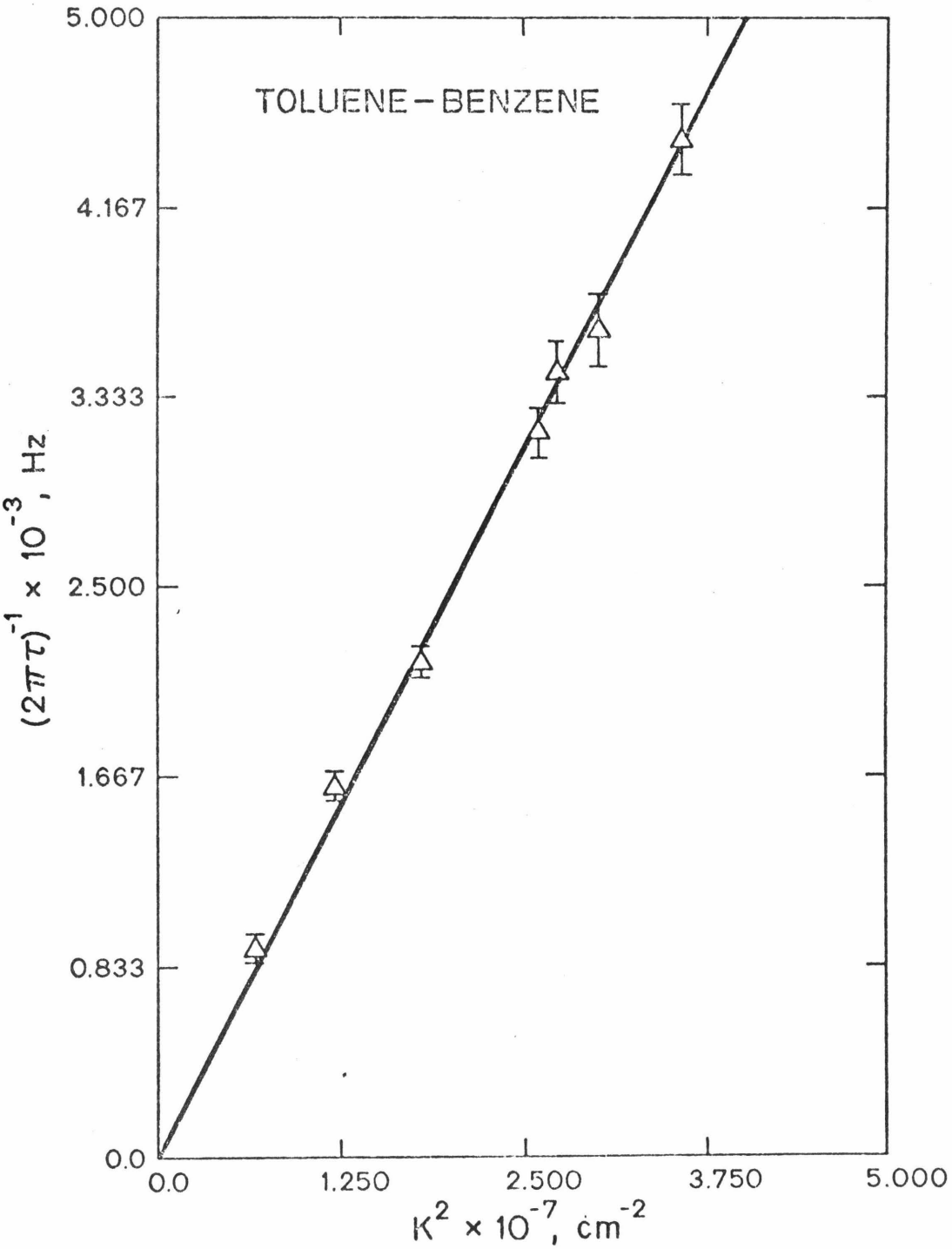
TOLUENE – BENZENE
5.000
4.167
3.333
2.500
1.667
0.833
0.0
$(2\pi\tau)^{-1} \times 10^{-3}$, Hz
0.0
1.250
2.500
3.750
5.000
$K^2 \times 10^{-7}$, cm^{-2}

Figure 11.

V

A LIGHT SCATTERING STUDY OF CRITICAL PHENOMENA IN ETHANE

Erdoğan Güları and C. J. Pings

(Preliminary draft for publication, complete with figures and references. For data not given in the draft see Tables XXVII to XXXIV.)

ABSTRACT

Extensive turbidity and linewidth measurements, in the temperature range $0.0005°C \leq \Delta T \leq 10.6°C$, have been made on the critical isochore of ethane. The results are:

$$K_T = 1.24\pm0.11\times10^{-3}(\varepsilon)^{-1.225\pm0.02}\ \text{atm}^{-1}$$

$$\xi = 1.64\pm0.20\times10^{-8}(\varepsilon)^{-0.644\pm0.02}\ \text{cm}$$

$$\bar{\eta} = 0.06\pm0.04$$

$$\lambda_T^x = 5.4\pm0.3\times10^{-6}(\varepsilon)^{-0.605\pm0.02}\ \text{cal sec}^{-1}\ \text{cm}^{-1}\ °\text{C}^{-1}$$

$$T_c = 32.19\pm0.01°C$$

$$\rho_c = 0.2044\pm0.0006\ \text{gr/cm}^3$$

where $\varepsilon = (\Delta T/T_c)$, and λ_T^x is the excess thermal conductivity. Our result for the isothermal compressibility and the excess thermal conductivity are in good agreement with independently made classical measurements.

By comparing the singular part of the linewidths with the Kawasaki linewidth expression containing no adjustable parameters we find that apart from the non-local viscosity correction correlation function modification and vertex corrections are needed to bring the theory into good agreement with data for all $k\xi$.

INTRODUCTION

First measurements of isothermal compressibility by light scattering near the critical point of a fluid were reported by Blosser and Drickamer[1], and the first measurements of Rayleigh linewidths were made by Alpert and coworkers[2] and by Ford and Benedek[3]. Since then there has been a great deal of both theoretical and experimental studies of critical phenomena based on using light scattering techniques.

In this paper we present extensive turbidity and linewidth measurements near the critical point of ethane and analyze the data in the light of some recent theoretical developments.

BRIEF THEORY

Turbidity τ is defined by

$$\tau = (1/L)\ \ln(I_o/I) \qquad (1)$$

where L is the path length in the fluid, I_o is the incident intensity and I is the transmitted intensity. According to Ornstein-Zernike theory, the intensity of light scattered, per unit length, volume and incoming intensity, by a fluid near its critical point is:

$$I(k) = AK_T \sin^2\phi/(1+k^2\xi^2) \qquad (2)$$

where A is given by $A = (\pi^2/\lambda^4)(\rho\partial\varepsilon'/\partial\rho)_T^2 BT$ with B the

Boltzmann constant, ε' the dielectric constant of the fluid, k the change in the wave vector of the scattered light, λ the wavelength of the incident light and ξ the correlation length. Integration[4] of Eq. (2) over all angles yields the following expression for the turbidity:

$$\tau = A\pi K_T[(2\alpha^2+2\alpha+1)/\alpha^3]\ln(1+2\alpha) - 2(1+\alpha)/\alpha^2 \qquad (3)$$

where $\alpha=2(k_o\xi)^2$ and k_o is the wave vector of the incident light. In the limit of small α Eq. (3) reduces to:

$$\tau = (8/3)\pi AK_T \ . \qquad (4)$$

In the hydrodynamic region ($k\xi<<1$), the Landau-Placzek theory based on linearized hydrodynamic equations predicts that the Rayleigh line will be Lorentzian in shape with a half width given by:

$$\Gamma = \chi k^2 \qquad (5)$$

where $\chi=\lambda_T/\rho C_p$ is the thermal diffusivity.

Using mode-mode coupling theory Kawasaki[5] has obtained the following expression for the singular part of the linewidth valid for all $k\xi$,

$$\Gamma = \frac{BTk^3}{8\pi\eta^*}\left[x + x^3 + (1-x^4)\tan^{-1}\left(\frac{1}{x}\right)\right] \qquad (6)$$

with η^* being the high frequency limit of shear viscosity and x is $1/k\xi$. For $k\xi<<1$ Eq. (6) reduces to Eq. (5) with $\chi=BT/6\pi\eta^*$. In the critical region, $k\xi>>1$, the linewidth

is given by $\Gamma=BT/16\eta^*$. The definition of the high frequency viscosity η^* had been ambiguous, but recently Kawasaki and Lo[6] removed this ambiguity by relating it to the experimentally measured shear viscosity,

$$\eta^* = \eta(k=0,T)/f(k\xi) \quad . \tag{7}$$

The function $f(k\xi)$ is given numerically if Ref. (6). For the case of binary mixtures Lo and Kawasaki[7] have obtained further numerical corrections to Eq. (6) taking care of the simplest vertex correction. Finally it has been suggested that Eq. (6) should be further modified to take into account deviations from the Ornstein-Zernike correlation function form[8,9].

EXPERIMENT

a. Materials

Ethane containing a nominal maximum impurity level of 50 ppm was obtained from Cryogenic Service Corporation of Glendale, California. A mass spectrometer analysis done by an independent laboratory was supplied with the sample cylinder. It showed 5 ppm methane, 5 ppm ethylene and 15 ppm propane. Two gas chromatograph analyses and one mass spectrometer analysis were done by us. The GC analysis of ethane, which was further purified by freezing and pumping to a high vacuum, showed $\sim$1-2 ppm methane, $\sim$1-2 ppm ethylene and no higher hydrocarbons. A second

GC analysis done on the ethane in the main cylinder showed 6-8 ppm methane, 5 ppm ethylene with no higher hydrocarbons. The mass spectrometer analysis done on the same sample showed no oxygen and water. It was not possible to detect nitrogen in any of the above analyses due to the fact that GC is not sensitive enough to detect parts per million amounts, and all the nitrogen peaks in the mass spectrum overlap with ethane peaks. We estimated the amount of nitrogen by freezing the ethane with liquid nitrogen and measuring the residual pressure. This procedure yielded an estimate of about 20 ppm.

b. Spectrometer

Our laser light scattering spectrometer has been described in detail elsewhere[10]. We have used a 400 point Saicor Sai-43A correlator to determine the autocorrelation function of the photocurrent.

c. Temperature Control and Measurement

The main features of our temperature control and measuring system were the same as those described in Ref. (11). However, several important improvements have been made. The temperature of the water bath was controlled to better than ±0.001°C with a Leeds and Northrup, L & N, series 60 controller and an L & N microvolt amplifier. The temperature of the light tight box containing the optics and the sample was controlled to better

than ±0.03°C and was kept at a temprature very close to the T_c of the ethane sample by a similar set up. The laboratory temperature was also kept as constant as possible and it never varied by more than 0.2°C during a measurement. In this way it was possible to control the temperature of the sample to ±0.0005°C. Platinum resistance thermometers were used for measuring and control. The resolution of the measuring circuit was 0.0003°C. The critical temperature was also measured with an NBS calibrated thermometer.

d. Density Measurements

Due to the scatter in the reported values of the critical parameters for ethane we determined our own critical density rather than relying on literature data. The volume of the scattering cell was carefully calibrated with distilled water, and the density was determined by weighing the cell before and after loading it with ethane. The weight of ethane in the cell could be determined with a precision of 0.05%. It was found that for densities slightly above or below the critical density the position of the meniscus changed by several millimeters if the temperature was lowered by 0.001° C below the phase separation temperature. The critical density was taken to be the density for which the position of the

meniscus did not change. This strict criteria required density changes as small as 0.01%. The accuracy of the critical density is believed to be about 0.3%.

e. Turbidity Measurements

Turbidity measurements were made by placing the phototube at zero degrees. Several different pinhole and lens combinations were used over a time period of six months and all the measurements were reproducible within the experimental error. The current from the EMI 9634QR phototube was measured by Keithley 602 Electrometer combined with a Hewlett Packard 7004A XY-recorder. The precision was better than 0.5%. The laser was stabilized by a feedback control circuit; the output never drifted by more than 1% during the course of a run.

Two cells were used in making the turbidity measurements. One was a double pass cell with a path length of 12 cm used for $0.1°C \leq \Delta T \leq 11°C$. The other cell was a piece of precision bore pyrex tubing having a path length of 0.889 cm. This cell was used for $\Delta T < 3°C$. To take care of gravity effects, if any, the beam height was adjusted to the meniscus height and as a further check measurements as a function of height were made at ΔT = 10 millidegrees. I_o was determined by a combination of measuring the intensity at large temperature distances from the critical and by measuring the transmitted

intensity without the sample and correcting for the different amounts of reflections at the interfaces.

f. Intensity Measurements

We have made intensity measurements at several angles with the aim of determining $I(0)^{-1}$ and thus extending the range of our isothermal compressibility determinations. Since we did not make extensive intensity measurements we did not have enough data to determine the correlation lengths from the intensity measurements accurately.

g. Linewidth Measurements

Our linewidth measurements cover the temperature range of $0.0008°C \leq \Delta T \leq 7.509°C$. The angular range examined was $1.50 \leq \theta \leq 110$. For large values of ΔT heterodyne detection at small angles was used. Our measurements at large angles were severely limited due to very large linewidths measured $\Gamma \simeq 50$ kHz. Thus if we went to higher scattering angles we could not get enough data points in the autocorrelation function to have high statistical accuracy.

Approximately half of our linewidths measured were taken by holding ΔT constant and changing the scattering angle. The other half was taken by holding the scattering angle constant while varying the ΔT. To detect gravitational effects almost all of our measurements below

ΔT = 0.020°C were taken as a function of height.

RESULTS AND DISCUSSION

We have determined the critical density of ethane to be ρ_c= 0.2044±0.0006 gr/cm^3. For the critical temperature we have obtained two values, T_c= 32.200°C for the sample which was further purified by freezing and pumping, and T_c= 32.182°C for the sample loaded directly by gas phase transfer from the main cylinder and used without further purification. While the sample that was further purified probably had much less methane and nitrogen, it came into contact with more valves and tubing and was loaded at close to the critical state conditions, thus it is not very clear what caused the difference in the critical temperatures. The "real T_c" probably is between the two. Based on the above two determinations our best estimate of the critical temperature is T_c= 32.19±0.01°C. Table I summarizes the best literature values together with our values of ρ_c and T_c.

a. Results of Turbidity Measurements

All of our 103 measurements are shown in Fig. 1. Using Eq. (4) absolute isothermal compressibilities were calculated from the turbidity data for $\Delta T \geq 0.5$°C. The term $(\rho\partial\varepsilon'/\partial\rho)_T^2$ was evaluated using the Lorentz-Lorenz law

and n = 1.119. This value of the refractive index was obtained from the measurements of J. Hadrich and coworkers [12] after a very small correction for wavelength dependence. We have also calculated the compressibilities from $I(0)^{-1}$ values determined from intensity measurements, these were converted to absolute values by matching them with those calculated from turbidity data at $\Delta T = 3.0°C$.

Fitting our isothermal compressibility data with the equation,

$$K_T = K_T^o(\Delta T/T_c)^{-\gamma} \qquad (9)$$

yields $K_T^o = 1.24\pm0.11\times10^{-3}$ atm^{-1} and $\gamma = 1.225\pm0.02$. The error limits quoted in this paper are what we believe to be realistic estimates of the errors rather than standard deviations obtained from least square fits. In making the least squares fit, K_T values below $\Delta T = 0.05°C$ were not used for possible effects of multiple scattering and those below $\Delta T = 1.0°C$ determined from turbidity measurements were not used for possible very small deviations from Eq. (4). Including these points do not change the quoted values of the parameters.

For comparison we have differentiated the PVT data of Sage et al [13] and Beattie [14] et al to obtain the isothermal compressibilities. Table II gives the K_T values determined in this way along with those calculated

using Eq. (9) with the parameters given above. As can be seen the agreement is very good. Blosser and Drickamer[1] have reported K_T values determined by light scattering, but their ΔT values are not stated making a comparison impossible. Beattie et al[14] also have three isotherms below $\Delta T=0.1°C$, but all of our attempts at obtaining meaningful K_T values from these failed. Due to the extreme flatness, the reported PVT data is not smooth and accurate enough for differentiation. All of our K_T data is shown in Fig. 2 along with those determined from literature PVT data.

Using Eqs. (3) and (9) we have calculated the long range correlation lengths as a function of ΔT from the turbidity data for $\Delta T<1.0°C$. A weighted linear least squares fit to

$$\xi = \xi_o(\Delta T/T_c)^{-\nu} \tag{10}$$

yields $\xi_o = 1.64\pm0.20$ Å and $\nu = 0.644\pm0.02$. The data above $\Delta T = 0.01°$ was weighted more than those below for several reasons: Below 0.01°C the correlation lengths become comparable to the wavelength of light, thus Eq. (3) may not be exact[15]. Multiple scattering may yield lower values of τ. Especially around $T=0.001°C$, small gravity effects that we could not detect may be present and the relative uncertainties in ΔT values are much higher, as a

result the error limits on the calculated correlation lengths can be as large as 50%. We feel that probably the first two reasons are mostly responsible for the small systematic deviations seen in Fig. 3 showing the correlation length data. Equal weighting of all the points change ν to 0.660.

We have also gained some insight into the process of thermal equilibration of the sample by monitoring the photocurrent as a function of time when a change in temperature was made. Fig. 4 shows a typical trace of photocurrent versus time. If we assume that the photocurrent reaches steady state when the sample reaches thermal equilibrium, then from Fig. 4 we can conclude that our sample reaches thermal equilibrium within ten minutes after a change of temperature. This can be compared to the reported value of several days by Puglielli and Ford[4] for SF_6 at a comparable state. The short thermal equilibrium is perhaps due to the good thermal contact achieved in our apparatus and the small volume of our cell, approximately 2 cm^3.

b. Results of Linewidth Measurements

From our meaurements in the hydrodynamic regime and in the nonlocal hydrodynamic regime, $k\xi \ll 1$ and $k\xi \leq 1$, we have determined the values of total thermal diffusivity as a function of ΔT using $\chi = \lim_{k^2 \to 0} \{\Gamma/[1+\frac{3}{5}k^2\xi^2]\}$.

These are shown in Fig. 5. As can be seen there are deviations from a linear behavior both at large and small ΔT values.

It was suggested by Sengers[16] that the normal part of the thermal conductivity should be subtracted off before making any comparisons with the theorethical predictions about the singular part. Using this idea it has been shown that Eq. (6) applies only to the singular part of the linewidth[8,17,18]. Taking the thermal conductivity as the sum of a singular part, λ_T^x, and a normal part, λ_T^n, which would have been the observed thermal conductivity in the absence of critical phenomena, we have for the linewidth,

$$\Gamma(k) = [\lambda_T^n/\rho C_p(k)]k^2 + \Gamma^s(k)[C_p^s(k)/C_p(k)] \quad (11)$$

where $\Gamma^s(k)$ $[\lambda_T^x(k)/\rho C_p^s(k)]k^2$ is the singular part of the linewidth predicted by the Kawasaki expression in Eq. (6).

In this study we have assumed $C_p^s = C_p - C_p(\rho=0,T)$. Also assuming[8,17] the Ornstein-Zernike k dependence for both $C_p^s(k)$ and $C_p(k)$ gives:

$$\Gamma(k) = [\lambda_T^n/(\rho C_p)][1+k^2\xi^2]k^2 + \Gamma^s(k)(C_p^s/C_p) \quad (12)$$

where $C_p = C_p(k=0)$ and λ_T^n are the thermodynamically measured quantities. The normal part of the thermal conductivity was evaluated from:

$$\lambda_T^n(\rho,T) = \lambda_T(0,T) + \tilde{\lambda}_T(\rho) \qquad (13)$$

From the data given in Vol. III of Thermophysical Properties of Matter[19] we obtained

$$\lambda_T(0,T) = 4.36\times10^{-5} + 3.13\times10^{-7}T(°C) \text{ cal sec}^{-1}\text{cm}^{-1}\text{°C}^{-1}.$$

This is in excellent agreement with

$$\lambda_T(0,T) = 4.40\times10^{-5} + 3.19\times10^{-7}T$$

determined from the data of Carmichael et al[20].
$\tilde{\lambda}_T(\rho_c)$ was evaluated from a plot of residual thermal conductivity given in Ref. (20) to be

$$\tilde{\lambda}_T(\rho_c) = 4.92\times10^{-5} \text{ cal sec}^{-1} \text{ cm}^{-1} \text{ °C}^{-1}.$$

We estimate the uncertainty in $\tilde{\lambda}_T$ to be ±6%.

The heat capacity at constant pressure was calculated from the thermodynamic relationship

$$\rho C_p = \rho C_v + T(\partial P/\partial T)_\rho^2 K_T \ . \qquad (14)$$

We evaluated the term $(\partial P/\partial T)_\rho$ by using the data of Sage et al[2] to get $(\partial P/\partial T)_\rho = 1.05\pm2\%$ atm/°C. For the isothermal compressibility we have used our own measurements and the heat capacity at zero density was taken to be $C_p = 0.43$ cal/gr-°C from Ref. (21). C_v was assumed to have a logarithmic temperature dependence and the data of Sage et al[2] was used to obtain $C_v = 0.67-0.06 \ln(\Delta T)$ cal/gr-°C. For the temperature range of our measurements the ratio C_p^s/C_p change from 0.92 to 1.00.

Using Eq. (14) with the quoted parameters we have

calculated the following C_p values:

$$T = 330°K \qquad C_p = 49.4 \text{ cal/mole-°K}$$

$$T = 340°K \qquad C_p = 37.5 \text{ cal/mole-°K}.$$

These can be compared with the tabulated values by Din[22], C_p values closest to the critical point we could find:

$$T = 330°K \qquad C_p = 48.5 \text{ cal/mole-°K}$$

$$T = 340°K \qquad C_p = 39.8 \text{ cal/mole-°K} \quad .$$

The agreement is very good considering the fact that we are extrapolating far beyond the range of the data used in calculating the parameters given above.

Using the expressions given for C_p and λ_T^n, the excess thermal conductivity λ_T^x was calculated from the total thermal diffusivity. A least squares fit of our data to the asymptotic power law $\lambda_T^x = \lambda_{To}^x (\Delta T/T_c)^{-\psi}$ yields $\lambda_{To}^x = 5.4 \pm 0.3 \times 10^{-6}$ cal $sec^{-1} cm^{-1} °C^{-1}$ and $\psi = 0.605 \pm 0.02$. In the least squares fitting only the data points above $\Delta T = 0.01°C$ were used. Including the points with smaller ΔT does not change the values of the parameters. Lenoir and coworkers[23] have measured the thermal conductivity of ethane for $T \simeq 9°C$ and got

$$\lambda_T = 1.73 \times 10^{-4} \text{ cal } sec^{-1} \text{ } cm^{-1} \text{ } °C^{-1},$$

and our analysis of their data gives

$$\lambda_T^x = 5.1 \times 10^{-5} \text{ cal } sec^{-1} \text{ } cm^{-1} \text{ } °C^{-1}.$$

These can be compared with our determinations at $T = 7.509°C$

$$\lambda_T = 1.62\times10^{-4} \text{ cal sec}^{-1} \text{ cm}^{-1} \text{ °C}^{-1}$$
$$\lambda_T^x = 5.6\times10^{-5} \text{ cal sec}^{-1} \text{ cm}^{-1} \text{ °C}^{-1}.$$

We would like to point out that Lenoir and coworkers did not make their measurements with the purpose of determining the thermal conductivity near the critical point. They report having a temperature gradient possibly as large as 6°C for a mean ΔT of about 9°C. Thus the comparison is only semi-quantitative in nature. All the excess thermal conductivity data is shown in Fig. 6. There are no systematic deviations from a linear behavior compared to Fig. 5.

For shear viscosity we have used tha data of Strumpf and Pings[24] taken on an isochore with $\rho = 0.2095$ gr/cm^3, after correcting the residual viscosity to the critical density. Zero density viscosity was taken from Carmichael et al[25]. Writing the viscosity as the sum of the normal viscosity and the excess viscosity, we have

$$\eta = \eta^n + \Delta\eta$$

with $\eta^n = \eta(\rho=0,T) + \tilde{\eta}(\rho_c) = 191.3+84.3(\Delta T/T_c)$ micropoises and $\Delta\eta$[24] $= -6.580 \ln(\Delta T/T_c) - 32.52$ micropoises.

Using the viscosity data along with our correlation length data, we have compared the singular part of our linewidths with Eq. (6) including the nonlocal viscosity correction in the range $0.0026 \leq k\xi \leq 10$. As can be seen in Fig. 6, the data fall below the theorethical prediction

by as much as 30% for $k\xi<0.01$. The deviation falls off to 10% around $k\xi=0.01$. Between $k\xi=0.01$ and $k\xi=0.5$, the predicted linewidth is systematically higher than the experimental data. Around $k\xi=1$ there is good agreement and for $k\xi>1$ the data are higher than the theory by 4-5%.

Fig. 7 can be compared with Fig. 8 where the normal part of the thermal conductivity was decreased by 3% and the coefficient of isothermal compressibility was increased by 5%; both changes are well within the limits of the uncertainties associated with these parameters. The agreement between the theory and the experiment is very good for $k\xi<1$ in Fig. 8 but the data are again higher than the theory by 4-5% for $k\xi>1$.

We have also tried the linewidth expression with a modified Ornstein-Zernike correlation function form. From our determinations of γ and ν, we get $\bar{\eta} = 0.06\pm0.04$. Using this value of $\bar{\eta}$ in the modified linewidth expression given by Chang et al[26], the result shown in Fig. 9 was obtained. In Fig. 9 the agreement between the theory and the experiment has improved considerably for $k\xi>1$, but the systematic deviations for $k\xi\leq0.5$ have increased.

Recently Lo and Kawasaki[7] have calculated the simplest vertex correction to the linewidth expression. Their results for a binary mixture are: -2.44% for $k\xi<<1$ and 0.40% for $k\xi>>1$. Since these results were specifically

obtained for binary mixtures, we did not use them in our analysis. If the vertex corrections for pure fluids are in the same direction, they will definitely improve the already good agreement between the theory and the experiment. Clearly the vertex corrections together with the correlation function correction will give very good agreement for all $k\xi$. For $k\xi>1$ we have tried evaluating the exponent z in the expression $\Gamma = Ck^z$. A typical result is $z = 2.96\pm0.06$ at $\Delta T = 0.006°C$.

Finally we would like to point out that closer to the critical point it is possible that the excess viscosity may not have the logarithmic temperature dependence determined from data taken for $\Delta T \geq 0.017°C$. Thus the behavior of the experimental data may change slightly for $k\xi>1$.

ACKNOWLEDGEMENTS

It is a pleasure to acknowledge helpful discussions with H. H. Reamer and the help of G. Griffith and the Chemical Engineering Shop in constructing the pressure cells used in this work. We are grateful to D. Powers for his help in the Gas Chromatograph analyses.

REFERENCES

1. L. G. Blosser and H. G. Drickamer, J. Chem. Phys. 19, 1244 (1951).

2. S. S. Alpert, Y. Yeh, and E. Lipworth, Phys. Rev. Lett. 14, 486 (1965).

3. N. C. Ford and G. B. Benedek, Phys. Rev. Lett. 14, 649 (1965).

4. V. G. Puglielli, and N. C. Ford, Phys. Rev. Lett. 25, 143 (1970).

5. K. Kawasaki, Phys. Lett. 30A, 325 (1969); Ann. Phys. 61, 1 (1970); Phys. Rev. A1, 1750 (1970).

6. K. Kawasaki and S. M. Lo, Phys. Rev. Lett. 29, 48 (1972).

7. S. M. Lo and K. Kawasaki, Phys. Rev. A5,421 (1972).

8. H. L. Swinney, D. L. Henry, and H. Z. Cummins, J. Phys. Supplement 33, 81 (1972).

9. B. Chu, S. P. Lee, and W. Tscharnuter, Phys. Rev. A7, 353 (1973).

10. Erdogan Gulari, R. J. Brown, and C. J. Pings to be published.

11. Erdogan Gulari, A. F. Collings, R. L. Schmidt, and C. J. Pings, J. Chem. Phys. 56, 6169 (1972).

12. J. Hadrich, F. W. Seeman, and P. Sliwinski, Z. Physikalische Chemie Neue Folge Bd. 70, 62 (1970).

13. B. H. Sage, D. C. Webster, and W. N. Lacey, Industrial and Engineering Chemistry 29, 658 (1937); H. H. Reamer,

R. H. Olds, B. H. Sage, and W. N. Lacey, ibid 36, 956 (1944).

14. J. A. Beattie, G. J. Su, and G. L. Simard, J. Amer. Chem. Soc. 61, 924 (1939).

15. S. Y. Larsen, R. D. Mountain, and R. Zwanzig, J. Chem. Phys. 42, 2187 (1965).

16. J. V. Sengers and P. H. Keyes, Phys. Rev. Lett. 26, 70 (1971).

17. T. K. Lim and H. L. Swinney, Phys. Rev. Lett. 27, 1776 (1971).

18. R. F. Chang, P. H. Keyes, J. V. Sengers, and C. O. Alley, Phys. Rev. Lett. 27,1706 (1971).

19. Thermophysical Properties of Matter, (TPM), V.3, Y. S. Toulukian main ed., Plenum Press (1970).

20. L. T. Carmichael, Virginia Berry, and B. H. Sage, J. Chem. and Eng. Data 8, 281 (1963).

21. TPM volume 6.

22. Thermodynamic Functions of Gasses, F. Din, Butterworths, London (1961).

23. J. M. Lenoir, W. A. Junk, and E. W. Comings, Chem. Eng. Prog. 49, 539 (1953).

24. H. J. Strumpf and C. J. Pings to be published.

25. L. T. Carmichael and B. H. Sage, J.Chem. and Eng. Data 8, 94 (1963).

26. R.F.Chang, P. H. Keyes, J. V. Sengers, and C.O.Alley, B.der B.G.fur Physik.Chemie, 76, 260 (1972).

TABLE I

Critical Temperature and Density of Ethane

Source	T_c(°C, '48)	ρ_c(gr/cm^3)
This study	32.19±0.01	0.2044±0.0006
Miniovich and Sorina[a]	32.20	0.2043±0.0007
Khazanova and Sominskaya[b]	32.19	0.2039±0.0007
Schmidt and Thomas[c]	32.18	-
Harrison, Moore and Douslin[d]	32.19	0.2066
Beattie, Su and Simard[14]	32.27	0.2033±0.002
Strumpf, Collings and Pings[24]	32.23	0.2055±0.002

a. V. M. Miniovich and G. A. Sorina, Russ. J. Phys. Chem. 45, 306(1971)

b. N. E. Khazanova and E. E. Sominskaya, ibid. 45, 88(1971)

c. E. Schmidt and W. Thomas, Forsch. Gebiete Ingenieurw. 20B, 161(1954)

d. R. H. Harrison, R. T. Moore and D. R. Douslin, Oral presentation 71st national meeting of the American Institute of Chemical Engineers.

TABLE II

Comparison of K_T Values Obtained by Differentiating the Literature PVT Data with Those Calculated from

$$K_T = 1.24\times10^{-3}(\Delta T/T_c)^{-1.225}\ atm^{-1}.$$

Source of PVT Data	$K_T(atm^{-1})$	$[K_T]_{calc.}(atm^{-1})$	T(°C)
Sage et al, Ref. (13)	0.393	0.391	2.98
Ref. (13)	0.181	0.170	5.58
Ref. (13)	0.169	0.170	5.58
Ref. (13)	0.0856	0.0725	11.1
Beattie et al, Ref. (14)	0.0478	0.0403	17.8
Ref. (13)	0.0184	0.0157	38.9

Figure Captions:

Fig. 1. Plot of Log(τ) vs. Log(ΔT), ■ data 12.85 cm path length cell, ○ data 0.889 cm path length cell, τ in cm^{-1} and ΔT in °C.

Fig. 2. Plot of Log(K_T) vs. Log(ΔT) on the critical isochore of ethane. □ this study from intensity measurements, ○ this study from turbidity measurements, ▲ from PVT data of Ref. (13), ♦ from PVT data of Ref. (14), the solid line is given by $K_T = 1.24(\Delta T/T_c)^{-1.225} \times 10^{-3}$ atm^{-1}.

Fig. 3. Plot of Log(ξ) vs. Log(ΔT), □ from turbidity measurements, ● from intensity measurements and solid line is given by $\xi = 1.64(\Delta T/T_c)^{-0.644}$ Å.

Fig. 4. Plot of phototube current vs. time.

Fig. 5. Plot of Log(χ) vs. Log(ΔT).

Fig. 6. Plot of Log(λ_T^x) vs. Log(ΔT), the solid line is is given by $\lambda_T^x = 5.4 \times 10^{-6}(\Delta T/T_c)^{-0.605}$ cal sec^{-1} cm^{-1} $°C^{-1}$.

Fig. 7. Plot of Log($6\pi\eta\Gamma^s/BTk^3$) vs. Log($k\xi$), the solid line represents $f(k\xi) \times$ Eq. (6), where $f(k\xi)$ is the nonlocal viscosity correction.

Fig. 8. Plot of Log($6\pi\eta\Gamma^s/BTk^3$) vs. Log($k\xi$), the solid line represents $f(k\xi) \times$ Eq. (6).

Fig. 9. Plot of Log($6\pi\eta\Gamma^s/BTk^3$) vs. Log($k\xi$), the solid line represents $f(k\xi) \times$ Eq. (6) ×Correlation function modification, obtained as described in the text.

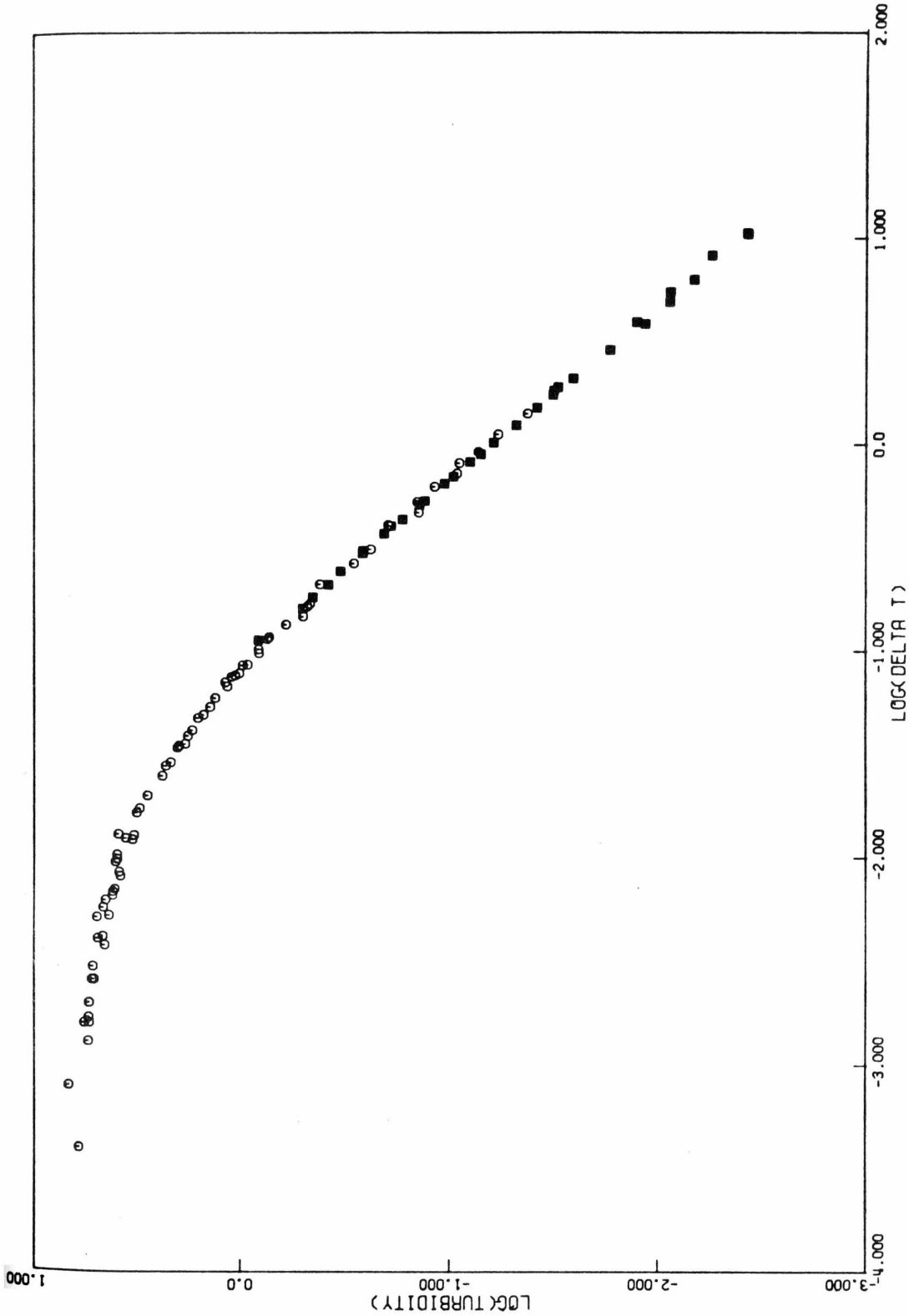
LOG(TURBIDITY)
1.000
0.0
-1.000
-2.000
-3.000
-4.000
2.000
1.000
0.0
-1.000
-2.000
-3.000
LOG(DELTA T)

Figure 1.

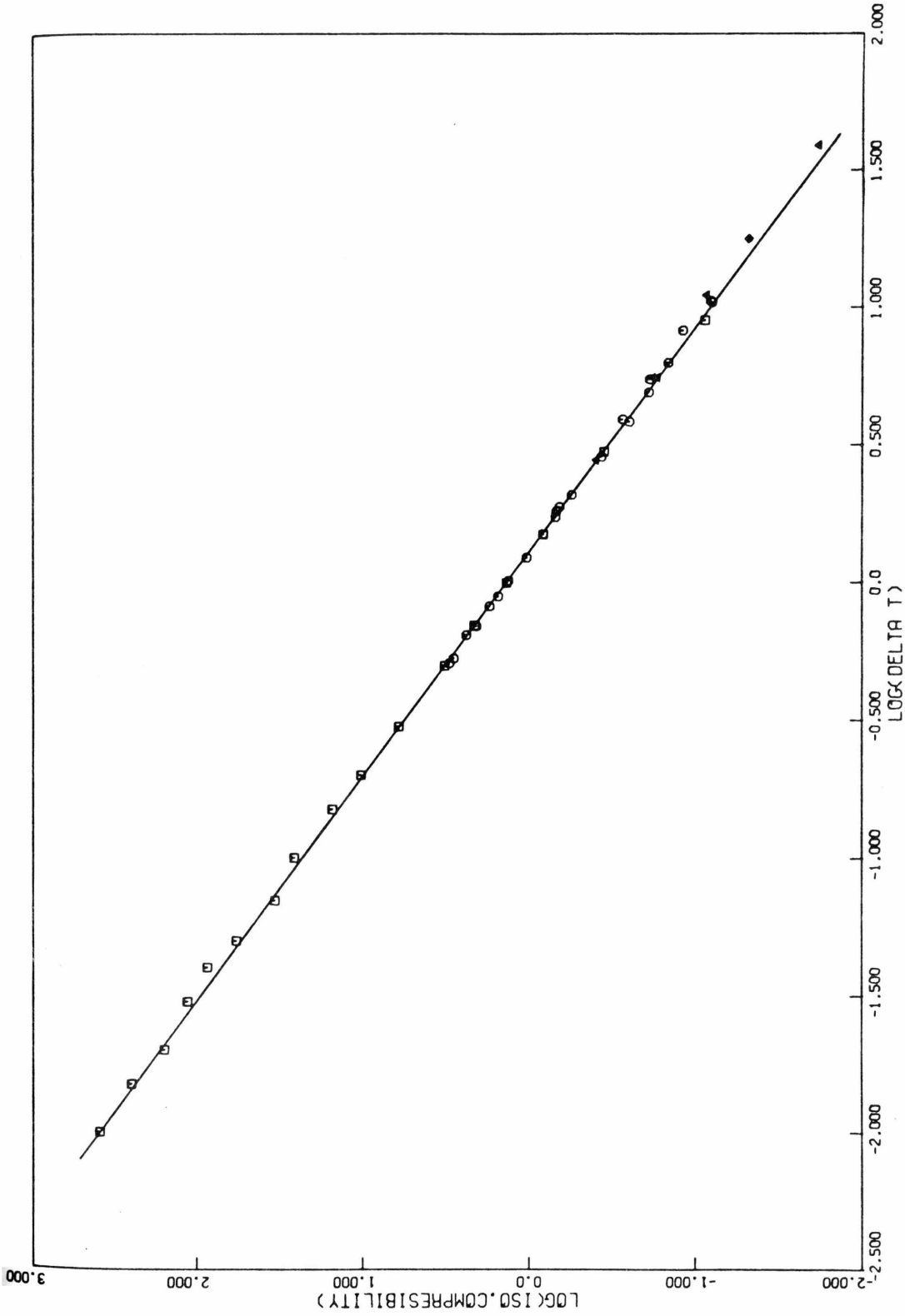
LOG(ISO.COMPRESIBILITY)
3.000
2.000
1.000
0.0
-1.000
-2.000
-2.500
LOG(DELTA T)
2.000
1.500
1.000
0.500
0.0
-0.500
-1.000
-1.500
-2.000

Figure 2.

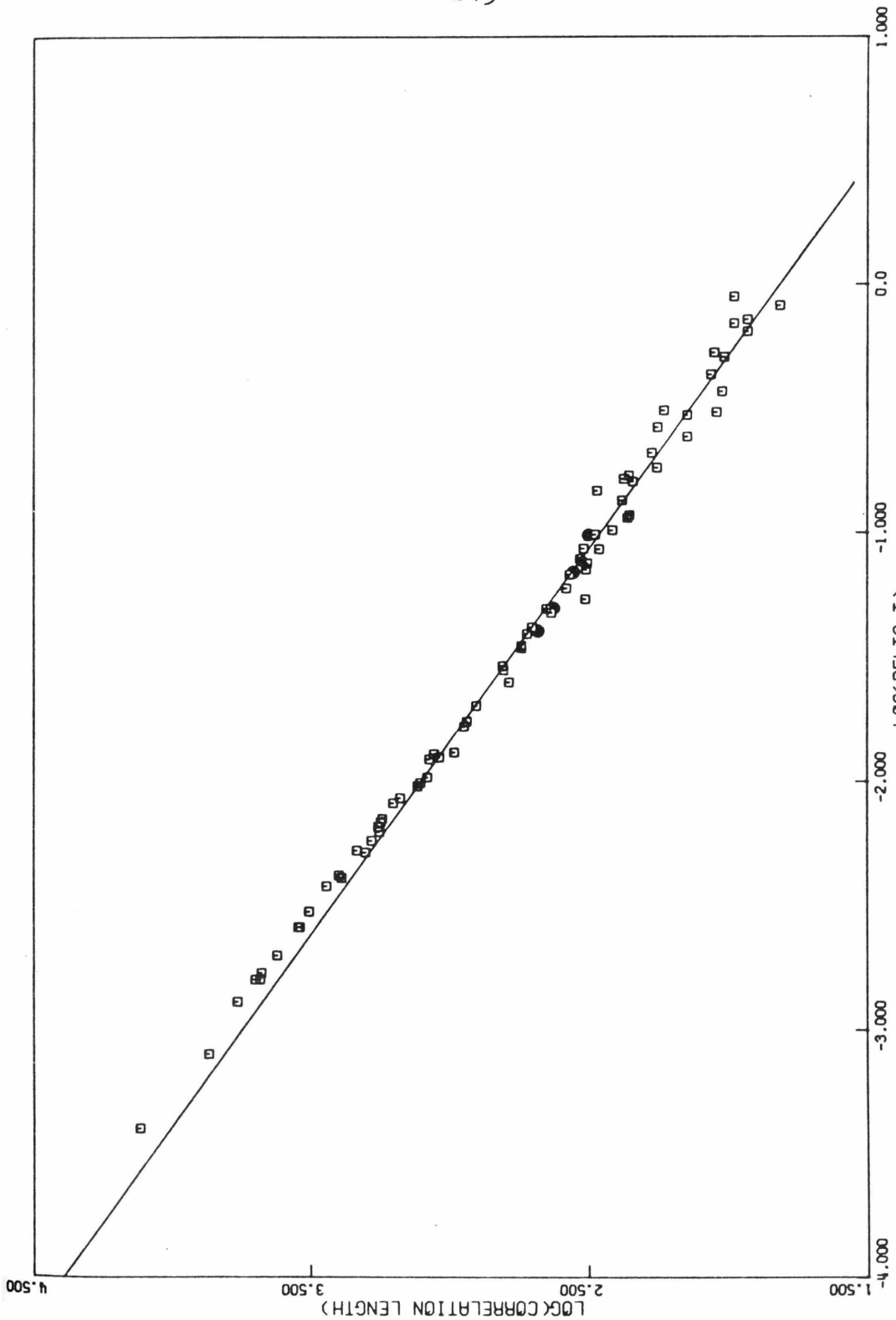
LOG(CORRELATION LENGTH)
1.500
2.500
3.500
4.500
-4.000
-3.000
-2.000
-1.000
0.0
1.000
LOG(DELTA T)

Figure 3.

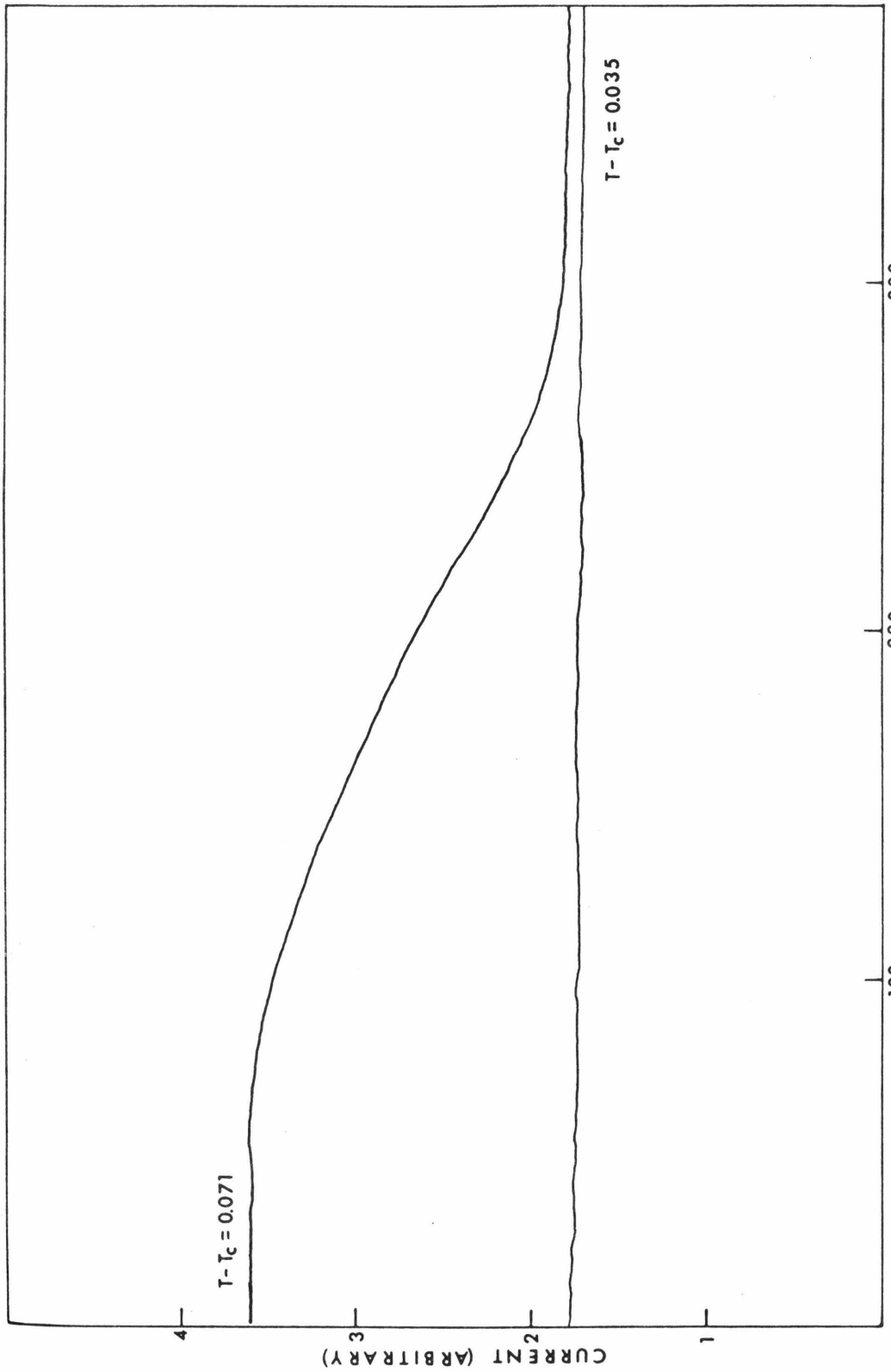
CURRENT (ARBITRARY)
4
3
2
1
100
200
300
TIME (SEC)
T-Tc = 0.071
T-Tc = 0.035

Figure 4.

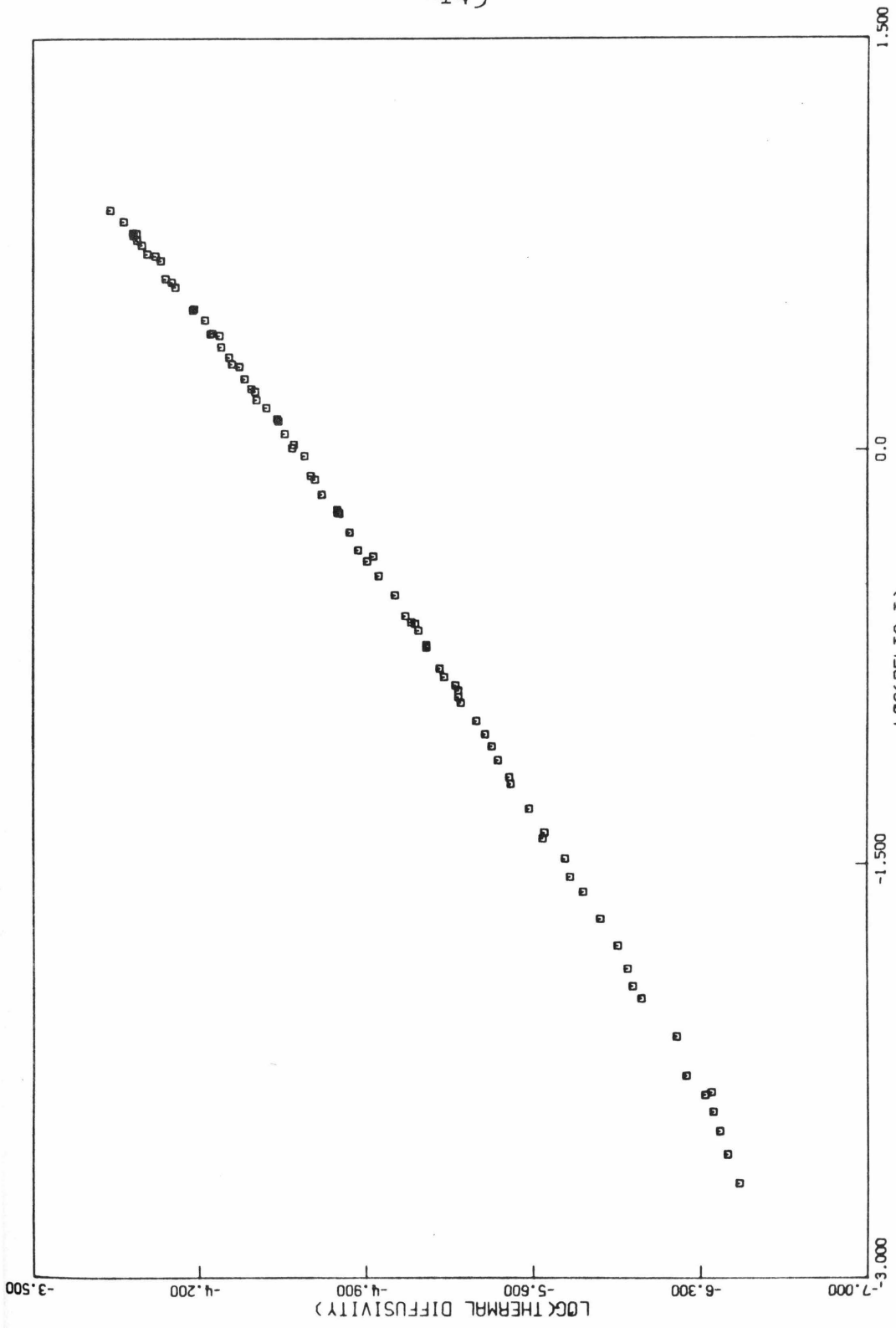
LOG(THERMAL DIFFUSIVITY)
-3.500
-4.200
-4.900
-5.600
-6.300
-7.000
-3.000
-1.500
0.0
1.500
LOG(DELTA T)

Figure 5.

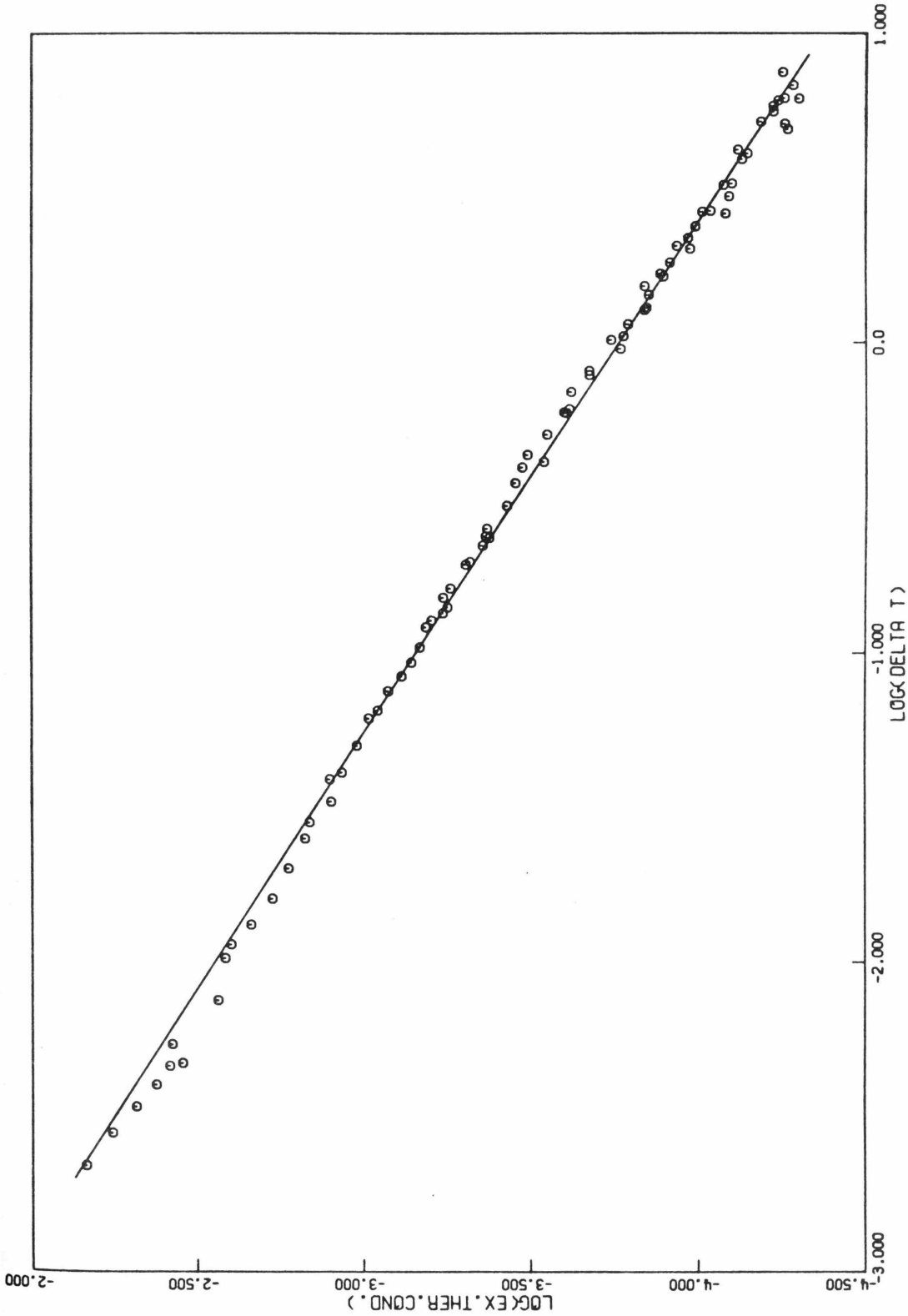
LOG(EX.THER.COND.)
-4.500
-4.000
-3.500
-3.000
-2.500
-2.000
LOG(DELTA T)
1.000
0.0
-1.000
-2.000
-3.000

Figure 6.

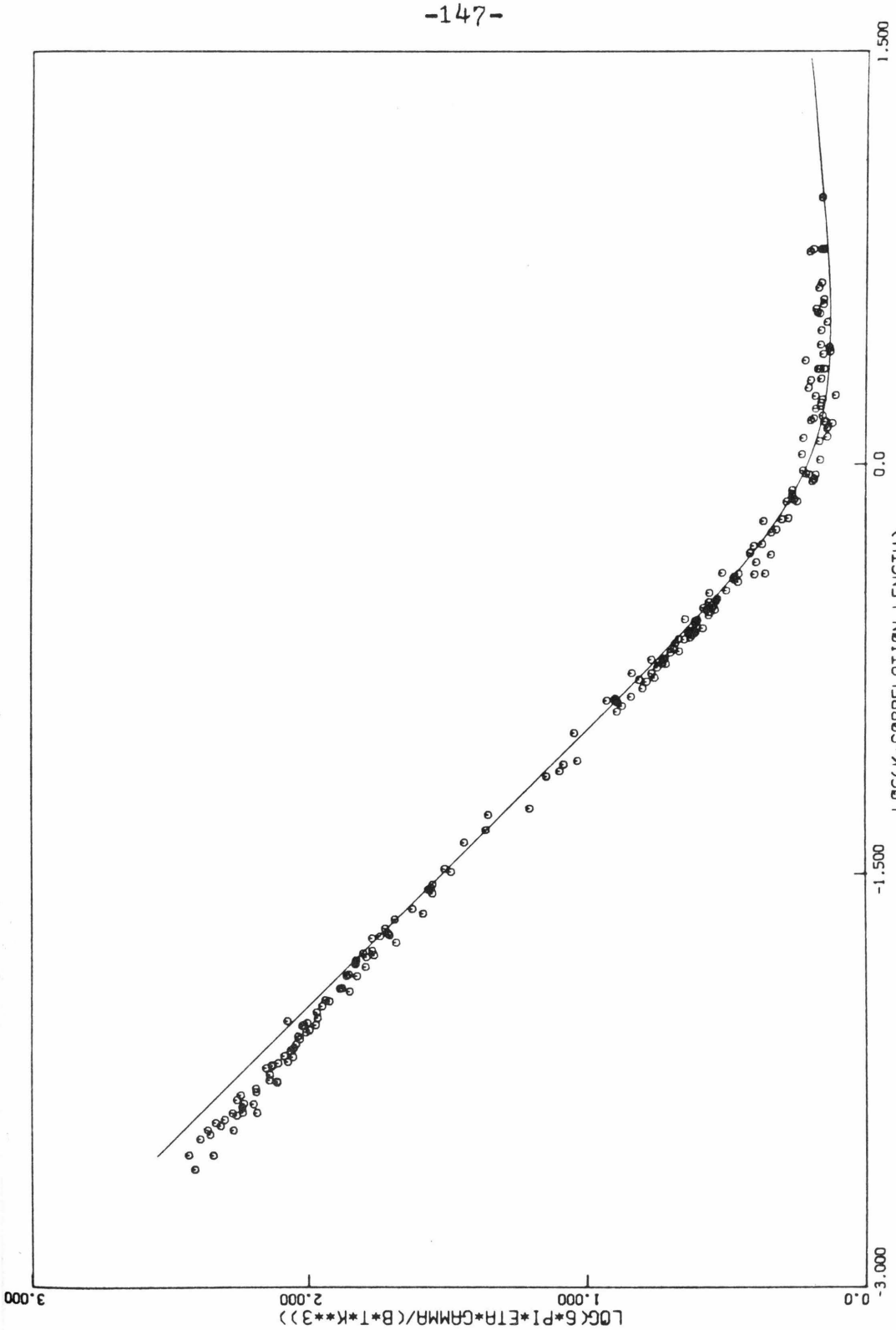
LOG(6*PI*ETA*GAMMA/(B*T*K**3))
3.000
2.000
1.000
0.0
-3.000
-1.500
0.0
1.500
LOG(K*CORRELATION LENGTH)

Figure 7.

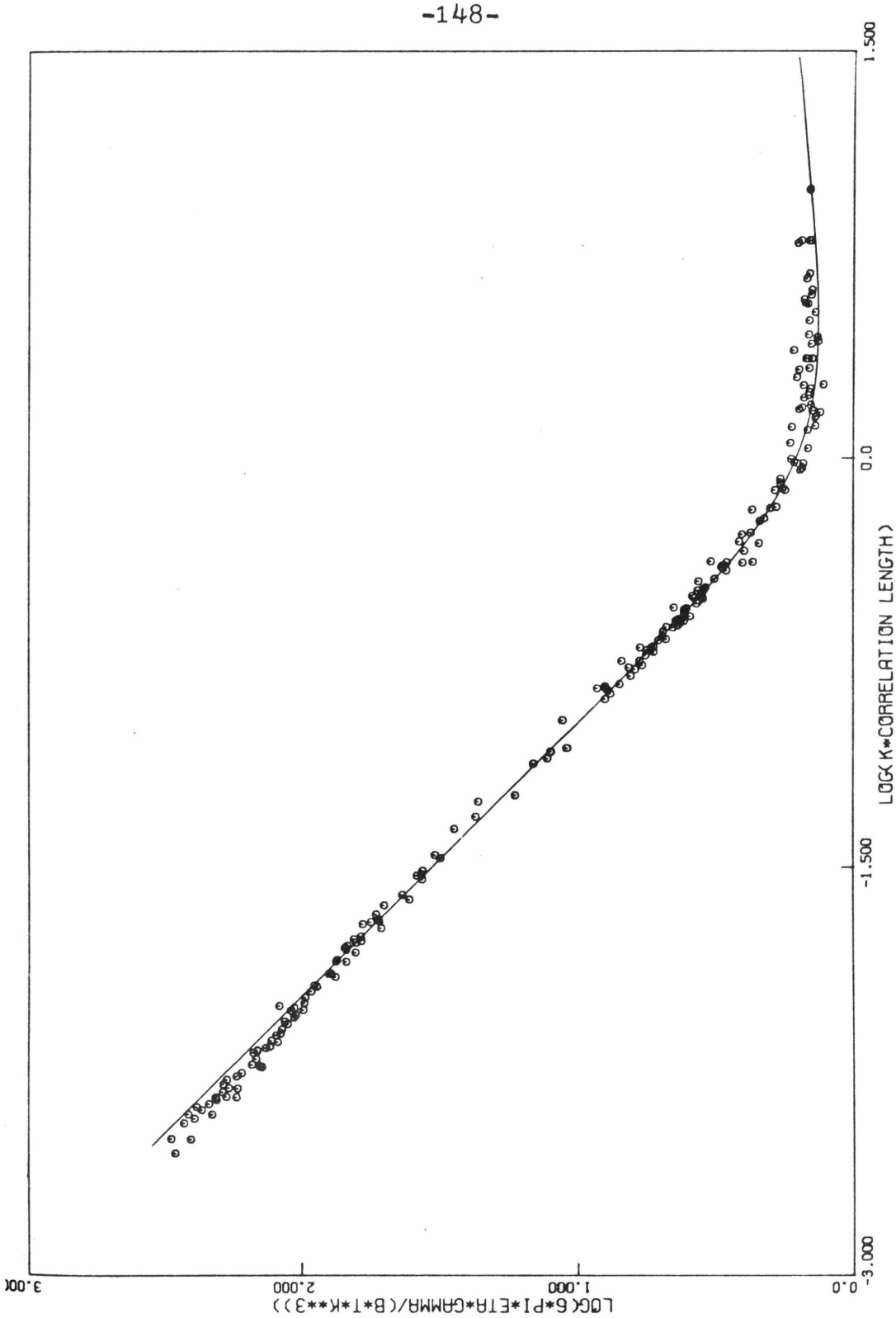
LOG(6*PI*ETA*GAMMA/(B*T*K**3))
3.000
2.000
1.000
0.0
-3.000
-1.500
0.0
1.500
LOG(K*CORRELATION LENGTH)

Figure 8.

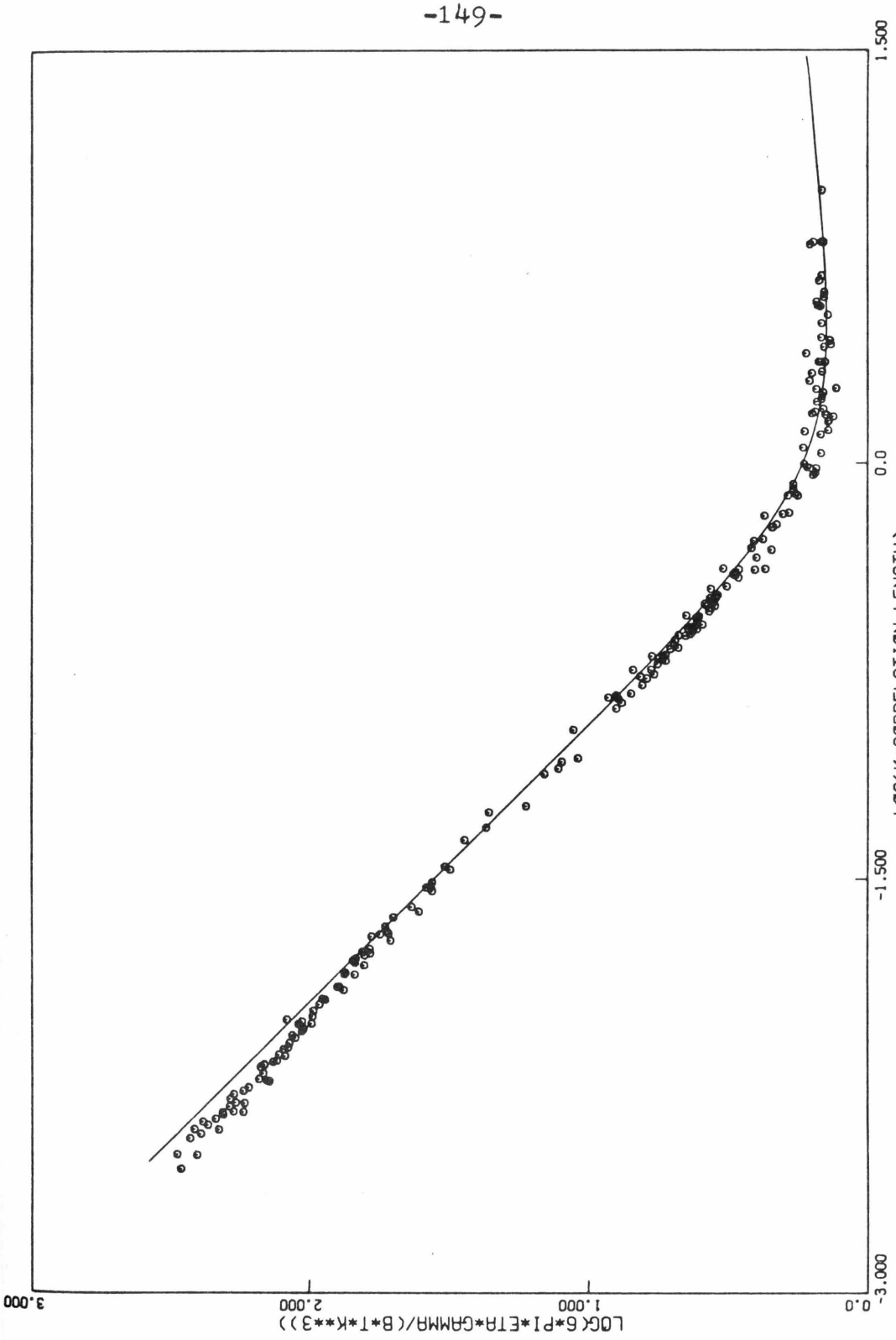
LOG(6*PI*ETA*GAMMA/(B*T*K**3))
0.0
1.000
2.000
3.000
-3.000
-1.500
0.0
1.500
LOG(K*CORRELATION LENGTH)

Figure 9.

VI. CONCLUDING REMARKS

During the time spent for this investigation the number of theorethical and experimental papers published on application of light scattering to critical phenomena have increased at least by an order of magnitude. This of course is an indication of the potential of the method. However, only two or three papers have appeared on the subject of determining the transport coefficients χ and D by laser light scattering, all with very limited data and inconclusive as to the potential of the technique. Section IV of this thesis, which will be submitted for publication in AIChE Journal, hopefully will remedy this problem with the extensive and conclusive data presented.

With the documentation of the viscosity anomaly for a wide variety of systems the only area of transport near the critical point not explored is the behavior of thermal conductivity in binary critical mixtures. It seems that this too can be studied using the present methods employed in laser light scattering. By choosing a system with a very small difference between the refractive indices of its components one can study the spectrum of thermal fluctuations along with the spectrum of concentration fluctuations as the critical point is approached.

Finally we may be reaching the practical limits of experimental technology in avoiding the problems caused by gravity and in improving the temperature control. There is not much one can do about gravity unless the experiments are done on satellites where gravitational forces are negligible. The present method of avoiding the gravitational problems by decreasing the sample height causes other experimental problems such as dealing with smaller samples and having larger errors. Today temperature controllers which can control within ±0.001°C are routine but the cost increases very rapidly if one wants better control. Mainly due to the thermal noises in the electrical circuits, the limit on temperature controlling seems to be about 10 microdegrees, a figure already reached in the water bath described in Proposition II. On the brighter side, significant advances can be made with the introduction of better detectors of the scattered light and much better correlators and spectrum analyzers may be in the market within a few years. These new electronic instruments may enable one to study even fast chemical reactions with light scattering, not feasible today due to very small change in the refractive index.

APPENDIX I

Experimental Details Not Given in Sections III, IV and V

A-Temperature Control:

In the studies of critical phenomena several different set ups were used in controlling the sample temperature. The main element was a model TVM 40 Tamson water bath sold by Neslab Instruments Durham, N.H.. By itself it could control the temperature to $\pm 0.003^{o}C$ and the temperature could be adjusted by about $0.005^{o}C$.

All the shear viscosity measurements were taken with the viscometer submerged in the water bath. The temperature control was achieved by using the water baths own controller.

The critical temperatures of the lutidine-water samples were measured by putting the sample in the light scattering cell into a larger test tube filled with water and submerging the test tube into the water bath. By this arrangement it was found that the fluctuations inside the test tube were less than $0.0003^{o}C$, the maximum sensitivity of the measuring circuit. Temperatures were measured in the test tube rather than the water bath.

During light scattering measurements the sample cell (precision bore nmr-tubing with wall thickness less than one mm) was put into a brass temperature control jacket similar to the one shown in fig.(1). The inner walls

of the heating jacket were quarter inch thick thus damping out the rapid fluctuations in temperature before they reached the sample.The brass jacket was insulated by putting it into a lucite jacket which in turn was further insulated by glass-wool or foam rubber insulation. Convection currents in the viewing slot were prevented by covering the slot with saran wrap.Water pumped from the water bath was circulated through hellical channels cut into the brass jacket.The temperature of the circulated water was controlled to $\pm 0.003^{\circ}C$. The temperature fluctuations in the center of the cell were measured to be less than $0.0005^{\circ}C$.The temperature of the sample was measured by inserting a miniature platinum resistance thermometer into a thermometer well drilled right next to the cell.

During the measurements of thermal diffusivity and mass diffusivity in pure fluids and binary mixtures away from their critical points no elaborate temperature controls were used other than the room temperature.The room temperature never changed by more than $0.5^{\circ}C$ during 12hrs. and most of the time it stayed constant to $0.1^{\circ}C$. The light tight box containing the sample and the detection equipment also acted as a stagnant air bath insulated from the room.Convection currents due to evaporation of the sample were prevented by filling the sample cell

completely and closing with teflon stopcocks which left no vapor space above the liquid.No measurements were taken until the sample was in thermal equilibrium with its surroundings.

Studies of critical phenomena in ethane were the most sophisticated in terms of temperature control.Again the main unit was the water bath but the temperature controller of the water bath was disconnected and only the heaters and the stirrer were used.A controller similar to the one described by H.J.Strumpf[36] was built and used to control the water bath temperature.The controller consisted of a wheatstone bridge with unequal arms and one of the arms was a precision variable resistor,Rubicon Bridge serial no 106276 made by Honeywell Instruments Co.,a Leeds and Northrup (L&N) microvolt amplifier cat.no: 9835-B together with a L&N series 60 proportional controller and a L&N Fincor Power Package.The sensor was a L&N 25.5 ohm platinum resistance element located in the water bath.The control inside the bath was about $\pm 0.0005^{o}C$ and could be kept constant for long periods of time provided no sudden jumps in room temperature occured.The necessary cooling for the bath was supplied by an auxiliary bath,Tamson model T3 circulating bath,cooled by a portable freon cooler,Tamson model PBC-4.The temperature of the cooling water was regulated to $\pm 0.02^{o}C$ and the

volume of the cooling water was kept constant.

During light scattering measurements water from the water bath was pumped by a 1/30 HP pump through insulated lines and circulated through the brass temperature control jacket.The inside of the brass jacket contained baffles to assure uniformity of temperature and flow. The rate of circulation was about two liters per minute resulting in a mean residence time of five seconds.By this arrangement the control inside the jacket was as good as the control in the water bath even though the net difference between the two reached 0.05°C when operating at temperatures much higher than the room temperature.

As in the lutidine-water case the brass jacket was insulated by lucite and foam insulation and the slot was covered by saran wrap.Furthermore the temperature of the light tight box was also controlled by a controller similar to the one described above for the water bath. The heating was accomplished with warm air blowers which heated and circulated the air.The temperature of the box was set as close to the critical temperature of ethane as possible and the control unit controlled the temperature within ±0.03°C for indefinite periods of time.The sensor for the controller was a 100 ohm platinum resistance thermometer.

Using the complex arrangement described above it was possible to control the sample temperature to within ±0.0003°C, the minimum amount our measuring circuit could detect, for several hours if the system was not disturbed. Disturbances due to sudden shifts in room temperature were minimized by operating the room temperature controller in manual mode which provided continuous cooling without causing any sudden jumps in temperature.

The brass jackets used in the ethane study are shown in figures (1) and (2) together with the pressure cells used. The complete temperature control set up is shown in fig.(3).

The temperature of the ethane sample was measured near the wall of the brass jacket and the critical temperature of ethane was used as a check against any differences between the sample temperature and the measured temperature.

B-Temperature Measurement:

Two doped platinum resistance thermometers with nominal resistances of 100 ohms were used in making all the measurements. The thermometers were manufactured by Electric Thermometrs Inc. Kearny, New Jersey, model number G-20. Calibration of both thermometers had been performed by P.Morrison, H.J.Strumpf and J.Karnicky[36].

The first thermometer,labeled resistance element 1 in the calibration tables was used throughout the measurements made on the lutidine-water system.This thermometer was put into a 1/8 in I.D. thin walled piece of copper tubing and the tubing was filled with silicone oil to improve thermal contact.The ice point resistance of this thermometer was checked frequently and it was also checked against the departmental standard,National Bureau of Standards calibrated,platinum resistance thermometer (ChE no 20121).About a year after all the lutidine-water data were taken an ice point check was made and it was found that the ice point resistance of the thermometer had shifted by an amount corresponding to a change of about $0.1^{o}C$ in the measured values,it was also observed that the ice point resistance of the thermometer was not reproducible.Upon these findings this thermometer was discarded and was not used anymore.Thus the absolute accuracies of the temperatures of the lutidine-water system are down to $\pm 0.1^{o}C$.However the relative accuracies stay the same due to the fact that all the critical temperatures were measured before and after taking the data and no significant differences were observed over a time span of a few days during which the measurements were taken.

The second thermometer used was of the same model as the first one,labeled resistance element 2 in the calibration tables, and was used for all the measurements taken on ethane.A very careful study of the reproducibility of the ice point resistance was made by cycling the thermometer between 100°C and -20°.It was found to have an ice point resitance of 99.8946±0.0004 ohms[37]. It was also checked against the standard thermometer described above and some systematic deviations from the calibration table were observed.The results of the calibration are given in table(I). A third thermometer of the same design as the standard thermometer was also calibrated for use as a secondary standard in our lab and the following calibration constants used in the Callendar equation relating the resistance of platinum to temperature were obtained: $\alpha=0.0039268_0\pm0.0000004$ and $\delta=1.485_2\pm0.0008$ which can be compared with $\alpha=0.0039268_5$ and $\delta=1.484_6$ determined by Ron Smith[38] using the same standard thermometer but a different potentiometer and standard resitor.The serial numbers of the thermometers are : for the standard L&N 676711 and for the secondary standard L&N 1708528 and the Chem.Eng.number of the secondary standard thermometer is 23446.

The resistances of the thermometers were determined by the circuit shown in fig.(4).The potentiometer used

was a six dial L&N guarded potentiometer,catalog no 7556. The variable resistor was an L&N decade resistance box of 0-10000 ohms adjustable at steps of 1 ohm.The standard resistor was an NBS recomended type L&N resistor with a nominal resistance of 100.0012±0.001 ohms at 25°C.A comparison with a known resistance showed that abetter value was 100.00204 ohms[36].The temperature dependence of the resistor was given by L&N to be:

$$R_t = R_{25}(1+7\times10^{-6}(t-25)-5\times10^{-7}(t-25)^2)$$

where t is the temperature in degrees Centigrade.Changes in the resistance were calculated by measuring the temperature of the standard resistor with a glass thermometer and using the above equation.The catalog no of the standard resistor is 4030-B and the serial no is 1759518.

Temperature determinations using resistance thermometry are based on the ratio of the resistance of the strain free platinum wire at the temperature of interest to its resistance at the ice point.The resistance of the thermometer is determined by measuring the voltage drop across it and by measuring the current.The current is measured by determining the voltage drop across the standard resistor thus the ratio of the resistances can be determined from:

$$R_t/R_0 = (E_t/I_t)/(E_0/I_0).$$

Thermal or stray voltages in the measuring circuit were very small about 0.1-0.3 microvolts and were corrected for by measuring the"zero current" voltages both in the thermometer and the standard resistor circuits.Any errors due to the potentiometer show up in the voltage ratios E_t/E_0,we have tried to keep this as small as possible by keeping the voltage drop across the standard at a constant value which was very close to but not less than 0.1 volts,since the ice point resistance of the thermometer is very close to the resistance of the standard resistor this resulted in a minumum change of dials on the potentiometer and the ice point resistance determination was free of potentiometer errors.Also the current used during the calibration of the thermometer was used during all the measurements.

All the temperatures were measured on the 1948 ITS scale and are reported in the 48 ITS scale.

C-Viscosity Measurements:

The shear viscosities were measured with a modified size 50 Cannon-Fenske capillary viscometer.The procedure suggested in NBS monogram 55 was used in calibrating the viscometer and in calculating the viscosities.The primary measured quantity in a flow viscometer is the time and the kinematic viscosity is related to the time by a second order polynomial: k.viscosity = $At + B/t^2$,with A and B

being the calibration constants of the viscometer.The calibration constants of the viscometer used in this study were determined to be $A=3.285\pm0.01\times10^{-3}$ centistokes/sec and $B=300.4\pm1$ centistokes-sec^2 by Dr.A.F.Collings.

Kinematic viscosities were converted to shear viscosities by multiplying with density.Since there were no density data in the literature we determined the densities as a function of temperature.A 10cc pycnometer calibrated with distilled water was used in measuring the densities.

D-Density Determination for Ethane:

Ethane densities were determined by weighing the sample cell before and after loading,the difference was taken as the weight of ethane.The densities were found by dividing the sample weight by the known cell volume. All the weighings of the 0.889cm path length cells were done with the ChE analytical balance made by WM Ainsworth and Sons Inc.Denver,Colorado,type BB no35973.A very careful study of the reproducibility of the balance indicated that it can reproduce within ±0.2mg over a time period of several days.

The sample cell was carefully conditioned before each weighing by immersing it into a good solvent,which

did not leave any residue upon evaporation, such as acetone or methyl alcohol for an hour to clean the outside surfaces properly. After cleaning, the container with the cell in it was evacuated for one hour to dessicate the cell and half an hour was given for thermal equilibration before weighing. This procedure resulted in an overall reproducibility of the cell weight within ±0.2mg.

The sample cell was loaded slightly above the critical density before weighing and the density was brought down to about 0.1-0.2% above the critical density when weighing. The weight was adjusted by venting the ethane from the cell and observing the gas bubbling out through a tube immersed in water. Further adjustment of the density was made after observing the behavior of the meniscus in the water bath. The density was adjusted until the meniscus appeared close to the geometrical center of the cell and was stable in position when the temperature was lowered by 0.001°C below the critical temperature. Again the density was adjusted by venting the ethane through a tube immersed in water and counting the bubles. The weight of each buble was calibrated and found to be about 0.025mg, thus it was possible to adjust the density by as little as 0.01%.

The volume of the cell was calibrated by filling the cell with distilled and degassed water after pumping

to a high vacuum. The volume was calculated by determining the net weight of water and dividing by the known density. Since the glass tubes used were precision bore it was also possible to calculate the volume within 0.5% from a knowledge of the physical dimensions of the cell. The precision of the volume calibration was 0.02%. The main source of error was the wighing step. The weight of ethane in the cell was about 0.40 grams and thus the precision in weighing was about 0.05%.

A similar procedure was used for the 12.85 cm path length cell. Since it had a much larger volume the limiting factor was not the precision of the weighing.

Finally all the densities were calculated from the volume calibration obtained at room temperature. Volume changes due to thermal expansion and gas pressure inside the cell were estimated to be less than 0.02% and therefore neglected.

REFERENCES

1. A. Einstein, Ann. Physik 33, 1275 (1910).

2. L. S. Ornstein and F. Zernike, Proc. Acad. Sci. , Amsterdam, 17, 793 (1914), 19, 1321 (1916); Physik. Z. 19, 134 (1918), 27, 761 (1926).

3. L. I. Mandelshtam, Zh. Russ. Fiz. Khim. Obshcjestva 58, 381 (1926).

4. L. D. Landau and G. Placzek, Physik. Z. Sovjetunion 5, 172 (1934).

5. M. E. Fisher, Reports on Prog. in Phys. 30, 615 (1967).

6. Introduction to Phase Transitions and Critical Phenomena, H. E. Stanley, Oxford University Press, (1971).

7. Molecular Scattering of Light, I. L. Fabelinskii, Plenum Press, (1968), p. 29 and appendix I.

8. L. D. Landau and E. M. Lifshitz, Statistical Physics, Addison Wesley, (1958).

9. L. D. Landau and E. M. Lifshitz, Fluid Mechanics, Pergamon Press, (1959).

10. P. H. Keyes, R. F. Chang, J. V. Sengers, and C. O. Alley, University of Maryland Preprints, Technical Report No. 73-018, p. 12.

11. V. G. Puglielli and N. C. Ford, Phys. Rev. Lett. 25, 143 (1970).

12. W. P. Kao and B. Chu, J. Chem. Phys. 50, 3986 (1969).

13. M. E. Fisher, J. Math. Phys. 5, 944 (1964).

14. P. Calmettes, I. Laques, and C. Laj, Phys. Rev. Lett. 28, 478 (1972).

15. Leon Van Hove, Phys. Rev. 95, 249 (1954).

16. R. D. Mountain, Rev. Mod. Phys. 38, 205 (1966); R. D. Mountain and J. M. Deutch, J. Chem. Phys. 50, 1103 (1969).

17. M. Fixman, J. Chem. Phys. 33, 1357 (1960).

18. R. A. Ferrell, N. Menyard, H. Schmidt, F. Schwabl, and P. Szepfaulsy, Phys. Rev. Lett. 18, 891 (1967) and Ann. Phys. 47, 565 (1968).

19. B. I. Halperin and P. C. Hohenberg, Phys. Rev. Lett. 19, 700 (1967) and Phys. Rev. 177, 952 (1969).

20. L. P. Kadanoff and J. Swift, Phys. Rev. 166, 89 (1968).

21. K. Kawasaki, Ann. Phys. 61, 1 (1970).

22. R. A. Ferrell, Phys. Rev. Lett. 24, 1169 (1970).

23. B. Chu, S. P. Lee, and W. Tscharnuter, Phys. Rev. A7, 353 (1973).

24. R. F. Chang, P. H. Keyes, J. V. Sengers, and C. O. Alley, B. der Bunsen-Gesellschaft fur Physik. Chemie 76, 260 (1972).

25. E. Gulari, A. F. Collings, R. L. Schmidt, and C.J. Pings, J. Chem. Phys. 56, 6169 (1972).

26. J. V. Sengers, B. der Bunsen-Gesellschaft fur Physik. Chemie 76, 234 (1972).

27. K. Kawasaki and S. M. Lo Phys. Rev. Lett. 29, 48 (1972).

28. S. M. Lo and K. Kawasaki, Phys. Rev. A5, 421 (1972).

29. H. L. Swinney, D. L. Henry, and H. Z. Cummins, J. Phys. Suppl. 33, 81 (1972).

30. T. K. Lim and H. L. Swinney and K. H. Langley and T. A. Kachnowski, Phys. Rev. Lett. 27, 1776 (1971).

31. B. Chu, Ann. Revs. Phys. Chem. 21, 145 (1970).

32. H. Z. Cummins and H. L. Swinney in Progress in Optics, Vol. VIII, Ch. III, E. Wolf editor, North Holland , (1970).

33. G. B. Benedek in Statistical Physics, Phase Transitions and Superfluidity, M. Chertien, E. P. Gross, and S. Deser eds., Gordon and Breach, (1968), Vol. II, p. 1.

34. L. Mandel and E. Wolf, J. Opt. Soc. Am. 53, 1315 (1965).

35. I. S. Reed, IRE Transactions on Information Theory IT-8, 194 (1962).

36. H. J. Strumpf, PhD thesis, California Institute of Technology.

37. Prof. C. J. Pings' group data book 6022 p. 150.

38. Ron Smith, PhD thesis, California Institute of Technology.

SCHEMATIC DRAWING OF HIGH PRESSURE LIGHT SCATTERING CELL

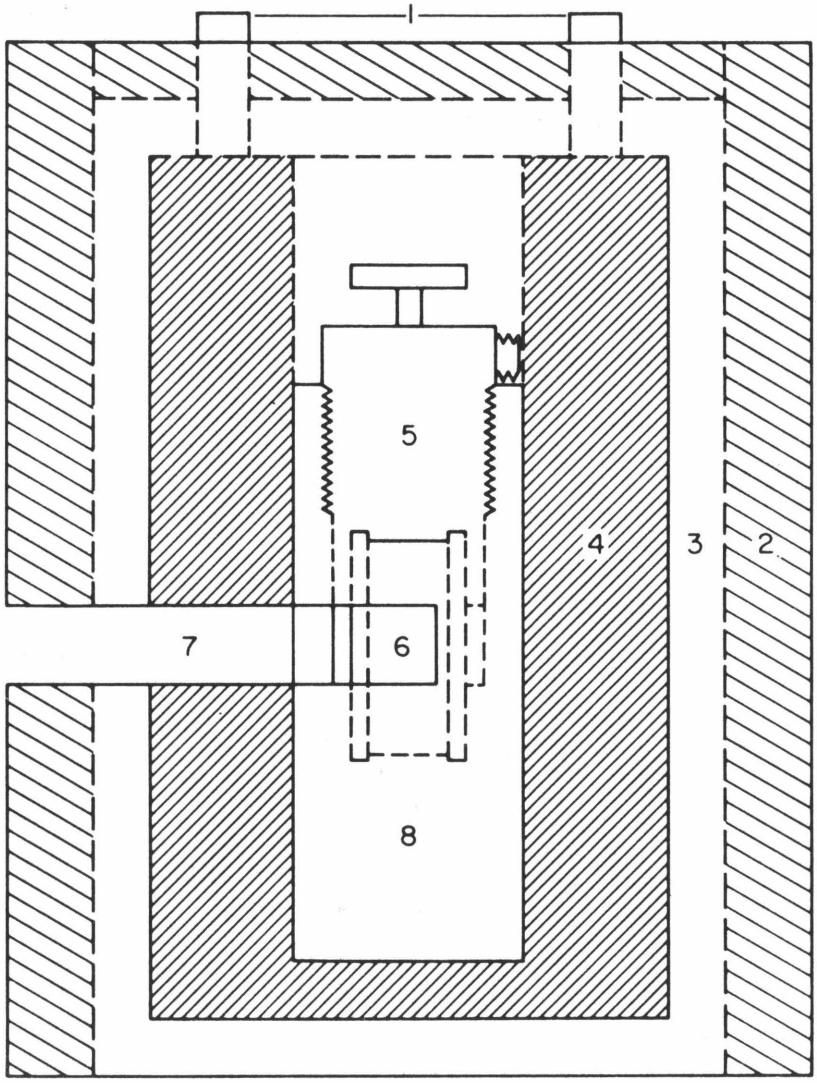

1- WATER INLET & OUTLET
2- FOAM INSULATION
3- LUCITE INSULATION
4- TEMPERATURE CONTROL JACKET
5- VALVE ASSEMBLY
6- GLASS CELL
7- VIEWING SLIT
8- SAMPLE CELL BODY

Figure 1. High pressure light scattering cell together with the temperature control jacket.

SCHEMATIC DRAWING OF DOUBLE PASS LIGHT SCATTERING CELL

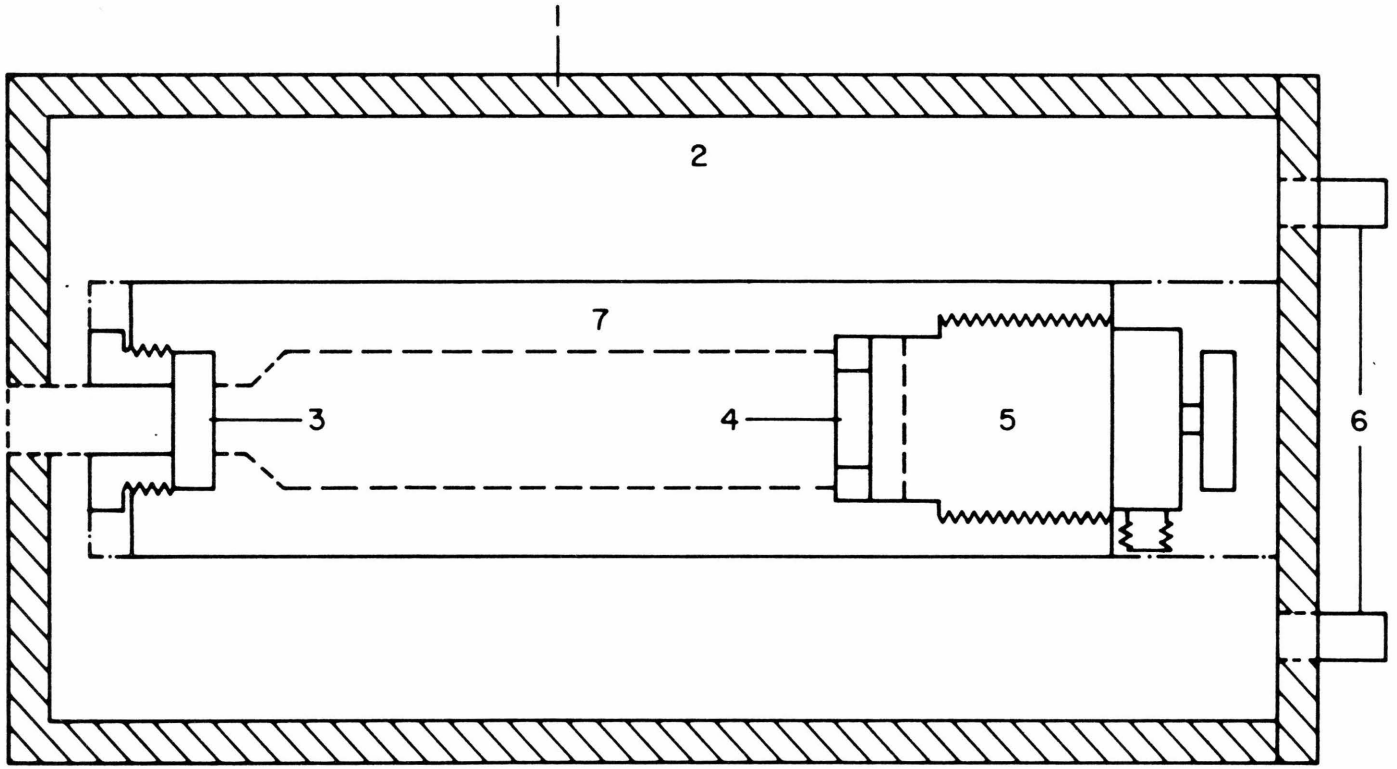

1 - LUCITE INSULATION
2 - TEMPERATURE CONTROL JACKET
3 - QUARTZ WINDOW
4 - MIRROR
5 - METAL TO METAL VALVE
6 - WATER CIRCULATION TUBES
7 - SAMPLE CELL

Figure 2. Double pass high pressure cell together with the temperature control jacket.

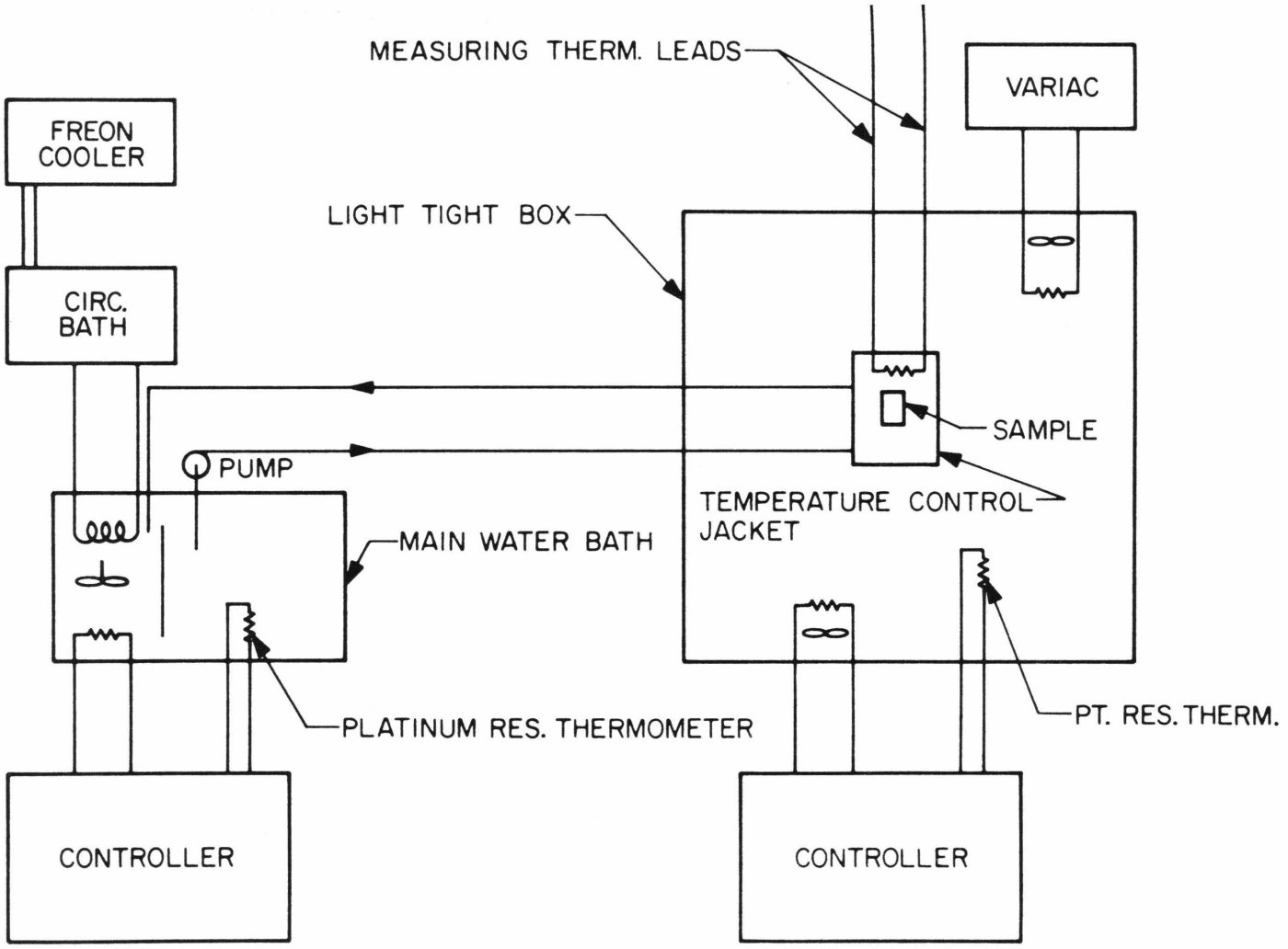

SCHEMATIC DRAWING OF TEMPERATURE CONTROL SYSTEM

Figure 3.

PLATINUM RESISTANCE THERMOMETER CIRCUIT

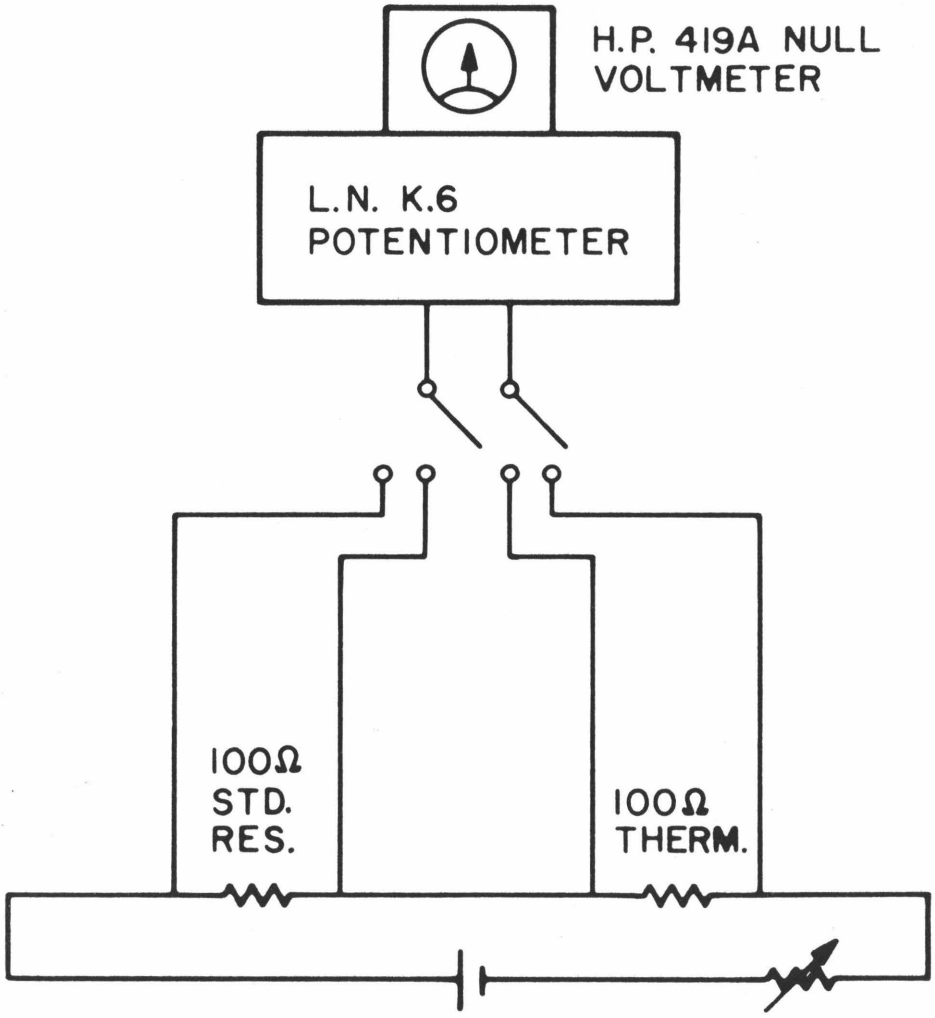

Figure 4.

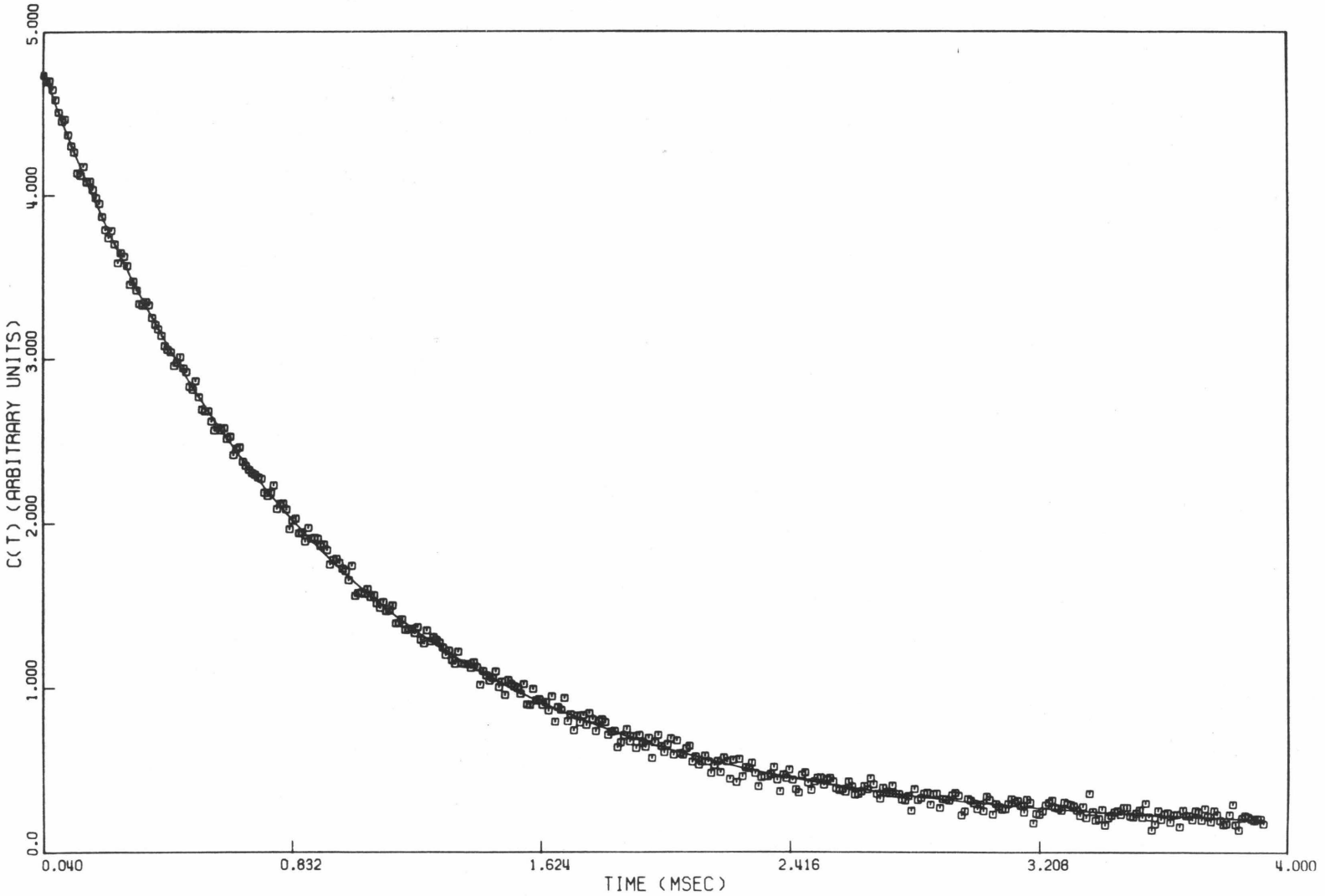

Figure 5. A typical photocurrent autocorrelation function, the solid line is the computer fit.

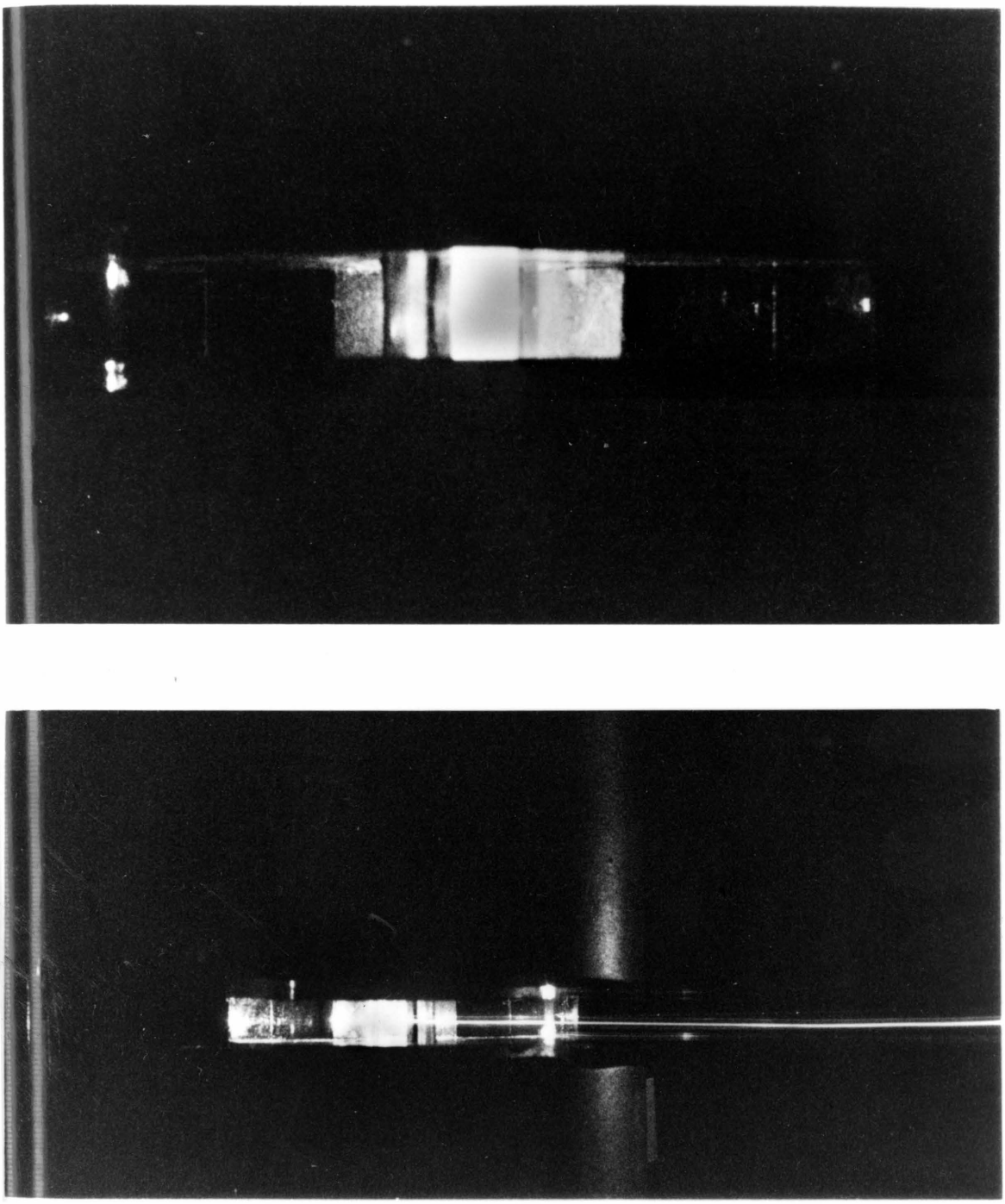

Figure 6. Critical opalescence in ethane:The lower picture far away from the critical temperature, ($\Delta T \sim 3.0^{o}C$),the upper picture close to the critical temperature,($\Delta T \sim 0.03^{o}C$),note that different exposure times are used,scattering from the dust in the air is the same in both but relative to the scattering from ethane near the critical point it is small.

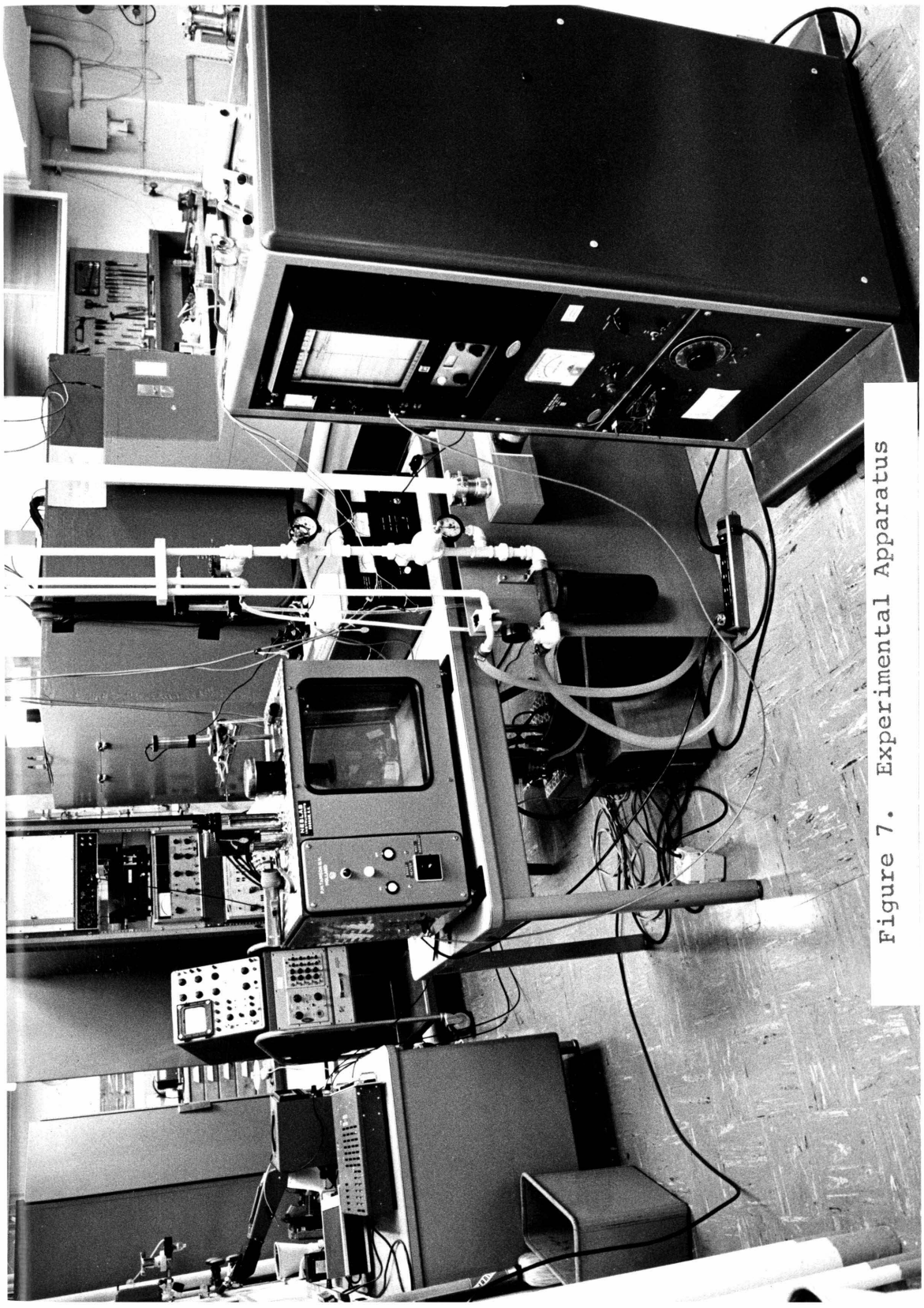

Figure 7. Experimental Apparatus

TABLE I

Calibration of the Measuring Thermometer Against the Chemical Engineering Standard Thermometer

T standard (°C)	T meas.th.(°C)	diff
22.5659	22.5669	0.0010
32.2168	32.2204	0.0036
42.3463	42.3520	0.0057
53.5191	53.5318	0.0127

TABLE II

Linewidth Data for the Lutidine- Water System

$\Theta = 25^{\circ}$ data taken with 15mm and 10mm precision bore nmr cells.

$\Delta T(^{\circ}C)$	$\Gamma/\pi(sec^{-1})$
7.485	688
5.108	584
4.146	528
3.138	416
2.790	447
2.423	400
1.799	365
1.740	343
1.322	301
1.189	279
1.030	273
0.876	250
0.704	212
0.680	203
0.525	181
0.504	171
0.397	143
0.388	147
0.300	134
0.257	120
0.213	111
0.212	115
0.164	104
0.118	75
0.087	74
0.035	44
0.029	38
0.012	28
0.010	27
0.003	25

(the uncertainty in ΔT is $\pm 0.001^{\circ}C$, and the uncertainty in the linewidth is about 5%)

TABLE II continued

$\Theta = 60^{\circ}$ data taken with the 10mm and the 15mm cells

$\Delta T(^{\circ}C)$	$\Gamma/\pi(sec^{-1})$
5.107	2996
4.151	2548
3.147	2423
2.789	2163
1.745	1756
1.798	1788
2.423	1878
1.318	1563
1.189	1417
1.032	1272
0.877	1182
0.703	1172
0.680	1060
0.528	898
0.504	891
0.399	772
0.386	782
0.299	632
0.257	582
0.214	569
0.212	602
0.162	488
0.118	413
0.081	383
0.035	264
0.025	256
0.014	236
0.010	221
0.002	180

(The uncertainty in ΔT is $= \pm 0.001^{\circ}C$, and the uncertainty in the linewidth is about 5%)

TABLE II continued

$\Theta = 90^{\circ}$ data taken with the 15mm and the 10mm cells

$\Delta T(^{\circ}C)$	$\Gamma/\pi(sec^{-1})$
5.109	5598
4.151	4988
2.789	4202
2.423	3976
1.799	3284
1.740	2892
1.315	2750
1.188	2430
1.032	2490
0.877	2202
0.703	1998
0.685	1983
0.522	1721
0.501	1648
0.395	1514
0.379	1274
0.296	1277
0.257	1117
0.214	1054
0.211	1111
0.164	940
0.118	879
0.081	759
0.035	648
0.021	563
0.013	540
0.007	495
0.001	457
0.183	1063
0.105	851
0.095	829
0.067	749
0.061	726
0.036	668
0.033	619
0.014	560
0.003	493

(The uncertainty in ΔT is $\pm 0.001^{\circ}C$ and the uncertainty in the linewidth is about 5%)

TABLE II continued

$\Theta = 90^{\circ}$ data taken with the 5mm cell

$\Delta T(^{\circ}C)$	$\Gamma/\pi(sec^{-1})$
0.185	1193
0.159	1074
0.094	943
0.071	823
0.048	773
0.044	775
0.033	729
0.028	677
0.019	663
0.017	643
0.010	668
0.002	646

$\Theta = 45^{\circ}$ data taken with the 15mm and 10 mm cells

0.876	687
0.397	481
0.388	469
0.257	368
0.164	281
0.118	202
0.035	141
0.012	114
0.003	72

$\Theta = 120^{\circ}$ data taken with the 15mm and 10 mm cells

3.147	6314
0.877	3725
0.257	1747
0.164	1524
0.118	1317
0.035	983

(The uncertainty in temperature is $\pm$ 0.001°C, and the uncertainty in the linewidth is about 5%)

TABLE III

Lutidine-Water System Diffusion Coefficients Calculated from the Linewidth Data

$\Delta T(^{\circ}C)$	$Dx10^{8}(cm^{2}/sec)$
5.108	28.8
4.146	25.5
3.138	21.8
2.790	21.6
2.423	18.6
1.799	17.7
1.740	16.7
1.322	15.2
1.030	12.9
0.876	12.0
0.703	10.4
0.680	9.74
0.525	8.64
0.504	8.11
0.397	7.13
0.300	6.19
0.257	5.59
0.212	5.25
0.164	4.49
0.118	3.55
0.035	1.88*
0.012	1.00*
0.087	3.24
0.025	1.57*
0.009	0.91*
0.003	0.35*

(The uncertainty in ΔT is $\pm 0.003^{\circ}C$ and the uncertainity in D is about 5%, those marked with an asterisk have larger uncertainties .)

TABLE IV

Turbidity Data of the Lutidine - Water System

$\Delta T(^{o}C)$	Turbidity(cm^{-1})
6.42	0.0543
3.326	0.1189
2.301	0.1571
1.415	0.2014
0.692	0.3210
0.364	0.5104
0.180	0.8746
0.095	1.435
0.040	2.309
0.017	3.031

(The uncertainties in ΔT are $\pm 0.003^{o}C$, the turbidities are accuarate to three significant figures.)

TABLE V

Intensity Data of the Lutidine-Water System Obtained in Run II

	$\Delta T(^{\circ}C)$										
Θ	3.325	1.906	0.940	0.679	0.479	0.361	0.238	0.127	0.050	0.038	0.017
30	0.288	0.562	1.349	2.045	3.177	4.498	7.552	15.72	42.52	55.19	119.9
40	0.275	0.544	1.317	2.022	3.167	4.488	7.555	15.61	41.82	54.47	116.7
50	0.245	0.504	1.261	1.939	3.058	4.348	7.314	14.87	39.44	51.20	109.3
55	0.241	0.498	1.243	-	3.027	4.269	7.212	14.59	38.49	49.46	105.2
60	0.238	0.498	1.256	1.929	3.053	4.304	7.238	14.64	38.19	48.83	104.7
65	0.242	0.498	1.254	-	3.033	4.309	7.184	14.52	37.40	47.99	102.7
70	0.241	0.498	1.252	1.925	3.009	4.288	7.122	14.29	36.43	46.48	100.5
75	0.239	0.498	1.258	-	3.018	4.283	7.078	14.11	35.64	45.53	97.98
80	0.242	0.498	1.247	1.903	2.975	4.216	6.935	13.68	34.46	44.06	93.98
85	0.243	0.498	1.250	-	2.972	4.194	6.900	13.47	33.62	42.88	91.52
90	0.245	0.498	1.243	1.889	2.934	4.129	6.766	13.15	32.45	41.30	88.58
95	0.243	0.498	1.238	-	2.902	4.071	6.677	12.85	31.32	40.14	85.12
100	0.244	0.498	1.238	1.862	2.913	4.080	6.628	12.66	30.63	39.04	82.79
105	0.244	0.498	1.237	-	2.897	4.033	6.542	12.35	29.54	37.77	79.45
110	0.243	0.498	1.235	1.871	2.886	3.983	6.453	12.08	28.60	36.46	76.49
120	0.244	0.498	1.218	1.839	2.814	3.892	6.191	11.40	26.43	33.67	70.29
130	0.250	0.498	1.204	1.806	2.732	3.596	5.885	11.01	24.06	30.37	63.27

(The uncertainty in ΔT is $\pm$ 0.003°C and the intensities are accurate to three significant figures)

TABLE V continued

Intensity Data of the Lutidine -Water System Measured in Run I

$\Delta T(^{\circ}C)$	θ=30	θ=40	θ=50	θ=60	θ=70	θ=80	θ=90	θ=100	θ=110	θ=120	θ=130
6.440	0.166	0.168	0.162	0.159	0.161	0.162	0.160	0.162	0.164	0.165	0.169
3.808	0.306	0.278	0.306	0.307	0.306	0.307	0.307	0.306	0.306	0.306	0.306
1.895	0.732	0.710	0.697	0.725	0.704	0.712	0.711	0.704	0.712	0.699	0.689
0.697	2.402	2.339	2.272	2.415	2.334	2.380	2.375	2.339	2.274	2.249	2.222
0.319	6.703	6.699	6.499	6.670	6.477	6.386	6.310	6.162	6.130	5.845	5.597
0.156	15.66	15.62	14.76	15.55	14.50	14.46	14.06	13.54	13.30	12.29	11.40
0.082	34.60	33.97	32.21	32.83	30.77	30.37	28.43	27.05	26.06	23.94	22.43
0.061	51.94	50.83	47.52	48.41	45.35	44.22	41.93	40.05	37.92	34.71	31.83
0.034	99.63	97.83	89.56	90.24	84.62	82.43	77.94	73.45	70.27	64.08	58.82

(The uncertainty in ΔT is $\pm$ 0.003°C, and the intensities are accurate to three significant digits)

TABLE VI

Extrapolated Zero Angle Intensities from the Lutidine-Water Intensity Data

Data of Run II:

$\Delta T(^{\circ}C)$	I(0)	%std.error
3.325	0.238	0.6
1.906	0.492	0.0
0.940	1.222	0.4
0.679	1.942	0.8
0.479	2.954	0.6
0.361	4.230	0.9
0.238	7.205	0.6
0.127	16.00	1.1
0.050	55.49	1.7
0.038	73.37	1.5
0.017	146.7	2.9
Data of Run I:		
6.440	0.162	1.1
3.808	0.298	1.8
1.895	0.720	0.7
0.697	2.396	1.4
0.319	6.930	1.4
0.156	16.65	3.3

TABLE VI continued

$\Delta T(^{o}C)$	I(0)	% std.error
0.082	37.69	3.1
0.061	56.95	3.5
0.034	109.0	3.3

(the uncertainty in ΔT is $\pm$ 0.003^{o}C)

TABLE VII

Lutidine-Water Correlation Lengths Obtained from the Intensity Data

$\Delta T(^{o}C)$	Corr.Length(A^{o})	% std.error
1.895	56	45
0.940	51	2
0.697	75	39
0.679	106	5
0.480	104	8
0.361	123	10
0.319	136	12
0.238	153	5
0.156	188	12
0.127	208	5
0.082	239	7
0.050	272	3

(The uncertainty in ΔT is + $0.003^{o}C$)

TABLE VIII

Density Data of the Lutidine - Water System

T(°C)	Density(gr/cc)
11.5	1.0013
15.7	0.9990
19.0	0.9971
23.2	0.9948
24.2	0.9942
26.2	0.9931
27.2	0.9923
28.2	0.9919
29.2	0.9912
30.2	0.9905
31.2	0.9898

(The temperatures are accurate to $\pm 0.1^{\circ}C$, and the densities are accurate to $\pm$ 0.0001gr/cc)

TABLE IX

Kinematic Viscosities for the Lutidine-Water System

$\Delta T(^{\circ}C)$	k.viscosity(centistokes)
27.42	5.014
23.71	4.250
20.55	3.729
18.34	3.421
17.11	3.268
14.94	3.019
14.37	2.962
12.45	2.776
11.15	2.662
10.50	2.608
10.22	2.585
9.392	2.520
8.484	2.456
7.335	2.377
6.375	2.314
5.385	2.257
4.414	2.205
3.935	2.184
3.441	2.157
2.473	2.127
1.650	2.109
1.008	2.113
0.646	2.131
0.443	2.155
0.276	2.193
0.257	2.199
0.231	2.196
0.197	2.207
0.160	2.225
0.129	2.241
0.106	2.264
0.313	2.180
0.080	2.282
0.063	2.309
0.038	2.349
0.025	2.376
0.017	2.411
0.013	2.424
0.007	2.441

(Uncertainty in ΔT is $\pm$ 0.003°C and the uncertainty in viscosity is 0.1%)

TABLE X

Toluene Thermal Diffusivity Data as a Function of Scattering Angle, T=20°C.

$\chi.10^3$ (cm^2/sec)	S.error.10^3 (cm^2/sec)	Θ (deg.)
0.893	0.063	2.58
0.914	0.017	2.24
0.816	0.048	1.90
0.941	0.019	1.57
0.805	0.014	1.23
0.831	0.017	1.79
0.831	0.014	1.62
0.880	0.012	1.40
0.830	0.010	1.23
0.818	0.013	1.23
0.791	0.007	1.06
0.975	0.040	2.23
0.877	0.024	2.23
0.837	0.019	1.86
0.850	0.016	1.59
0.839	0.024	1.59
0.850	0.022	1.14
0.816	0.011	0.81
0.850	0.012	1.14
0.856	0.044	2.24

TABLE XI

Benzene Thermal Diffusivity Data as a Function of Scattering Angle, T=20.0°C.

$\chi.10^3$ (cm^2/sec)	S.error.10^3 (cm^2/sec)	θ (deg.)
1.004	0.016	2.23
1.026	0.016	2.23
0.933	0.020	1.56
0.929	0.013	1.56
0.959	0.018	1.56
0.909	0.012	1.23
0.891	0.016	1.23
0.948	0.018	1.11
0.977	0.019	0.89
0.982	0.013	0.89

TABLE XII

Carbon Disulfide Thermal Diffusivity Data as a Function of Scattering Angle, T=20°C.

$\chi.10^3(cm^2/sec)$	S.error.$10^3(cm^2/sec)$	θ(deg.)
1.12	0.02	1.48
1.16	0.03	2.08
1.06	0.04	2.39
1.12	0.02	1.76
1.13	0.02	1.14
1.03	0.02	1.45

TABLE XIII

10% by Volume Acetone-Carbon Disulfide Mutual Diffusion Data as a Function of Scattering Angle, T=20°C.

$D.10^5$ (cm^2/sec)	S.error.10^5 (cm^2/sec)	θ (deg.)
Data taken with the 100mm path length cell:		
2.23	0.02	1.47
2.42	0.02	1.47
2.14	0.03	2.73
2.66	0.02	2.10
2.61	0.04	3.36
2.39	0.04	4.62
2.38	0.04	3.99
2.49	0.05	5.25
2.45	0.04	5.88
Data taken with the 30 mm path length cell:		
2.18	-	3.12
2.29	-	3.74
2.40	-	4.99
2.24	-	6.23
2.45	-	7.50

TABLE XIV

10% by Weight Acetone-Carbon Disulfide Mutual Diffusion Data as a Function of Scattering Angle, T=18.2°C.

$D.10^5$ (cm^2/sec)	S.error.10^5 (cm^2/sec)	θ (deg.)
2.23	0.04	1.16
2.29	0.02	1.16
2.28	0.01	1.47
2.23	0.02	1.47
2.24	0.03	1.80
2.24	0.01	1.80
2.21	0.04	2.11
2.24	0.02	2.11
2.30	0.01	2.75
2.22	0.01	3.38
2.06	0.05	3.38

TABLE XV

Methanol-Benzene Mutual Diffusion Data as a Function of Scattering Angle, T=20°C.

$D.10^5(cm^2/sec)$	$S.error.10^5(cm^2/sec)$	θ(deg.)
10% by volume methanol data:		
0.890	0.010	2.25
0.810	0.006	2.93
0.836	0.006	3.61
0.850	0.008	4.28
30% by volume methanol data:		
0.790	0.005	1.61
0.794	0.004	2.30
0.770	0.005	3.0
0.781	0.004	3.69
0.825	0.005	4.38

TABLE XVI

Miscellaneous Mutual Diffusion Data, T=20°C.

System and conc.	$D.10^5$ (cm^2/sec)	θ(deg.)
CH_3OH-CS_2 :		
2% by vol.methanol	1.28	9.25
CH_3CH_2OH-CS_2:		
16.7% by vol.ethanol	0.65	3.16
	0.58	6.31
	0.63	9.42
25.0% by vol.ethanol	0.527	9.56
33.3% by vol.ethanol	0.513	9.69
50.0% by vol.ethanol	1.07	9.99
75.0% by vol.ethanol	1.32	10.3
85.7% by vol.ethanol	2.08	10.7
$CH_3CH_2CH_2OH$-CS_2:		
20.0% by vol.ethanol	0.850	9.45
	0.819	12.5
	0.780	6.33
$CH_3CH_2CH_2CH_2OH$-CS_2:		
21.0% by vol.butanol	1.08	9.44
50.0% by vol.butanol	1.06	9.86
33.3% by vol.butanol	1.04	15.9
	0.97	3.23

TABLE XVI continued

System and conc.	$D.10^5$ (cm^2/sec)	θ (deg.)
$CH_3CH_2CH_2CH_2OH$-CS_2:		
75.0% by vol.butanol	1.29	10.24
Propanol-water:		
24% by vol.propanol	0.173	14.7
Heptyl alcohol-CS_2		
25.0% by vol.heptyl alcohol	1.02	9.54

TABLE XVII

Refractive Indicies for Pure Liquids Used in Determining the Thermal Diffusivities by Light Scattering ,Wavelength = 4880 Angstroms

Substance	Temperature(°C)	R.Index
Acetone	19.9	1.361
Benzene	20.0	1.491
Bromobenzene	19.9	1.552
Carbon Tetrachloride	20.0	1.460
Ethyl Alcohol	19.8	1.362
n-Hexane	19.9	1.375
Methyl Alcohol	19.7	1.324
Toluene	20.0	1.486
Carbon Disulfide	20.0	1.616

TABLE XVIII

Refractive Indicies of Acetone-Benzene System, $T=20.4^{\circ}C$, $\lambda=4880$ Å.

Vol.% acetone	Refractive index
2.0	1.492
5.0	1.489
12.0	1.479
20.0	1.469
32.0	1.453
44.0	1.436
56.0	1.420
68.0	1.404
80.0	1.387
92.0	1.370

TABLE XIX

Refractive Indicies of n-Hexane-Benzene System, $T=19.9^{o}C$, $\lambda=4880$ Å.

Vol.% n-hexane	Refractive index
5.0	1.482
10.0	1.481
20.0	1.471
30.0	1.458
40.0	1.439
50.0	1.433
60.0	1.421
70.0	1.410
80.0	1.397
90.0	1.386

TABLE XX

Refractive Indicies of Ethanol-Benzene System, T=18.6°C, λ=4880 Å.

Vol.% ethanol	Refractive index
5.0	1.489
10.0	1.483
20.0	1.468
40.0	1.443
60.0	1.414
80.0	1.388
90.0	1.375

TABLE XXI

Refractive Indicies of Methyl Alcohol-Butyl Alcohol System, $T=19.5^{o}C$ and $\lambda=4880$ Å.

Vol.% methanol	Refractive Index
20.0	1.382
40.0	1.373
60.0	1.360
80.0	1.341

TABLE XXII

Refractive Indicies of Carbon Tetrachloride-Carbon Disulfide System, $T=18.6^{\circ}C$, $\lambda=4880$ Å.

Vol.% carbon tetrachloride	Refractive index
10.0	1.596
20.0	1.578
40.0	1.541
60.0	1.515
80.0	1.488
90.0	1.472

TABLE XXIII

Refractive Indicies of Nitromethane-Benzene System, the Wavelength is 4880 Angstroms and the Temperature = 20°C.

Mole fraction nitromethane	R.index
0.155	1.476
0.293	1.464
0.415	1.453
0.525	1.442
0.624	1.430
0.713	1.421
0.794	1.408
0.869	1.398
0.939	1.385

TABLE XXIV

Refractive Indicies of Toluene-Bromobenzene System, T=19.9, λ=4880 Å.

Vol.% toluene	Refractive index
12.5	1.541
37.5	1.532
62.5	1.516
80.0	1.505

TABLE XXV

Refractive Indicies of Methanol-Benzene System, T=20.0, λ=4880 Å.

Vol.% methanol	Refractive index
2.0	1.489
5.0	1.488
10.0	1.477
20.0	1.459
15.0	1.467
30.0	1.445
40.0	1.429
50.0	1.407
60.0	1.394
70.0	1.372
80.0	1.361
90.0	1.346
95.0	1.341

TABLE XXVI

Miscellaneous Refractive Index Data, λ=4880 Å.

Substance	T(°C)	R.index
Lutidine-water critical conc.(0.0658 mol.frac.lut.)	33.0	1.387
Acetone-carbon disulfide		
10% by vol. acetone	20.0	1.583
10% by wt. acetone	18.2	1.575

TABLE XXVII

Ethane Turbidity Data Obtained With The 12.85cm Path Length Cell

$T-T_c$(°C)	Turbidity(cm^{-1})
10.59	0.003719
8.266	0.005495
6.304	0.006698
4.931	0.008780
3.853	0.01151
2.877	0.01689
2.092	0.02541
1.505	0.03782
1.018	0.06110
0.822	0.07928
0.646	0.1052
0.510	0.1387
0.404	0.1895
0.306	0.2576
0.244	0.3300
0.183	0.4485
0.114	0.8210
0.161	0.5007
0.210	0.3783
0.298	0.2591
0.434	0.1670
0.532	0.1305
0.697	0.09525
0.893	0.07036
1.236	0.04754
1.738	0.03167
1.822	0.03138
1.892	0.02997
3.930	0.01264
5.500	0.008722
10.46	0.003685

TABLE XXVII continued

Ethane Turbidity Data Obtained With The 0.889cm Path Length Cell

$T-T_c$(°C)	Turbidity(cm^{-1})
0.371	0.2045
0.811	0.08934
1.409	0.04208
1.116	0.05826
0.918	0.07223
0.722	0.09164
0.624	0.1176
0.527	0.1422
0.211	0.4148
0.408	0.1960
0.469	0.1398
0.311	0.2371
0.115	0.7419
0.0766	1.059
0.0476	1.598
0.0343	2.006
0.0201	2.784
0.0174	3.035
0.0099	3.903
0.102	0.8193
0.0596	1.323
0.028	2.278
0.0096	3.970
0.165	0.4764
0.0982	0.8164
0.0784	1.014
0.0540	1.398
0.0416	1.702
0.0357	1.842
0.0291	2.156
0.0123	3.289
0.148	0.4987
0.118	0.7283
0.0857	0.9771
0.0753	1.104
0.0710	1.182
0.0351	1.967

TABLE XXVII continued

$T-T_c$ (°C)	Turbidity (cm^{-1})
0.0166	3.141
0.0125	3.552
0.0104	3.908
0.0131	3.858
0.266	0.2489
0.170	0.4629
0.135	0.6039
0.0863	0.9255
0.0677	1.156
0.0494	1.507
0.0391	1.786
0.0250	2.368
0.0129	3.235
0.0013	5.400
0.0052	4.885
0.0008	6.728
0.0058	4.554
0.0016	5.640
0.0026	5.170
0.0030	5.112
0.0063	4.437
0.0041	4.843
0.0004	6.004
0.0042	4.567
0.0071	3.999
0.0086	3.808
0.0017	5.363
0.0020	5.338
0.0026	5.059
0.0069	4.081
0.0053	4.263
0.0016	5.330
0.0038	4.473
0.0082	3.762
0.0066	4.106

TABLE XXVIII

Ethane Correlation Lengths Obtained

From The Turbidity Data

$T-T_c(^oC)$	Correlation Length(angstroms)
0.822	65
0.646	85
0.510	103
0.532	112
0.697	95
0.893	95
0.722	85
0.306	110
0.371	105
0.244	140
0.183	180
0.161	220
0.210	188
0.298	140
0.434	115
0.311	170
0.115	230
0.0766	336
0.0476	430
0.0343	550
0.0201	800
0.0174	865
0.102	260
0.0596	380
0.0280	639
0.165	237
0.0982	300
0.0784	340
0.0540	325
0.0416	504
0.148	295
0.118	226
0.0857	290
0.0753	320
0.0710	323
0.0351	550
0.0291	643
0.0166	885

TABLE XXVIII continued

$T-T_c$ (°C)	Correlation Length (A°)
0.0131	960
0.266	179
0.170	227
0.135	240
0.0863	330
0.0677	370
0.0494	448
0.0391	525
0.0250	610
0.0125	1087
0.0104	1200
0.0123	1180
0.0129	1135
0.0038	2770
0.0016	5000
0.0053	2150
0.0069	1760
0.0026	3500
0.0020	4170
0.0017	4750
0.0086	1500
0.0071	1740
0.0042	2500
0.0041	2440
0.0063	1780
0.0030	3200
0.0026	3450
0.0016	4800
0.0058	1900
0.0052	2000
0.0013	5800
0.0096	1300
0.0099	1270
0.0082	1590
0.0066	1800
0.0004	13000
0.0008	7350

TABLE XXIX

Ethane Intensity Data After Sinθ And Attenuation Corrections

θ=30		θ=40		θ=70		θ=110	
Δ T(^{o}C)	I	Δ T	I	ΔT	I	ΔT	I
9.0	0.60	9.0	0.49	9.0	0.48	9.0	0.42
2.868	2.33	3.382	1.62	3.095	1.71	3.099	1.58
1.565	4.62	1.429	4.66	1.616	3.84	1.618	3.36
1.029	7.35	1.016	6.795	1.025	6.71	1.020	5.79
0.736	10.9	0.718	10.4	0.732	10.0	0.725	8.70
0.512	16.6	0.504	16.1	0.535	14.7	0.521	12.4
0.310	30.5	0.308	29.9	0.335	26.4	0.314	22.3
0.152	75.6	0.160	70.0	0.189	54.1	0.173	44.9
0.107	124	0.101	135	0.110	94.6	0.103	89.1
0.079	161	0.074	180	0.079	142	0.072	115
0.061	226	0.056	245	0.069	171	0.052	154
0.042	348	0.038	371	0.045	266	0.036	216
0.031	499	0.028	541	0.035	341	0.025	339
0.022	750	0.023	655	0.029	429	0.018	554
0.016	1100	0.017	1030	0.020	674	0.014	698
0.012	1740	0.013	1350	0.014	1110	0.012	978
0.010	2130	0.009	2090	0.012	1210	0.009	1290

(Note that there is no calibration data taken for this cell due to the fact that we did not want to risk contaminating the cell with another fluid.For this reason the intensity data is only reliable enough to determine the zero angle intercepts.)

TABLE XXX

Interpolated Zero Angle Intensities Obtained From The Intensity Data

$\Delta T(^{o}C)$	I(arbitrary)
9.0	0.481
3.0	1.94
1.50	4.48
1.00	7.46
0.700	11 7
0.500	17.6
0.300	33.2
0.200	56.2
0.150	83.3
0.100	142
0.070	186
0.050	318
0.040	424
0.030	625
0.020	862
0.015	1370
0.010	2130

TABLE XXXI

Isothermal Compressibilities Calculated From The Interpolated Zero Angle Intensity Data

$\Delta T(^{o}C)$	$K_T(atm^{-1})$
9.0	0.0876
3.0	0.353
1.50	0.817
1.00	1.36
0.700	2.12
0.500	3.21
0.300	6.05
0.200	10.2
0.150	15.2
0.100	25.8
0.070	33.8
0.050	57.9
0.040	86.7
0.030	114
0.020	157
0.015	249
0.010	388

TABLE XXXII

Isothermal Compressibilities Calculated From The 12.85cm Path Length Cell Turbidity Data

$\Delta T(^{o}C)$	$K_T(atm^{-1})$
10.59	0.0811
8.266	0.119
6.304	0.146
4.931	0.191
3.853	0.250
2.877	0.366
2.092	0.551
1.505	0.820
1.018	1.325
0.822	1.720
0.646	2.370
0.510	3.007
0.532	2.830
0.697	2.070
0.893	1.530
1.236	1.030
1.738	0.687
1.822	0.681
1.892	0.650
3.930	0.274
5.500	0.189
10.46	0.0791

TABLE XXXIII

Ethane Linewidth Data

(The data are given in exponential format to the base 10)

$\Delta T(^{\circ}C)$	$\Gamma(sec^{-1})$	$\Gamma_s(sec^{-1})$	$k(cm^{-1})$	$\frac{6\pi\Lambda\Gamma_s}{BTk^3}$	$k\xi$
0.127	7.87E 1	6.83E 1	3.77E 3	1.19E 2	9.31E-3
0.134	2.10E 2	1.79E 2	6.29E 3	6.75E 1	1.50E-2
0.127	2.07E 2	1.78E 2	6.29E 3	6.72E 1	1.55E-2
0.093	1.64E 2	1.45E 2	6.29E 3	5.51E 1	1.90E-2
0.084	1.56E 2	1.38E 2	6.29E 3	5.29E 1	2.02E-2
0.234	5.81E 2	4.62E 2	8.81E 3	6.22E 1	1.47E-2
0.221	6.13E 2	5.01E 2	8.81E 3	6.77E 1	1.52E-2
0.196	5.64E 2	4.68E 2	8.81E 3	6.34E 1	1.64E-2
0.161	5.08E 2	4.32E 2	8.81E 3	5.89E 1	1.87E-2
0.084	2.95E 2	2.61E 2	8.81E 3	3.63E 1	2.84E-2
0.065	2.56E 2	2.31E 2	8.81E 3	3.23E 1	3.34E-2
5.193	1.88E 4	7.69E 3	1.34E 4	2.70E 2	3.03E-3
4.214	1.58E 4	6.99E 3	1.34E 4	2.46E 2	3.47E-3
3.274	2.22E 4	5.68E 3	1.34E 4	2.00E 2	4.08E-3
2.980	1.08E 4	4.89E 3	1.34E 4	1.73E 2	4.34E-3
2.671	9.66E 3	4.47E 3	1.34E 4	1.58E 2	4.65E-3
2.653	9.98E 3	4.84E 3	1.34E 4	1.71E 2	4.67E-3
2.379	9.48E 3	4.97E 3	1.34E 4	1.76E 2	5.01E-3
2.183	8.47E 3	4.38E 3	1.34E 4	1.55E 2	5.30E-3
2.015	7.39E 3	3.66E 3	1.34E 4	1.30E 2	5.58E-3
1.821	7.18E 3	3.88E 3	1.34E 4	1.38E 2	5.95E-3
1.675	6.97E 3	3.98E 3	1.34E 4	1.42E 2	6.28E-3
1.429	5.88E 3	3.41E 3	1.34E 4	1.22E 2	6.96E-2

TABLE XXXIII continued

$\Delta T(^{o}C)$	$\Gamma(sec^{-1})$	$\Gamma_s(sec^{-1})$	$k(cm^{-1})$	$\frac{6\pi\Gamma_s\eta}{BTk^3}$	$k\xi$
1.300	5.36E 3	3.15E 3	1.34E 4	1.14E 2	7.40E-3
1.150	4.87E 3	2.96E 3	1.34E 4	1.07E 2	8.00E-3
1.051	4.52E 3	2.81E 3	1.34E 4	1.02E 2	8.48E-3
0.956	4.11E 3	2.58E 3	1.34E 4	9.41E 1	9.02E-3
0.811	3.80E 3	2.55E 3	1.34E 4	9.34E 1	1.00E-2
0.693	3.40E 3	2.36E 3	1.34E 4	8.70E 1	1.11E-2
0.595	2.94E 3	2.08E 3	1.34E 4	7.70E 1	1.22E-2
0.592	2.90E 3	2.04E 3	1.34E 4	7.55E 1	1.23E-2
0.504	2.66E 3	1.95E 3	1.34E 4	7.27E 1	1.36E-2
0.395	2.17E 3	1.64E 3	1.34E 4	6.17E 1	1.59E-2
0.297	1.71E 3	1.34E 3	1.34E 4	5.09E 1	1.91E-2
0.221	1.49E 3	1.21E 3	1.38E 4	4.22E 1	2.39E-2
0.161	1.20E 3	1.02E 3	1.38E 4	3.57E 1	2.93E-2
0.093	8.64E 2	7.69E 2	1.38E 4	2.75E 1	4.17E-2
0.065	6.84E 2	6.22E 2	1.38E 4	2.25E 1	5.26E-2
6.817	3.19E 4	1.05E 4	1.59E 4	2.21E 2	3.02E-3
3.924	2.03E 4	8.93E 3	1.59E 4	1.88E 2	4.31E-3
6.164	3.94E 4	1.38E 4	1.84E 4	1.87E 2	3.73E-3
4.906	3.11E 4	1.13E 4	1.84E 4	1.53E 2	4.32E-3
3.274	2.20E 4	9.56E 3	1.84E 4	1.30E 2	5.61E-3
2.671	1.97E 4	9.96E 3	1.84E 4	1.35E 2	6.39E-3
2.653	1.97E 4	9.99E 3	1.84E 4	1.36E 2	6.42E-3
2.379	1.69E 4	8.36E 3	1.84E 4	1.14E 2	6.89E-3
2.183	1.62E 4	8.53E 3	1.84E 4	1.16E 2	7.28E-3
2.018	1.52E 4	8.13E 3	1.84E 4	1.11E 2	7.66E-3
1.821	1.42E 4	7.96E 3	1.84E 4	1.09E 2	8.18E-3

TABLE XXXIII continued

$\Delta T(^{\circ}C)$	$\Gamma(sec^{-1})$	$\Gamma_s(sec^{-1})$	$k(cm^{-1})$	$\frac{6\pi\Omega\Gamma_s}{BTk^3}$	$k\xi$
1.675	1.28E 4	7.21E 3	1.84E 4	9.91E 1	8.64E-3
1.429	1.14E 4	6.71E 3	1.84E 4	9.27E 1	9.57E-3
0.221	2.74E 3	2.23E 3	1.89E 4	3.06E 1	3.26E-2
3.924	3.48E 4	1.50E 4	2.10E 4	1.38E 2	5.67E-3
0.041	1.59E 3	1.46E 3	2.64E 4	7.74E 0	1.35E-1
0.039	1.61E 3	1.49E 3	2.64E 4	7.90E 0	1.39E-1
0.028	1.37E 3	1.29E 3	2.64E 4	6.89E 0	1.72E-1
0.065	8.28E 3	7.40E 3	5.13E 4	5.25E 0	1.95E-1
0.041	6.18E 3	5.66E 3	5.13E 4	4.08E 0	2.62E-1
0.039	6.65E 3	6.16E 3	5.13E 4	4.44E 0	2.71E-1
0.395	4.74E 4	3.55E 4	6.36E 4	1.25E 1	7.56E-2
0.221	4.37E 4	3.53E 4	7.59E 4	7.46E 0	1.31E-1
0.196	3.99E 4	3.27E 4	7.59E 4	6.93E 0	1.42E-1
0.161	3.43E 4	2.85E 4	7.59E 4	6.09E 0	1.61E-1
0.134	3.06E 4	2.60E 4	7.59E 4	5.59E 0	1.81E-1
0.127	2.93E 4	2.50E 4	7.59E 4	5.37E 0	1.87E-1
0.093	2.35E 4	2.05E 4	7.59E 4	4.45E 0	2.29E-1
0.065	1.84E 4	1.64E 4	7.59E 4	3.60E 0	2.88E-1
0.041	1.45E 4	1.33E 4	7.59E 4	2.96E 0	3.88E-1
0.039	1.58E 4	1.47E 4	7.59E 4	3.27E 0	4.00E-1
0.693	1.49E 5	1.05E 5	8.75E 4	1.39E 1	7.24E-2
0.592	1.27E 5	9.06E 4	8.75E 4	1.21E 1	8.00E-2
0.297	7.31E 4	5.71E 4	8.75E 4	7.79E 0	1.25E-1
0.395	1.06E 5	8.32E 4	8.79E 4	1.11E 1	1.04E-1
0.221	5.78E 4	4.64E 4	8.79E 4	6.30E 0	1.52E-1
0.234	7.74E 4	6.16E 4	9.98E 4	5.71E 0	1.66E-1
0.196	6.86E 4	5.59E 4	9.98E 4	5.20E 0	1.86E-1

TABLE XXXIII continued

$\Delta T(^{\circ}C)$	$\Gamma(sec^{-1})$	$\Gamma_s(sec^{-1})$	$k(cm^{-1})$	$\frac{6\pi\eta\Gamma_s}{BTk^3}$	$k\xi$
0.161	6.21E 4	5.19E 4	9.98E 4	4.87E 0	2.11E-1
0.134	5.25E 4	4.43E 4	9.98E 4	4.18E 0	2.38E-1
0.127	5.15E 4	4.38E 4	9.98E 4	4.13E 0	2.46E-1
0.121	5.00E 4	4.27E 4	9.98E 4	4.04E 0	2.54E-1
0.104	4.46E 4	3.85E 4	9.98E 4	3.66E 0	2.80E-1
0.084	4.05E 4	3.57E 4	9.98E 4	3.41E 0	3.21E-1
0.065	3.44E 4	3.07E 4	9.98E 4	2.96E 0	3.79E-1
0.041	2.64E 4	2.41E 4	9.98E 4	2.36E 0	5.10E-1
0.221	9.83E 4	7.98E 4	1.12E 5	5.31E 0	1.92E-1
0.234	1.25E 5	1.01E 5	1.23E 5	5.00E 0	2.05E-1
0.196	1.14E 5	9.42E 4	1.23E 5	4.69E 0	2.30E-1
0.134	8.18E 4	6.90E 4	1.23E 5	3.48E 0	2.93E-1
0.127	8.17E 4	6.96E 4	1.23E 5	3.51E 0	3.04E-1
0.121	8.00E 4	6.86E 4	1.23E 5	3.47E 0	3.13E-1
0.104	7.19E 4	6.22E 4	1.23E 5	3.16E 0	3.45E-1
0.093	6.48E 4	5.63E 4	1.23E 5	2.87E 0	3.71E-1
0.084	5.68E 4	4.91E 4	1.23E 5	2.51E 0	3.96E-1
0.065	4.84E 4	4.25E 4	1.23E 5	2.19E 0	4.67E-1
0.041	4.21E 4	3.82E 4	1.23E 5	2.00E 0	6.28E-1
0.028	3.77E 4	3.48E 4	1.23E 5	1.84E 0	8.04E-1
0.221	1.39E 5	1.12E 5	1.34E 5	4.25E 0	2.32E-1
0.034	4.98E 4	4.56E 4	1.34E 5	1.84E 0	7.74E-1
0.221	1.60E 5	1.28E 5	1.45E 5	3.84E 0	2.51E-1
0.093	9.26E 4	8.00E 4	1.45E 5	2.47E 0	4.38E-1
0.041	6.30E 4	5.70E 4	1.45E 5	1.81E 0	7.42E-1
0.028	5.72E 4	5.26E 4	1.45E 5	1.69E 0	9.49E-1

TABLE XXXIII continued

$\Delta T(^{\circ}C)$	$\Gamma(sec^{-1})$	$\Gamma_s(sec^{-1})$	$k(cm^{-1})$	$\frac{6\pi\Lambda\Gamma_s}{BTk^3}$	$k\xi$
0.033	6.85E 4	6.22E 4	1.56E 5	1.60E 0	9.17E-1
0.018	7.88E 4	7.31E 4	1.66E 5	1.58E 0	1.44E 0
0.033	9.14E 4	8.23E 4	1.76E 5	1.46E 0	1.04E 0
5.111	1.34E 4	4.92E 3	1.18E 4	2.57E 2	2.68E-3
3.242	9.30E 3	4.32E 3	1.18E 4	2.27E 2	3.60E-3
2.062	6.38E 3	3.44E 3	1.18E 4	1.81E 2	4.82E-3
1.279	4.06E 3	2.40E 3	1.18E 4	1.29E 2	6.55E-3
0.786	2.86E 3	1.93E 3	1.18E 4	1.05E 2	8.96E-3
0.609	2.30E 3	1.62E 3	1.18E 4	8.92E 2	1.06E-2
0.412	1.62E 3	1.20E 3	1.18E 4	6.68E 2	1.36E-2
0.237	1.12E 3	9.08E 2	1.18E 4	5.15E 2	1.94E-2
0.140	7.33E 2	6.20E 2	1.18E 4	3.58E 2	2.72E-2
0.061	4.30E 2	3.88E 2	1.18E 4	2.30E 2	4.63E-2
0.011	1.32E 2	1.27E 2	1.18E 4	7.88E 0	1.37E-1
0.011	1.41E 2	1.36E 2	1.18E 4	8.46E 0	1.37E-1
0.011	1.32E 2	1.26E 2	1.18E 4	7.86E 0	1.37E-1
0.004_7	6.80E 1	6.61E 1	1.18E 4	4.22E 0	2.42E-1
0.004_7	6.58E 1	6.39E 1	1.18E 4	4.08E 0	2.42E-1
0.002_8	5.72E 1	5.62E 1	1.18E 4	3.64E 0	3.38E-1
0.003_4	6.07E 1	5.94E 1	1.18E 4	3.82E 0	2.98E-1
0.004_0	6.41E 1	6.25E 1	1.18E 4	4.01E 0	2.69E-1
0.004_6	6.89E 1	6.71E 1	1.18E 4	4.29E 0	2.46E-1
6.080	7.56E 4	2.90E 4	2.51E 4	1.55E 2	5.13E-3
4.100	5.21E 4	2.22E 4	2.51E 4	1.19E 2	6.62E-3
1.640	2.33E 4	1.31E 4	2.51E 4	7.10E 1	1.19E-2
1.022	1.63E 4	1.05E 4	2.51E 4	5.80E 1	1.62E-2

TABLE XXXIII continued

$\Delta T(^{o}C)$	$\Gamma(sec^{-1})$	$\Gamma_s(sec^{-1})$	$k(cm^{-1})$	$\frac{6\pi\eta\Gamma_s}{BTk^3}$	$k\xi$
0.434	8.59E 3	6.53E 3	2.51E 4	3.71E 1	2.81E-2
0.082	2.06E 3	1.80E 3	2.51E 4	1.08E 1	8.25E-2
0.028	1.12E 3	1.05E 3	2.51E 4	6.48E 0	1.63E-1
0.028	1.12E 3	1.05E 3	2.51E 4	6.48E 0	1.63E-1
0.013	6.72E 2	6.41E 2	2.51E 4	4.06E 0	2.66E-1
0.013	6.70E 2	6.39E 2	2.51E 4	4.05E 0	2.66E-1
0.013	6.76E 2	6.46E 2	2.51E 4	4.09E 0	2.66E-1
0.010	5.94E 2	5.71E 2	2.51E 4	3.64E 0	3.13E-1
0.010	5.97E 2	5.73E 2	2.51E 4	3.66E 0	3.13E-1
0.005_4	4.12E 2	4.00E 2	2.51E 4	2.60E 0	4.74E-1
0.005_4	4.12E 2	4.00E 2	2.51E 4	2.60E 0	4.74E-1
0.205	1.15E 5	9.44E 4	1.22E 5	4.82E 0	2.21E-1
0.132	8.43E 4	7.20E 4	1.22E 5	3.73E 0	2.93E-1
0.082	5.11E 4	4.37E 4	1.22E 5	2.30E 0	3.99E-1
0.048	4.52E 4	4.08E 4	1.22E 5	2.18E 0	5.63E-1
0.032	3.87E 4	3.56E 4	1.22E 5	1.93E 0	7.31E-1
0.014	3.22E 4	3.03E 4	1.22E 5	1.68E 0	1.24E 0
0.006_6	2.94E 4	2.80E 4	1.22E 5	1.59E 0	2.02E 0
0.003_1	2.54E 4	2.40E 4	1.22E 5	1.40E 0	3.29E 0
0.295	1.97E 5	1.53E 5	1.44E 5	4.67E 0	2.07E-1
0.152	1.32E 5	1.11E 5	1.44E 5	3.45E 0	3.17E-1
0.107	1.05E 5	9.08E 4	1.44E 5	2.86E 0	3.97E-1
0.029	5.47E 4	5.01E 4	1.44E 5	1.64E 0	9.23E-1
0.018	4.51E 4	4.16E 4	1.44E 5	1.38E 0	1.26E 0
0.013_6	4.61E 4	4.29E 4	1.44E 5	1.44E 0	1.50E 0
0.014_1	4.94E 4	4.61E 4	1.44E 5	1.54E 0	1.47E 0

TABLE XXXIII continued

$\Delta T(^{\circ}C)$	$\Gamma(sec^{-1})$	$\Gamma_s(sec^{-1})$	$k(cm^{-1})$	$\frac{6\pi\eta\Gamma_s}{BTk^3}$	$k\xi$
0.014_7	4.52E 4	4.19E 4	1.44E 5	1.40E 0	1.43E 0
0.015_0	4.30E 4	3.97E 4	1.44E 5	1.33E 0	1.41E 0
0.015_8	4.46E 4	4.12E 4	1.44E 5	1.38E 0	1.36E 0
0.011_0	4.58E 4	4.27E 4	1.44E 5	1.44E 0	1.72E 0
0.011_5	4.63E 4	4.33E 4	1.44E 5	1.46E 0	1.67E 0
0.012_0	4.66E 4	4.35E 4	1.44E 5	1.46E 0	1.63E 0
0.012_4	4.84E 4	4.52E 4	1.44E 5	1.52E 0	1.59E 0
0.007_4	4.67E 4	4.39E 4	1.44E 5	1.50E 0	2.22E 0
0.007_4	4.59E 4	4.31E 4	1.44E 5	1.47E 0	2.22E 0
0.007_4	4.44E 4	4.17E 4	1.44E 5	1.42E 0	2.22E 0
0.006_1	4.45E 4	4.18E 4	1.44E 5	1.43E 0	2.51E 0
0.005_9	4.21E 4	3.94E 4	1.44E 5	1.35E 0	2.57E 0
0.005_6	4.23E 4	3.96E 4	1.44E 5	1.36E 0	2.66E 0
0.005_4	4.52E 4	4.26E 4	1.44E 5	1.46E 0	2.72E 0
0.003_6	4.50E 4	4.24E 4	1.44E 5	1.48E 0	3.53E 0
0.003_4	4.63E 4	4.37E 4	1.44E 5	1.52E 0	3.66E 0
0.003_2	4.36E 4	4.10E 4	1.44E 5	1.43E 0	3.81E 0
0.003_0	4.34E 4	4.08E 4	1.44E 5	1.43E 0	3.97E 0
0.000_8	4.27E 4	4.00E 4	1.44E 5	1.45E 0	9.30E 0
0.092	1.38E 5	1.21E 5	1.65E 5	2.53E 0	5.02E-1
0.064	1.02E 5	8.96E 4	1.65E 5	1.90E 0	6.34E-1
0.038	7.96E 4	7.13E 4	1.65E 5	1.54E 0	8.80E-1
0.023	7.36E 4	6.74E 4	1.65E 5	1.47E 0	1.21E 0
0.018	7.01E 4	6.45E 4	1.65E 5	1.42E 0	1.43E 0
0.010	6.99E 4	6.51E 4	1.65E 5	1.46E 0	2.04E 0
0.008_2	7.83E 4	7.36E 4	1.65E 5	1.66E 0	2.38E 0

TABLE XXXIII continued

$\Delta T(^{o}C)$	$\Gamma(sec^{-1})$	$\Gamma_s(sec^{-1})$	$k(cm^{-1})$	$\frac{6\pi\eta\Gamma_s}{BTk^3}$	$k\xi$
0.003_2	6.87E 4	6.43E 4	1.65E 5	1.49E 0	4.37E 0
0.002_0	7.28E 4	6.83E 4	1.65E 5	1.60E 0	5.91E 0
0.160	2.21E 5	1.85E 5	1.80E 5	2.98E 0	3.82E-1
0.084	1.47E 5	1.28E 5	1.80E 5	2.10E 0	5.76E-1
0.058	1.20E 5	1.06E 5	1.80E 5	1.77E 0	7.30E-1
0.041	1.02E 5	9.06E 4	1.80E 5	1.52E 0	9.16E-1
0.022	8.89E 4	8.09E 4	1.80E 5	1.38E 0	1.35E 0
0.005	9.03E 4	8.42E 4	1.80E 5	1.51E 0	3.56E 0
0.015	9.51E 4	8.81E 4	1.80E 5	1.53E 0	1.77E 0
0.006_3	8.84E 4	8.22E 4	1.80E 5	1.46E 0	3.06E 0
0.003_4	8.67E 4	8.06E 4	1.80E 5	1.46E 0	4.56E 0
0.002_2	9.12E 4	8.51E 4	1.80E 5	1.56E 0	6.03E 0
0.002_2	8.58E 4	7.97E 4	1.80E 5	1.46E 0	6.03E 0
0.002_2	8.44E 4	7.82E 4	1.80E 5	1.43E 0	6.03E 0
0.069	2.49E 5	2.15E 5	2.36E 5	1.56E 0	8.65E-1
0.022	1.92E 5	1.72E 5	2.36E 5	1.29E 0	1.78E 0
0.012	1.97E 5	1.79E 5	2.36E 5	1.37E 0	2.66E 0
5.831	3.93E 4	1.54E 4	1.84E 4	2.08E 2	3.87E-3
1.527	1.24E 4	7.33E 3	1.84E 4	1.01E 2	9.17E-3
1.150	9.63E 3	6.03E 3	1.84E 4	8.41E 1	1.10E-2
0.811	7.43E 3	5.07E 3	1.84E 4	7.15E 1	1.38E-2
0.693	6.71E 3	4.75E 3	1.84E 4	6.74E 1	1.52E-2
0.595	5.75E 3	4.12E 3	1.84E 4	5.88E 1	1.68E-2
0.395	4.37E 3	3.38E 3	1.84E 4	4.89E 1	2.19E-2
7.509	6.58E 4	2.52E 4	2.10E 4	2.31E 2	3.74E-3
6.817	6.01E 4	2.36E 4	2.10E 4	2.17E 2	3.98E-3

TABLE XXXIII continued

$\Delta T(^{o}C)$	$\Gamma(sec^{-1})$	$\Gamma_s(sec^{-1})$	$k(cm^{-1})$	$\frac{6\pi\Omega\Gamma_s}{BTk^3}$	$k\xi$
6.189	5.28E 4	1.97E 4	2.10E 4	1.82E 2	4.23E-3
5.594	4.84E 4	1.89E 4	2.10E 4	1.74E 2	4.52E-3
1.918	1.97E 4	1.11E 4	2.10E 4	1.04E 2	9.00E-3
1.675	5.65E 4	3.20E 4	3.85E 4	4.84E 1	1.80E-2
1.150	4.09E 4	2.52E 4	3.85E 4	3.87E 1	2.30E-2
0.121	3.13E 4	2.72E 4	7.58E 4	5.86E 1	1.93E-1
1.051	1.95E 5	1.22E 5	8.75E 4	1.60E 1	5.54E-2
0.693	1.49E 5	1.05E 5	8.75E 4	1.39E 1	7.24E-2
0.592	1.27E 5	9.06E 4	8.75E 4	1.21E 1	8.01E-2
0.221	7.79E 4	6.32E 4	9.98E 4	5.86E 0	1.72E-1
0.036	3.58E 4	3.31E 4	1.12E 5	2.33E 0	6.20E-1
0.234	1.79E 5	1.44E 5	1.45E 5	4.33E 0	2.42E-1
0.028	8.65E 4	7.96E 4	1.66E 5	1.70E 0	1.09E 0
0.013	9.96E 4	9.28E 4	1.80E 5	1.61E 0	1.89E 0

The following expressions for C_p, λ_T^n, Ω, and ξ were used in calculating columns 3,5 and 6 from columns 1,2 and 4:

$$C_p = 0.67-0.06\ln(\Delta T)+T(\Delta T/T_c)^{-1.225}x1.619x10^{-4}$$

$$\lambda_T^n = 9.26x10^{-5}+(3.13x10^{-7})(\Delta T+32.18)$$

$$=(191.3+84.3(\Delta T/T_c)+\Delta\Omega)x10^{-6}, \text{with } \Delta\Omega \equiv 0 \text{ for } T \geq 2.18^{o}C, \Delta\Omega = -6.58\ln(\Delta T/T_c)$$

$$-32.52, \text{for } \Delta T < 2.18 \text{ ; and } \quad \xi = 1.64x10^{-8}(\Delta T/T_c)^{-0.644} .$$

TABLE XXXIV

Ethane Thermal Diffusivities, χ, Thermal Conductivities, λ_T, and Excess Thermal Conductivities, λ_T^x, as a Function of ΔT. The Units are Cm^2/Sec and $Cal./Cm^2\text{-}Sec(C^o/Cm)$ Respectively. The Data are Given in Exponential Format to the Base 10.

$\Delta T(^oC)$	χ	λ_T	λ_T^x
7.509	1.50E-4	1.62E-4	5.63E-5
6.817	1.31E-4	1.58E-4	5.23E-5
6.189	1.20E-4	1.61E-4	5.55E-5
6.164	1.16E-4	1.56E-4	5.03E-5
5.831	1.16E-4	1.65E-4	5.99E-5
5.594	1.10E-4	1.65E-4	5.98E-5
5.193	1.04E-4	1.70E-4	6.50E-5
4.906	9.17E-5	1.59E-4	5.42E-5
4.214	8.76E-5	1.81E-4	7.61E-5
3.924	7.97E-5	1.79E-4	7.40E-5
3.274	6.64E-5	1.84E-4	7.92E-5
2.980	6.00E-5	1.85E-4	8.08E-5
2.671	5.59E-5	1.96E-4	9.19E-5
2.653	5.70E-5	2.02E-4	9.72E-5
2.379	5.13E-5	2.06E-4	1.02E-4
2.183	4.75E-5	2.11E-4	1.07E-4
2.016	4.29E-5	2.10E-4	1.06E-4
1.821	4.08E-5	2.26E-4	1.22E-4
1.675	3.83E-5	2.34E-4	1.30E-4
1.527	3.64E-5	2.48E-4	1.44E-4
1.429	3.31E-5	2.44E-4	1.40E-4
1.300	2.98E-5	2.47E-4	1.43E-4
1.150	2.77E-5	2.66E-4	1.62E-4
1.051	2.53E-5	2.71E-4	1.67E-4
0.956	2.29E-5	2.74E-4	1.70E-4
0.811	2.15E-5	3.15E-4	2.11E-4
0.693	1.94E-5	3.42E-4	2.39E-4
0.595	1.66E-5	3.54E-4	2.51E-4
0.592	1.64E-5	3.51E-4	2.47E-4
0.504	1.48E-5	3.85E-4	2.82E-4
0.395	1.25E-5	4.37E-4	3.33E-4
0.297	9.54E-6	4.74E-4	3.70E-4

TABLE XXXIV continued

$\Delta T(^{o}C)$	χ	λ_T	λ_T^x
0.234	7.85E-6	5.21E-4	4.18E-4
0.221	7.60E-6	5.42E-4	4.38E-4
0.196	7.05E-6	5.82E-4	4.78E-4
0.192	7.05E-6	5.96E-4	4.93E-4
0.161	6.19E-6	6.50E-4	5.46E-4
0.134	5.17E-6	6.79E-4	5.76E-4
0.127	5.17E-6	7.25E-4	6.22E-4
0.121	5.05E-6	7.51E-4	6.48E-4
0.104	4.35E-6	7.79E-4	6.76E-4
0.093	3.99E-6	8.19E-4	7.16E-4
0.084	3.74E-6	8.70E-4	7.66E-4
0.065	3.16E-6	1.01E-3	9.02E-4
0.041	2.25E-6	1.26E-3	1.16E-3
0.039	2.29E-6	1.36E-3	1.26E-3
0.033	1.85E-6	1.35E-3	1.25E-3
5.110	9.67E-5	1.60E-4	5.52E-5
3.242	6.74E-5	1.88E-4	8.40E-5
2.062	4.62E-5	2.20E-4	1.16E-4
1.279	2.94E-5	2.48E-4	1.45E-4
0.786	2.07E-5	3.14E-4	2.11E-4
0.609	1.67E-5	3.45E-4	2.42E-4
0.412	1.17E-5	3.91E-4	2.88E-4
0.237	8.14E-6	5.32E-4	4.29E-4
0.140	5.31E-6	6.61E-4	5.58E-4
0.061	3.11E-6	1.06E-3	9.59E-4
0.011	9.69E-7	2.60E-3	2.50E-3
0.004_7	4.53E-7	3.60E-3	3.50E-3
0.004_6	4.82E-7	3.93E-3	3.82E-3
0.004_0	4.45E-7	4.30E-3	4.20E-3
0.003_4	4.17E-7	4.93E-3	4.83E-3
0.002_8	3.88E-7	5.81E-3	5.71E-3
0.002_2	3.45E-7	6.95E-3	6.84E-3
6.080	1.20E-4	1.63E-4	5.79E-5
4.100	8.26E-5	1.76E-4	7.13E-5
2.618	5.21E-5	1.87E-4	8.29E-5
1.640	3.69E-5	2.31E-4	1.27E-4
1.022	2.58E-5	2.85E-4	1.82E-4
0.434	1.36E-5	4.25E-4	3.22E-4
0.028	1.76E-6	1.55E-3	1.45E-3
0.013	1.02E-6	2.28E-3	2.18E-3
0.010	8.91E-7	2.71E-3	2.60E-3
0.005_4	5.76E-7	3.86E-3	3.76E-3

TABLE XXXIV continued

T(°C)	χ	λ_T	λ_T^x
0.350	1.12E-5	4.54E-4	3.50E-4
0.250	8.63E-6	5.29E-4	4.25E-4
0.150	5.93E-6	6.78E-4	5.75E-4
0.075	3,53E-6	9.43E-4	8.40E-4
0.050	2.61E-6	1.15E-3	1.04E-3
0.025	1.56E-6	1.60E-3	1.49E-3
0.020	1.32E-6	1.78E-3	1.68E-3
0.016	1.12E-6	1.98E-3	1.88E-3
0.007_6	6.33E-7	2.84E-3	2.73E-3

(The estimated accuracies are as follows: in ΔT about $0.0006^{o}C$-$0.001^{o}C$, in χ about 3%, in λ_T about 6-10% and in λ_T^x it changes from about 20% for the smallest values to about 6-10% for $\lambda_T^x > 10^{-4}$. The estimated errors in the thermal conductivities are larger because one has to use C_p and normal thermal conductivity data to calculate them from the thermal diffusivity data. The following expressions were used for C_p and λ_T^n :

$$C_p = 0.67 - 0.06\ln(\Delta T) + T(\Delta T/T_c)^{-1.225} \times 1.62 \times 10^{-4}$$

$$\lambda_T^n = 9.3 \times 10^{-5} + (3.19 \times 10^{-7}) \times (\Delta T + 32.2) \quad .)$$

Proposition I

Determination of Spectrum of Light Scattered by a Dilute Ternary Solution

Abstract

The spectrum of light scattered by a dilute ternary solution is determined.It is found that the spectrum consists of three peaks,two Brillouin peaks and a central peak which is the sum of three Lorentzians.

Introduction[1]

The intensity of the scattered light is related to the space-time Fourier transform of the autocorrelation function of the dielectric constant.To calculate this quantity the approach suggested by Landau and Placzek[2] is used in this work.The space and time response of the system to a perturbation from the equilibrium state is calculated using (i) linearized hydrodynamic equations to determine the modes by which the system returns to equilibrium as well as the relative amplitudes of each mode,and (ii) the thermodynamic fluctuation theory to provide initial values for the correlation functions. The case where the multicomponent diffusion coefficients can be replaced by the effective diffusivities is considered. We neglect hydrodynamic effects from Dufour and Soret effects.The latter can be done because of the fact that

our system is very dilute with respect to the solutes.

Light Scattering Formalism

In thermodynamic fluctuation theory the random thermal motion of molecules in a fluid is considered to produce fluctuations in a set of complete, local thermodynamic variables. These fluctuations result in local variations in the dielectric constant and therefore scattering light. The intensity of the light is given by the expression[3]

$$I(R,\underline{k},w) = I_o(Nk_o^4/32\pi^3R^2)\ \sin^2\phi\ S(\underline{k},w) \qquad (1)$$

where $\underline{k}$ is the change in the wave vector and $\underline{w}$ is the change in the frequency of the incident light upon scattering. R is the distance to the point of observation, ϕ is the angle between the electric vector of the incident light and the scattering plane, N is the Avagadro's number, I_o is the incident intensity and I is the scattered intensity. The relationship between the magnitude of $\underline{k}$ and the incident wave vector k_o is:

$$k = 2nk_o\sin(\Theta/2) \qquad (2)$$

where n is the refractive index and Θ is the scattering angle. In equation (1) $S(\underline{k},w)$ is the generalised structure factor defined by:

$$S(\underline{k},w) = 2\mathrm{Re}\int_0^\infty dt\int d\underline{r}d\underline{r}'\langle\delta\epsilon(\underline{r}+\underline{r}',t)\,\delta\epsilon(\underline{r}',0)\rangle x \exp(i(\underline{k}.\underline{r}-wt)) \quad (3)$$

where $\delta\epsilon(\underline{r},t)$ is the fluctuation in the local dielectric constant at the point $\underline{r}$ at time t.In terms of Fourier-Laplace transforms

$$S(\underline{k},w) = 2\mathrm{Re}\langle\epsilon(\underline{k},iw)\epsilon(-\underline{k})\rangle, \quad (4)$$

$$\hat{\epsilon}(\underline{k},s) = \int_0^\infty dt\int dr\,\delta\epsilon(\underline{r},t)\exp(i\underline{k}.\underline{r}-st) \quad (5)$$

$$\epsilon(\underline{k}) = \int d\underline{r}\,\delta\epsilon(\underline{r},0)\exp(i\underline{k}.r) \; . \quad (6)$$

The caret is used to indicate a Laplace-time transform. If only k is indicated as a variable the time independent initial value is implied.The angular bracket $\langle\ldots\ldots\rangle$ indicates an average over the initial states of the system.Our basic concern is to compute $S(\underline{k},w)$ for a three component solution.

We begin by relating the fluctuations in the local dielectric constant to fluctuations in the local thermodynamic quantities such as temperature,concentration and pressure:

$$\delta\epsilon(\underline{r},t) = (\partial\epsilon/\partial P)_{T,C_1,C_2}\delta P(\underline{r},t) + (\partial\epsilon/\partial T)_{P,C_1,C_2}\delta T(\underline{r},t) + (\partial\epsilon/\partial C_1)_{P,T,C_2}\delta C_1(\underline{r},t) + (\partial\epsilon/\partial C_2)_{P,T,C_1}\delta C_2(\underline{r},t) \; . \quad (7)$$

We shall use the linearized hydrodynamic equations to describe the time dependence of the fluctuations.For this system these are the continuity equation

$$(\partial\rho/\partial t) + \mathrm{div}(\underline{v}) = 0 \ , \tag{8}$$

the longitidunal part of the Navier-Stokes equation

$$\rho_o(\partial\underline{v}/\partial t) = -\mathrm{grad}(p) + (4/3\eta_s+\eta_v)\mathrm{grad}\ \mathrm{div}(\underline{v}), \tag{9}$$

and the two diffusion equations

$$\partial C_1/\partial t = D_1\nabla^2 C_1 \tag{10}$$

$$\partial C_2/\partial t = D_2\nabla^2 C_2 \ , \tag{11}$$

and the energy equation

$$C_p(\partial T/\partial t) + T_o(\partial S/\partial P)_{T,C} = K\nabla^2 T \ . \tag{12}$$

In these equations T is the temperature,C_p is the specific heat at constant pressure,$\underline{v}$ is the mass velocity. Other quantities appearing in these equations are the transport coefficients:K is the thermal conductivity, η_s and η_v are the shear and volume viscosities respectively,D_1 and D_2 are the diffusion coefficients for component 1 and 2.Equilibrium values are denoted by the subscript zero.We would like to emphasize the fact that the above equations are valid for dilute mixtures only.

We must next express eqs.(8)-(12) in terms of the variables that have been chosen to characterize the local state of the fluid.For a ternary fluid we must choose four such variables.While any four independent variables will suffice for the calculation,certain choices will prove a good deal more conveninet than the others.The criterion we shall use to select four state variables (x_1,x_2, x_3,x_4) is that the probability of a fluctuation $W(x_1,x_2,$ $x_3,x_4)$ is statistically independent,ie.e. $W(x_1,x_2,x_3,x_4)=$ $h_1(x_1)h_2(x_2)h_3(x_3)h_4(x_4)$.The Boltzmann principle gives the probability W as

$$W \propto \exp(\Delta S_T/k_B) \qquad (13)$$

where ΔS_T is the change in the entropy of a system plus surroundings caused by the fluctuation.If for convenince we choose our system to contain one gram of solution then,

$$\Delta S_T/k_B = -(1/2k_BT_o)(\delta S\delta T-\delta V\delta P +\delta C_1\delta\mu_1+ \delta C_2\delta\mu_2) \ . \qquad (14)$$

It is easy to show that in the Gaussian approximation $\langle\delta T\delta P\rangle\neq 0$ and $\langle\delta C_1\delta C_2\rangle\neq 0$.Hence the obvious candidates (T,P, C_1,C_2) do not satisfy our criterion of independence.

If we consider the set of variables (Ψ,P,x,C) where

$$\Psi = T-(T_o\alpha_T/C_p\rho_o)P \ , \qquad (15)$$

$$x = C_1+dC_2$$

$$2d = ((\partial\gamma_1/\partial C_2)_{C_1,T,P} + (\partial\gamma_2/\partial C_1)_{T,P,C_2})/(\partial\gamma_1/\partial C_1)_{T,P,C_2} \tag{16}$$

and

$$C = C_2 \tag{17}$$

The set of variables (Ψ,P,x,C) is a unique linear combination of the set (T,P,C_1,C_2) which is a statistically independent set. We express fluctuations in the dielectric constant, in terms of spatial Fourier transforms, as:

$$\epsilon(\underline{k},t) = (\partial\epsilon/\partial P)_{\psi,C,x} P(\underline{k},t) + (\partial\epsilon/\partial\psi)_{P,C,x} \Psi(\underline{k},t) + (\partial\epsilon/\partial x)_{P,C,\psi} x(\underline{k},t) + (\partial\epsilon/\partial C)_{P,x,\psi} C(\underline{k},t) \tag{18}$$

The probability distribution is obtained by substituting for ΔS_T in equation (13) will be used to obtain the quantities $\langle |P(\underline{k})|^2 \rangle$, $\langle |\psi(\underline{k})|^2 \rangle$, $\langle |x(\underline{k})|^2 \rangle$ and $\langle |C(\underline{k})|^2 \rangle$. Since k^{-1} is much grater than the range of molecular correlations this is an acceptable procedure.

The next thing to do is to use equations (8)-(12) to obtain $\psi(\underline{k},t), P(\underline{k},t), x(\underline{k},t), C(\underline{k},t)$.

Calculation of the Correlation Function Matrix

Rewriting the linearised hydrodynamic equations in terms of the variables $\Psi, P, x, C, Y=\mathrm{div}(\underline{v})$:

$$(\partial\rho/\partial T)_{P,C} (\partial\Psi/\partial t) + (1/c_o^2)(\partial P/\partial t) + (\partial\rho/\partial C_1)_{C,P,T} \frac{\partial x}{\partial t} +$$

$$D(\partial C/\partial t) + \rho_o Y = 0 \quad \text{(continued from previous page)} \tag{19}$$

$$\partial x/\partial t = D_1 \nabla^2 x + d(D_2 - D_1)\nabla^2 C \tag{20}$$

$$\partial C/\partial t = D_2 \nabla^2 C \tag{21}$$

$$\partial Y/\partial t = -\nabla^2 P/\rho_o + a\nabla^2 Y \tag{22}$$

$$\partial \Psi/\partial t = \chi \nabla^2 (\Psi + (T_o \alpha_T/\rho_o C_p)P) \tag{23}$$

In terms of Fourier-Laplace transforms this set of equations in matrix form, is :

$$M \cdot \hat{N}(\underline{k},s) = T \cdot N(\underline{k}) \tag{24}$$

Where $N(\underline{k},s)$ is a column vector with the elements $\psi(\underline{k},s)$, $P(\underline{k},s), x(\underline{k},s), C(\underline{k},s), (\underline{k},s)$. The 5X5 matrix M has the form:

$$M = \begin{Bmatrix} s(\partial\rho/\partial T)_{P,C} & s/c_o^2 & s(\partial\rho/\partial C_1)_{P,T,C_2} & Ds & \rho_o \\ 0 & 0 & (s+D_1k^2) & d(D_2-D_1)k^2 & 0 \\ 0 & 0 & 0 & (s+D_2k^2) & 0 \\ 0 & -k^2/\rho_o & 0 & 0 & (s+ak^2) \\ (s+\chi k^2) & (T_o\alpha_T/\rho_o C_p)\chi k^2 & 0 & 0 & 0 \end{Bmatrix}$$

and the matrix T has the form:

$$T = \begin{Bmatrix} (\partial\rho/\partial T)_{P,C} & 1/c_o^2 & (\partial\rho/\partial C_1)_{P,T,C_2} & D & 0 \\ 0 & 0 & 1 & 0 & 0 \\ 0 & 0 & 0 & 1 & 0 \\ 0 & 0 & 0 & 0 & 1 \\ 1 & 0 & 0 & 0 & 0 \end{Bmatrix}$$

The general form of the solutions is:

$$N_i(\underline{k},s) = (1/\det M)\sum_j P_{ij}(\underline{k},s)N_j(\underline{k}) \qquad (25)$$

In the above matrices we have used

$$c_o = ((\partial P/\partial \rho)_{S,C})^2 \text{ ,adiabatic speed of sound} \qquad (26)$$

$$a = (4/3\eta_s + \eta_v)/\rho_o \qquad (27)$$

$$\chi = K/\rho_o C_p \qquad (28)$$

$$D = ((\partial \rho/\partial C_2)_{T,P,C_1} - d(\partial \rho/\partial C_1)_{T,P,C_2}) \qquad (29)$$

We are interested in correlation functions of the form $N_i(\underline{k},s)N_j(-\underline{k})$,from equation (25) it follows that

$$\langle N(\underline{k},s)N(-\underline{k})\rangle = (P_{ij}(\underline{k},s)/\det M)\langle |N_j(\underline{k})|^2\rangle \qquad (30)$$

as we have assumed that N_i are statistically independent.

An expression for the correlation functions is obtained by taking the inverse Laplace transform of eq.(30).

$$N_i(\underline{k},t)N_j(-\underline{k}) = \langle N_j(\underline{k})|^2\rangle /2\pi(\int_{-\infty}^{\infty}((\exp(\ iwt).$$
$$P_{ij}(\underline{k},iw))/\det(M(\underline{k},s))dw \qquad (31)$$

In order to perform this inversion we must obtain the roots of det M.We seek approximate roots of det M considering as small dimensionless quantities $(\chi k/c_o)$,(ak/c_o) $(D_1 k/c_o)$ and $(D_2 k/c_o)$.In typical experiments $k\sim 10^5$ cm^{-1}, and $c_o \sim 10^5$cm/sec,so that these quantities are on the

the order of 10^{-2},10^{-2},$10^{-4}$and 10^{-4} respectively.To the terms linear in small quantities one obtains:

$$\det(M(\underline{k},s)) = (s+D_1k^2)(s+D_2k^2)(s+\chi k^2)(s+ic_ok+\Gamma k^2)x$$
$$(s-ic_ok+\Gamma k^2). \qquad (32)$$

The roots related to the stationary modes (which are exact),

$$s = -D_1k^2 \qquad (33)$$

$$s = -D_2k^2 \qquad (34)$$

the third root which is approximate is:

$$s = -\chi k^2 \qquad (35)$$

and the two roots related to the two propagating modes are (approximate):

$$s = -ic_ok-\Gamma k^2 \qquad (36)$$

$$s = +ic_ok-\Gamma k^2 \qquad (37)$$

where $\Gamma = a/2$.

We are now in a position to take the inverse Laplace transform indicated in equation (31),to terms linear in the designated small quantities one finds:

$$\langle \Psi(k,t)\Psi(-\underline{k}) \rangle / \langle |\Psi(k)|^2 \rangle = (1/c_o^2)\exp(-\chi k^2 t) \qquad (38)$$

$$\langle P(k,t)P(-k) \rangle / \langle |P(k)|^2 \rangle = (1/c_o^2)((\Gamma k/c_o)\exp(-\Gamma k^2 t)+$$
$$\exp(ic_ok t)) \qquad (39)$$

$$\langle x(k,t)x(-k) \rangle / \langle |x(k)|^2 \rangle = \exp(-D_1k^2t) \qquad (40)$$

$$\langle C(k,t)C(-k) \rangle / \langle |C(k)|^2 \rangle = \exp(-D_2k^2t) \qquad (41)$$

with these results and using equation (3) we obtain our final expression for $S(\underline{k},w)$:

$$S(\underline{k},w) = (\partial\epsilon/\partial\psi)^2_{P,C,x}(2k_BT_o{}^2/C_p)(\chi k^2/((\chi k^2)^2+w^2)(c_o^{-2})$$
$$+(c_o^{-2})(\partial\epsilon/\partial P)^2_{C,x,}\ (k_BT_o\rho_o/\beta_s)((\Gamma k^2/((\Gamma k^2)^2+$$
$$(w+c_ok)^2))+(\Gamma k^2/((\Gamma k^2)^2+(w-c_ok)^2)))+$$
$$(\partial\epsilon/\partial x)^2_{T,P,C}(2k_BT_o/(\partial\mu/\partial x)_{P,T,C}).(D_1k^2/((D_1k^2)^2$$
$$+w^2))+(\partial\epsilon/\partial C)^2_{T,P,x}2k_BT_o(D_2k^2/((D_2k^2)^2+w^2))/$$
$$((\partial\nu_2/\partial C)_{P,x,}-d(\partial\nu_1/\partial C)_{P,x}) \qquad (42)$$

where β_s is the adiabatic compressibility and α_T is the coefficient of thermal expansion. Note that all the initial averages of the fluctuations are evaluated and substituted.

Finally we note that from thermodynamics:

$$(\partial\epsilon/\partial P)_{C,x,\psi} = (\partial\epsilon/\partial P)_{T,C,x}+(T_o\alpha_T/\rho_oC_p)(\partial\epsilon/\partial T)_{P,C,x} \qquad (43)$$

$$(\partial\epsilon/\partial C)_{P,T,x}= (\partial\epsilon/\partial C)_{T,P,C} -d(\partial\epsilon/\partial C_2)_{T,P,C_1} \qquad (44)$$

with d being defined as before. This relates the dielectric constant derivatives to measurable quantities.

Discussion

The spectrum associated with a dilute ternary solution consists of three peaks.Two Brillouin peaks centered at frequencies $w=\pm c_o k$ and have a Lorentzian line shape with width Γk^2.The central peak consists of super position of Lorentzians with widths $D_1 k^2$,$D_2 k^2$,and χk^2.

Experimentally the three Lorentzians in the central peak can be resolved if $\chi \gg D_1 \gg D_2$.If the conditions are met determining all three transport coefficients simultaneously by light scattering would be a very attractive way.The above conditions are met by solutions of macromolecules in a binary mixture.

REFERENCES

1. See R. D. Mountain, J. Chem. Phys. 50, 1103 (1969) and Revs. Mod. Phys. 38, 205 (1966) for a more detailed discussion.

2. L. D. Landau and G. Placzek, Physik. Z. Sovjetunion 5, 172 (1934).

3. L. D. Landau and E. Liftschitz, Electrodynamics of Continuous Media, Ch. 14.

Appendix to Proposition I

We would like to add that getting the statistically independent variables and the probability distribution is not a trivial problem, rather complex algebraic manipulations and thermodynamic derivatives are involved.

After expanding ΔS_T given in equation (14) in a Taylor series using the independent variables we get:

$$\Delta S_T/k_B = -(1/2k_BT_o)\Big((\partial S/\partial \psi)_{P,C,x}(\delta\psi)^2 -$$

$$(\beta_s(\partial S/\partial P)_{C,x,\psi}+(\partial V/\partial P)_{C,x,\psi})(\delta P)^2 +$$

$$(\partial \mu_1/\partial x)_{P,C,\psi}(\delta x)^2 + ((\partial \mu_2/\partial C)_{P,x,\psi} -$$

$$d(\partial \mu_1/\partial C)_{P,x,\psi})(\delta C)^2\Big)$$

Also note that μ_1 and μ_2 used here and in the text are not ordinary chemical potentials. For one gram of solution the two are related by:

$$\mu_1 = ((\mu_1'/m_1)-(\mu_2'/m_2)) \; ; \mu_2 = ((\mu_1'/m_1)-(\mu_3'/m_3))$$

where the primed quantities are the normal chemical potentials and m's are the molecular wts.

Using the given expression for $\Delta S_T/k_B$ and evaluating various thermodynamic variables we find the time average of the fluctuations $\langle|C(\underline{k})|^2\rangle$ etc. and substituting in we get the final expression for $S(\underline{k},w)$ given in the text.

Proposition II

Abstract

It is proposed that a heat leak calorimeter be built to measure the heat capacities of pure fluids at constant volume and binary critical mixtures at constant pressure. The proposed calorimeter is mainly for use in the temperature range 10°C to 50°C, where other types of calorimeters are not very accurate.

Introduction

At the moment little heat capacity data exists for both pure fluids and binary mixtures near their critical points. Notable exceptions are; for pure fluids the works of Voronel[1] and Edwards[2], for binary mixtures the works of Cope, Reamer and Pings[3] and Schmidt, Jura and Hildebrand[4].

The main reason for the lack of data is the difficulty of the experiments involved. Adiabatic calorimeters are very hard to construct and operate, ice calorimeters measure the integrated heat capacity all the way down to the ice point and as a result do not yield accurate differential data. Both types of calorimeters require relatively large samples, about 50cc, to obtain good accuracies, but close to the critical point gravity becomes a serious problem and obtaining small fluid heads with large samples require complicated sample vessels.

For pure fluids the important heat capacity is C_v, the heat capacity at constant volume.For binary mixtures the quantity of interest is C_p,the heat capacity at constant pressure.

In recent years several accurate and simple heat leak microcalorimeters were built and used successfully in measuring heats of reactions of biological reactions[5,6], particularly of those that took a long time to reach completion.

It is proposed to modify a heat leak microcalorimeter so as to be able to use it to measure heat capacities within a few millidegrees of the critical point simply and accurately.The proposed modifications are:

(1)-Putting the whole calorimeter into a very good temperature control bath.

(2)-Addition of a very sensitive temperature measuring circuit.

(3)-Operating the calorimeter in a non isothermal fashion to measure heat capacities.

(4)-Design of high pressure constant volume cells to be used with pure fluids and constant pressure cells to be used with binary liquid critical mixtures.

(5)-Modifiying the electrical calibration circuit to use a lead acid battery.

(6)-Modifying the heat flow detection circuit to accomodate

commercially available thermolectric modules in the U.S.A.

(7)-Evacuating the empty space around the sample cells to improve the precision.

The Principle of Operation

In adiabatic calorimeters the sample is thermally insulated from its surroundings as well as possible and the heat leaking into the sample is treated as a small correction.A known amount of electrical energy is dissipated in the sample and the increase in the sample temperature is measured,thus C_v or C_p is calculated from:

$C=(\Delta Q/\Delta T)$-corrections (1)

In the first heat leak calorimeters,used to measure heat capacities of liquids with moderate accuracy,a constant temperature differential was maintained between the shield and the sample together with a recording of temperature as a function of time.Assuming that $Q=K\Delta Tt$, where K is the overall proportionality constant and since ΔT is constant the heat capacity was calculated from:

$C=(Q(t_2)-Q(t_1))/(T(t_2)-T(t_1))$ (2)

t=time

To get an absolute value of Q therefore C the calorimeter had to be calibrated with a sample whose heat capacity was known.Today this type of calorimeter is not used.

In the newer heat leak calorimeters,used to measure heats of reaction,the heat is leaked from the sample to

a surrounding heat sink through the elements used to measure the temperature difference between the sample and the sink.Berzinger and Kitzinger[5] used a thermopile containing about ten to twenty thousand thermocouple junctions in series.Wadso[6] used themoelectric devices instead of thermopiles.

Thermolectric devices are better than thermopiles in three aspects:they have much lower internal resistance, they generate ten times the voltage for the same temperature difference,and finally they have very high thermal conductivities.

When a temperature difference is introduced across a thermolectric module a Seebeck voltage V is produced and the Seebeck coefficient may be written as $a_m=(V/\Delta T)$, this is schematically shown in figure (1).Assuming that the heat conducted across the module is proportional to ΔT :

$$\Delta Q=K_m \Delta T=K_m a_m V \qquad (3)$$

K_m is the module thermal conductivity

and the total heat leaked across the module is given by:

$$Q=\int_o^t \Delta Q dt=\int_o^t K_m a_m V dt = K\int_o^t V dt \qquad (4)$$

Thus by integrating the voltage with time we will be able to measure the heat conducted through the module within a constant factor.The constant of proportionality can be obtained very simply in either of the two ways:

(a)-By generating a known amount of heat in the cell and leaking it out.

(b)-By putting in a sample whose heat capacity is known.

Description of the Calorimeter

(Includes all of the proposed modifications)

The calorimeter consists of four main parts:the water bath used to control the temperature,the metal heat sink, the sample cell assembly,and the electronics needed to amplify and integrate the output voltage from the thermo-electric modules.

The water bath:Since the water bath controls the temperature of the heat sink and in turn the sample cell it has to satisfy two very strict requirements:It should be possible to change the temperature in steps of 0.001°C or better and the temperature control should be very good. These two requirements are actually related due to the fact that one needs to know the temperature change ΔT in order to be able to determine the heat capacity from $C=Q/\Delta T$. Thus if we want to have 1% precision in our measurements taken in 0.001°C steps then the temperature control should be better than 10 micro degrees Centigrade.Finally the water bath should also have a large controlled volume into which the calorimeter can be put.Such a water bath was built and described by M.E.Harvey[7] of the National Bureau of Standards.The following is an excerpt from

the abstract of reference (7):"The bath and its associated temperature controller operate at any temperature between 18°C and 28°C which is not more than 6°C below the ambient temperature.The bath provides a temperature stability of of ± 25°μC over a 24 h period when measured with a 100-sec time constant.The short term stability measured with a 0.7-sec time constant is between ±70μC° and ±7μC° depending on the location within the bath and the magnitude of the energy exchange between the heating and cooling mechanisms.The bath temperature change caused by an ambient temperature change of 2°C is less than 5μ°C".The controller for the water bath was designed by N.T.Larsen(8).

The only change proposed in the water bath is to switch to water cooling instead of cooling by air injection.This would extend the useful temperature range of the water bath greatly from 18°C-28°C to 10°C-50°C.The proposed cooling system consists of a Tamson T3/low circulating water bath and a Neslab freon cooler cooling the circulating bath.Water controlled to ±0.02°C from the circulating bath will be pumped through a bifibrillar cooling coil in the calorimeter bath.

The heat sink:The heat sink is the simplest of all the components of the calorimeter.It is just a cylindrical block of copper which has a central bore into which the cell and the dummy cell assembly fits.It serves three

purposes:Damps out the very short term temperature fluctuations,serves as a source or sink of thermal energy, due to its high thermal conductivity maintains a very uniform temperature on the inner surfaces in contact with the cell assembly.Copper seems to be the best metal suited for use as a heat sink.It has very high thermal conductivity and is resistant to corrosion by water.Figure (2) shows the suggested heat sink design.

The sample cell assembly consists of two parts:The constant volume or constant pressure cell,the thermoelectric modules which detect the heat flow.Figure (3) shows the constant volume cell.The design objectives in designing a constant volume calorimeter cell are:High strength to weight ratio,high thermal conductivity,low heat capacity and finally a high sample volume to total volume ratio. Beryllium-copper alloys meet the material specifications very well.The tensile strength is close to that of steel and the thermal conductivity is close to that of copper. Another problem one has to worry about close to the critical point is the change in density as a function of height due to gravity.The only way to minimise it is to keep the sample height small.Since the effect of gravity on C_v is not known very well it is impossible to predict what sample height will be optimum.Figure (3) was drawn with a sample height of five millimeters.If smaller heights

are needed the design shown in figure (3) can easily be adapted.Figure (4) shows a constant pressure cell to be used for measurements on binary liquid critical mixtures. Since the effect of gravity,if any,is assumed to be much smaller than pure fluids figure (4) was drawn with a proposed sample height of 12mm.The constant volume cell does not have a valve,due to the fact that a valve would introduce a lot of unwanted weight and a possible source of contamination.Instead it is proposed that the cell be loaded at a temperature well above the critical temperature and the soft copper tubing be closed off by pinching it with a clamp.

The thermoelectric modules to be used are Cambion model 801-1015-01.Four of them are needed,two on each side of the sample cell and all four will be connected in series.Each one of these modules have 40 pairs of thermoelectric couples and typically generate 0.0160volts/C^{o}, have resistances of about 0.2 ohms and overall thermal conductivities of 0.60 wat/C^{o}.The modules are made by Cambridge Thermionic Corporation,Cambridge ,Mass. .

To increase the accuracy of the calorimetric measurements a dummy cell assembly having exactly the same physical dimensions as the sample cell assembly is also needed.The dummy cell will either contain nothing or some calorimetric standard fluid.Connected differentially with

the sample cell assembly the output will either be com - pletely due to the sample fluid or it will be the difference of the sample fluid and the standard fluid.

Electronics:The signal from the modules will be amplified by either a Keithley 150B Microvolt Ammeter or by a Hewlett Packard 419A DC Null Voltmeter.The amplified signal will be recorded by a Sargent SR recorder having a ball and disc integrator.Digital recorders and integrators would probably increase the precision as would signal averaging using a signal averager such as Sai 43A made by the Signal Analysis Corporation,but these are expensive additions and are not needed for the calorimeter described here.Electrical calibration circuit will consist of a Nuclear Chicago Model 8600 Scaler Timer,a lead acid battery to supply electrical energy at constant voltage, a standard resistor in series with the calibration heater wound around the sample cell.The potential drop across the heater and the standard resistor will be measured by a Leeds and Northrup K6 Universal Potentiometer.Measurement of absolute temperatures will be done by using a platinum resistance thermometer in series with a standard resistor and the K6 potentiometer.The electrical calibration set up is shown figure (5),the temperature measurement set up is shown in figure (6).The overall calorimeter set up is shown in figure (7).Measurement of

relative temperatures will be made with the bath control thermometer.

Proposed Method of Operation

A typical run will consist of the following steps:

(1)-Load the cell at a temperature higher than the critical and seal the loading tube.

(2)-Determine the density by using either literature PVT data or by weighing the cell.Small changes in the density can be made by crushing the loading tubing.

(3)-Assemble the cell and the thermoelectric modules.

(4)-Put the cell into the copper heat sink evacuate the air out and seal the vacuum.

(5)-Put the heat sink into the water bath and set the starting temperature,let everything come to equilibrium for a few hours.

(6)-Make an electrical calibration check by turning on the heater.Measure the voltage drop across the standard resistor and the heater,measure the time of the electrical heat input,measure the integrated area on the recorder.Calculate the calibration constant if O.K. turn of the heater and let everything equilibrate for a while.

(7)-Measure the bath temperature on the controller,increase it by ΔT,wait until everything reaches steady state and measure the new temperature.Calculate C_v from-

$$Cv = Q/\Delta T = K(\text{calib.const.}) \times \int V dt \; /\Delta T \qquad (5)$$

(8)-Decrease the temperature by the same ΔT.Measure the new temperature and calculate the heat capacity as in (7).
(9)-If the calculated heat capacities agree by both methods decrease the temperature and continue making new measurements.
The above procedure is for making C_v measurements C_p determinations would be similar.

The precision of the measurements can be improved by: Making a number of measurements and averaging, making measurements with the dummy cell empty and full and finally by keeping the mean temperature the same while changing the temperature interval.

Estimated precision of the calorimeter,based on a six gram load of ethane and an average C_v of 0.6 cal/gr-C^o, with the uncertainties in Q measurements and ΔT measurements being the same as in references (6) and (7) respectively (Table 2.ref.6 and fig.3.ref.7) is as follows:
(a)-Large temperature interval measurements $\Delta T \sim 0.1C^o$ Q ~360mcal,uncertainty in Q determination ~0.03%,uncertainty in ΔT determination ~0.005%,thus the overall precision is better than 0.05%.(b)-medium temperature interval measurements $\Delta T \sim 0.01C^o$;Q~36mcal,0.07% precision in Q determination,0.05% precision in ΔT determination ,overall precision is about 0.15%.(c)-Small temperature interval measurements $\Delta T \sim 0.001C^o$,Q ~3.6mcal ,1% uncertainty in

Q determination and 0.5% uncertainty of ΔT determination is 0.5%,thus the overall precision is about 2%.

The relative precision of the calorimeter depends on three things:The time of equlibrium,the amount of heat flowing in and out,and the precision with which ΔT can be measured.The constant volume cell has a very high surface area where the metal is in contact with the fluid resulting in a short equilibrium time.The amount of heat flowing in or out depends on the sample size,for binary mixtures the sample size is about 50 cc's this large volume combined with larger heat capacities makes the heat flow about twice as large as the pure fluids.However there is a trade off it takes longer for a large sample to equiliberate.The precision with which ΔT can be determined seem to be the limiting factor,from fig.(3) of Ref.(7) this limit is seen to be about $\pm 5 \mu C^{o}$.It is very hard if not impossible to improve upon the above given resolution in temperature.Thus the best one can do using any type of calorimeter is to obtain a precision of about 1% when making measurements at $0.001C^{o}$ intervals.

Finally it is also possible for the proposed calorimeter to perform better or worse than the above estimates.

Acknowledgement:

I would like to acknowledge helpful discussions with H.H.Reamer.

REFERENCES

1. A. Voronel and Y. R. Chaskin, Soviet Physics JETP 24, 263 (1967).

2. C. Edwards, J. A. Lipa, and M. J. Buckingham, Phys. Rev. Lett. 20, 496 (1968).

3. A. F. G. Cope, H. H. Reamer and C. J. Pings, B. der Bunsen-Gesellschaft 76, 319 (1972).

4. H. Schmidt, G. Jura, and J. H. Hildebrand, J. Phys. Chem. 63, 297 (1959).

5. T. H. Benzinger and C. Kitzinger, Methods Biochem. Anal. 8, 309 (1960).

6. Ingemar Wadso, Acta Chemica Scandinavica 22, 927 (1968).

7. M. E. Harvey, The Review of Scientific Instruments 39, 13 (1968).

8. N. T. Larsen, ibid, 39, 1 (1968).

Figure Captions

Figure 1. A schematic drawing of a thermoelectric module.

Figure 2. Copper heat sink,dimensions in mm.

Figure 3. Constant volume cell

Figure 4. Constant pressure cell

Figure 5. Electrical calibration circuit

Figure 6. Schematic drawing of the thermometer circuit

Figure 7. Schematic drawing of the total calorimeter. Water bath controls and the vacuum system not shown.

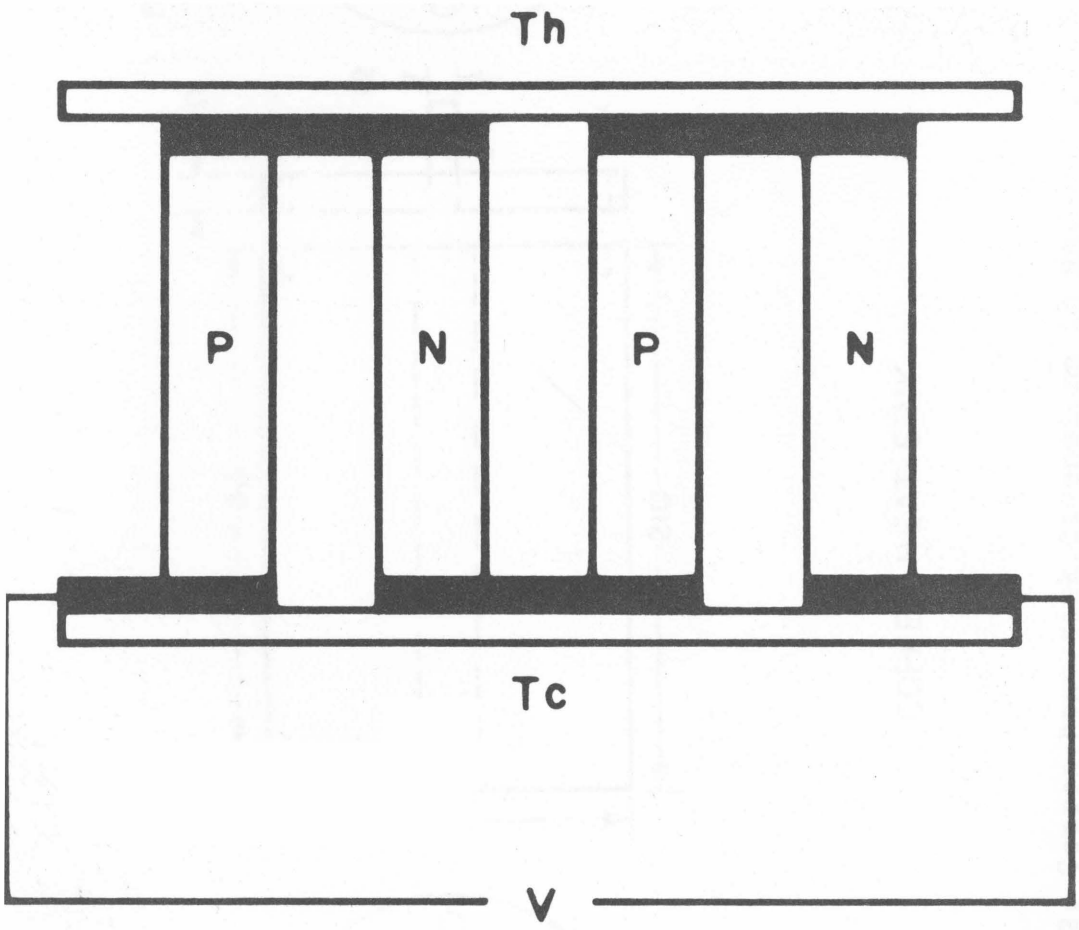

Figure 1. A schematic drawing of a thermoelectric module.

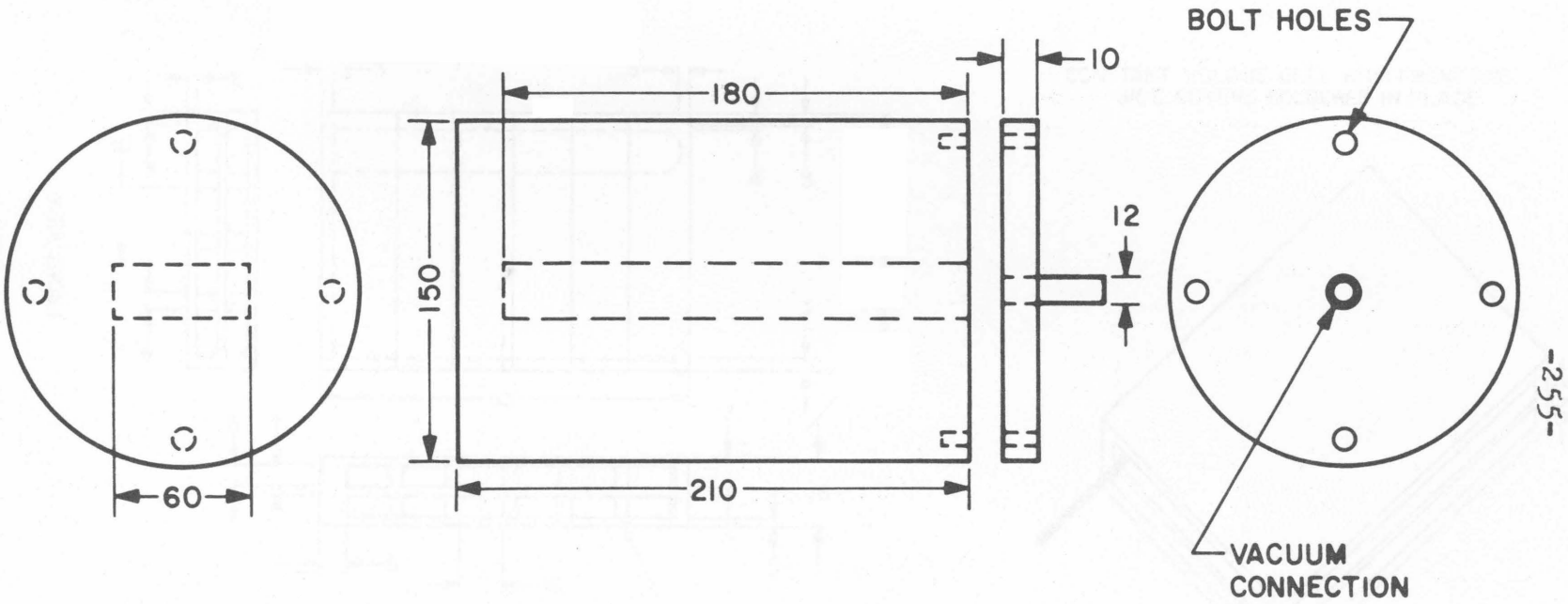

COPPER HEAT SINK

Figure 2. Copper heat sink,dimensions in mm.

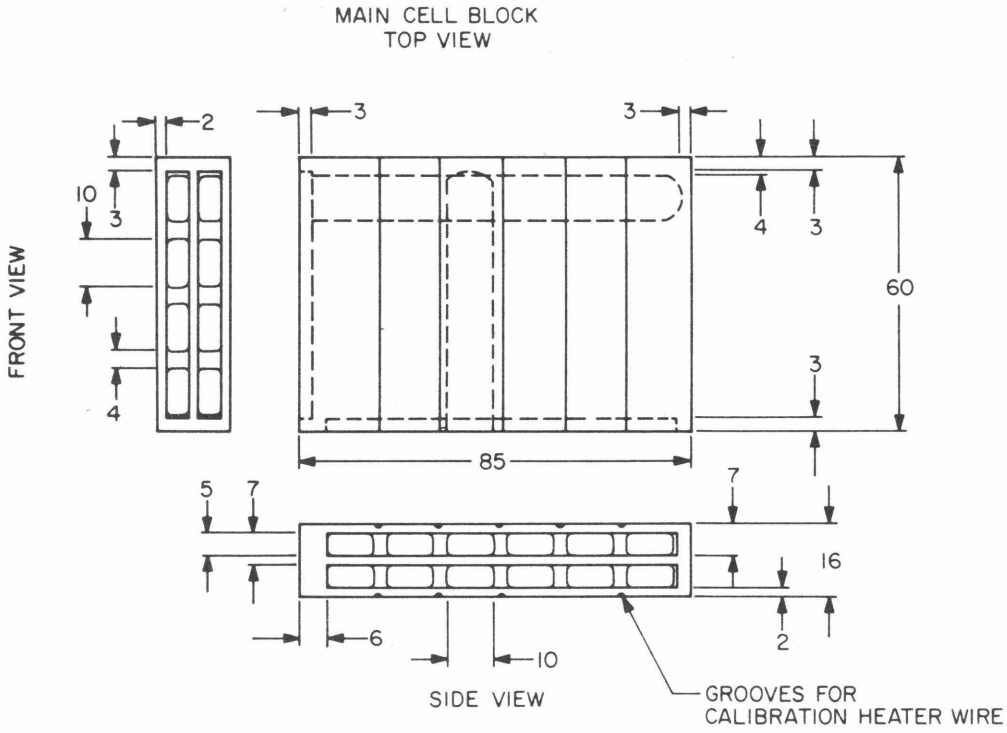

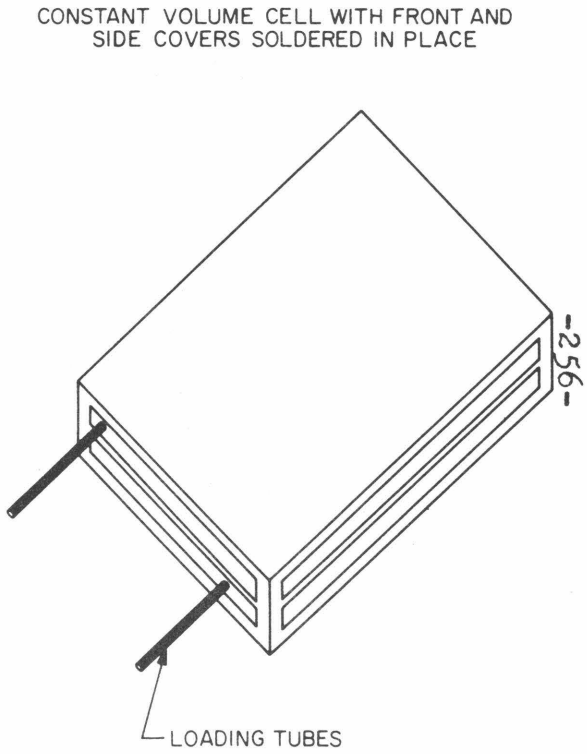

Figure 3. Constant volume cell

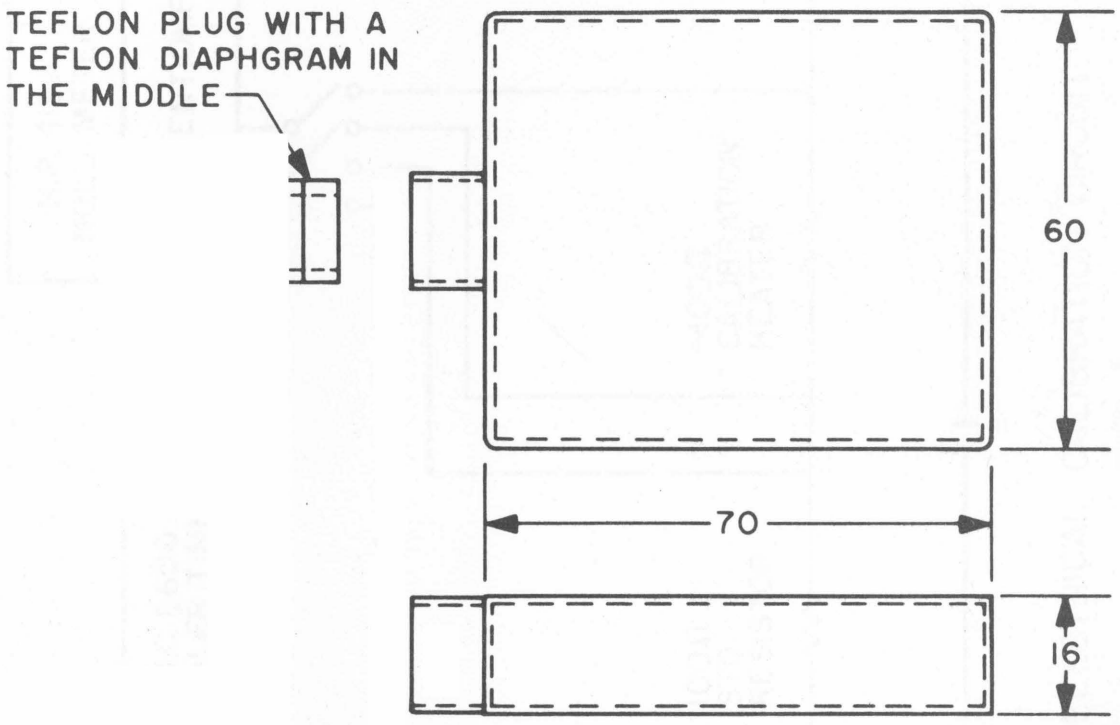

CONSTANT PRESSURE CELL

Figure 4. Constant pressure cell

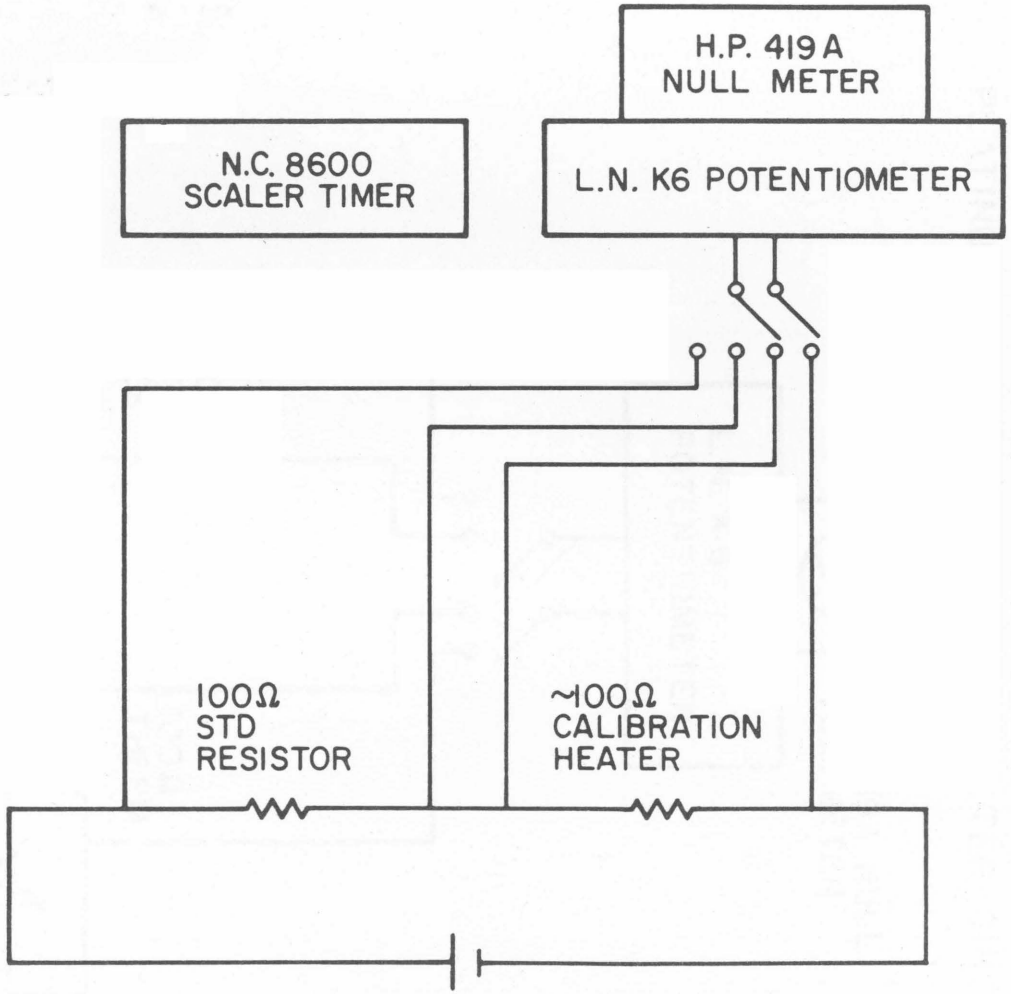

ELECTRICAL CALIBRATION CIRCUIT

Figure 5.

PLATINUM RESISTANCE THERMOMETER CIRCUIT

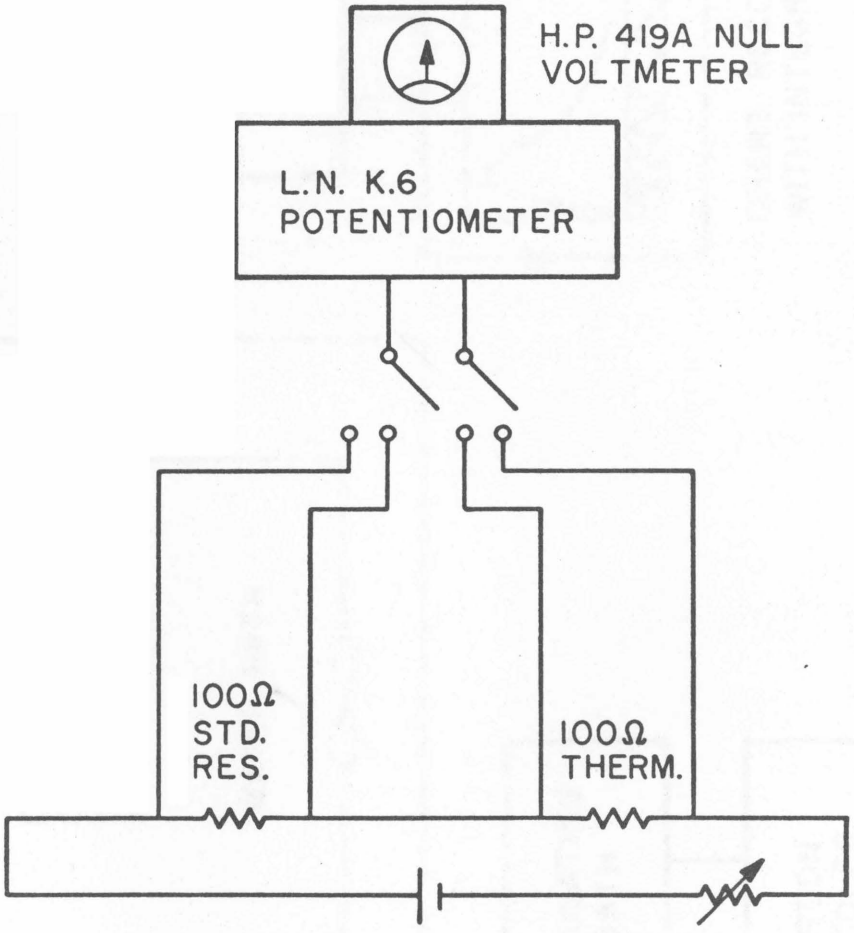

Figure 6. Schematic drawing of the thermometer circuit

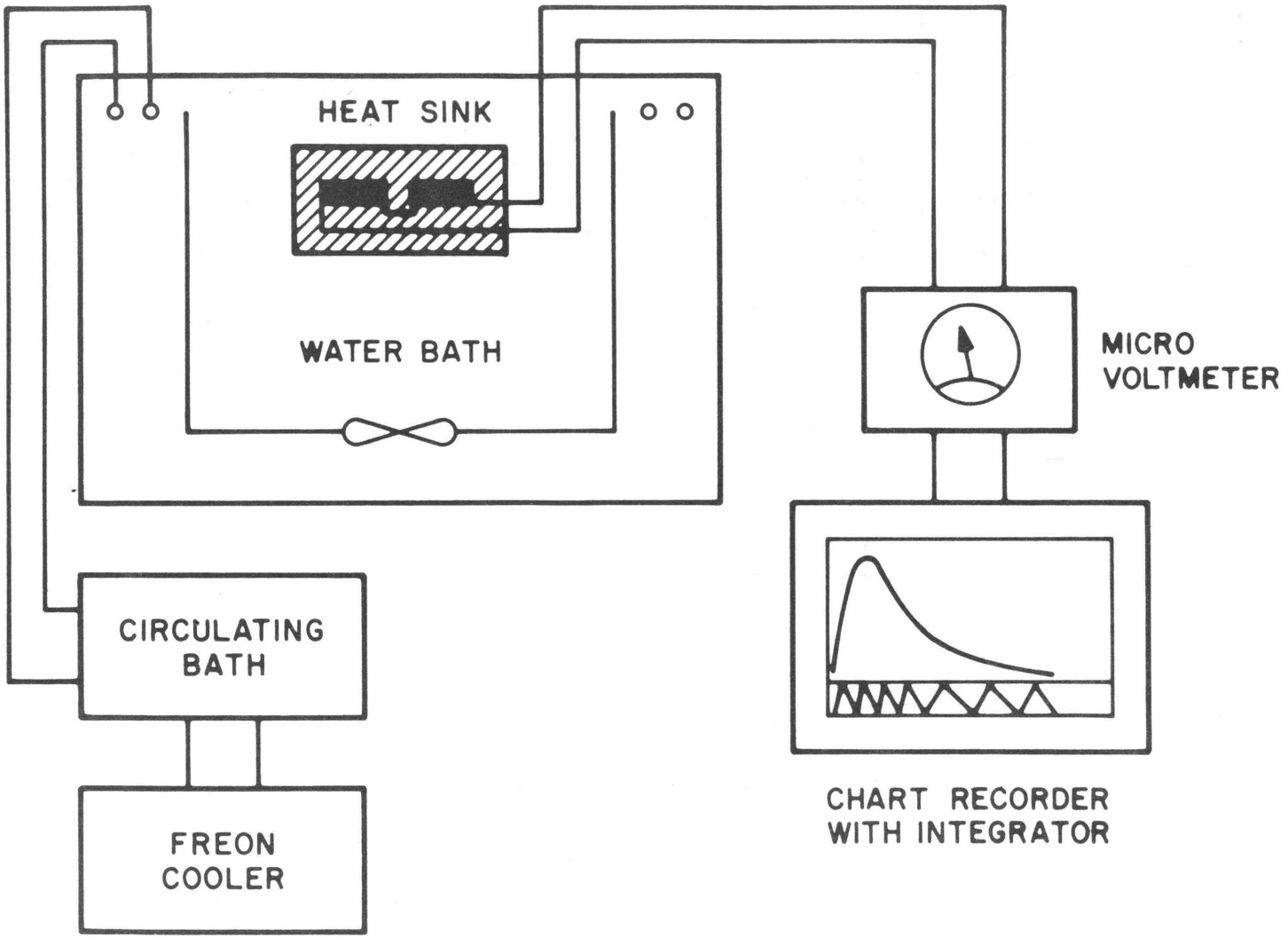

Figure 7. Schematic drawing of the total calorimeter. Water bath controls and the vacuum system not shown.

Proposition III

Measurements of Shear Viscosity of Solutions of Ethanol in Carbon Disulfide and Analysis in Terms of Einstein-Simha Equations.

There has been a good deal of interest in the aqueous solutions of electrolytes[1,2] and aqueous solutions of neutral solutes[3], but not much work has been done on the viscosity of neutral solutes in organic solvents. This work explores the behavior of viscosity of solutions of ethanol in carbon disulfide.

For the shear viscosity η of spherical particles moving in a continuous medium Einstein[4] derived:

$$\eta = \eta_0(1+2.5\bar{\Phi}) \qquad (1)$$

where η_0 is the viscosity of the solvent and $\bar{\Phi}$ is the volume fraction of the solute particles. Equation (1) is valid only for $\bar{\Phi} \leq 0.03$. The hydrodynamic theory of spherical particles was later extended by Guth, Simha, and others[5] to higher solute concentrations and higher powers of $\bar{\Phi}$ was added to eq.(1), with the coefficient of the square terms varying between 4.32 to 14.1[5]. With the addition of the square term (1) becomes :

$$\eta/\eta_0 = 1+2.5\bar{\Phi} + C\bar{\Phi}^2 \quad . \qquad (2)$$

Equations (1),(2) are the basic equations used for analysing the viscosity data of electrolytes,nonelectrolytes and macromolecules[3].Eq.(2) has been found to be sufficiently accurate for $\phi \leq 0.25$.Another equation used for analysing the viscosity data at relatively high concentrations is[6]:

$$\eta/\eta_o = 1+B'm+D'm^2 \qquad (3)$$

where m is the molal concentration.Equation (3) can be rewritten as:

$$\eta/\eta_o = 1+B\bar{\phi}+D\bar{\phi}^2 \quad . \qquad (4)$$

Simha[7] has derived an expression for the coefficient B for the case of nonspherical particles.

Experimental

Reagent grade carbon disulfide and absolute ethyl alcohol were used and the solutions were prepared volumetrically.

A size 50 Cannon-Fenske viscometer was calibrated at 20°C with distilled water,reagent grade benzene,toluene,and carbon disulfide to determine the calibration coefficients in the working equation of the viscometer:

$$(\eta/\rho) = At + A'/t \quad . \qquad (5)$$

A and A' were found to be 0.003362 and -1.72 respectively,

when t was measured in seconds.The viscometer was mounted conventionally in a Tamson model 40 viscometer bath. Times were measured by a Lab-Chron timer to ±0.05 sec. Flow times were between 90 and 220 seconds.Temperature was controlled at 20° to better than ±0.01°C.

Experimentally it was observed that the excess volume of mixing was very small,less than 0.1%,therefore all the densities were calculated using:

$$\rho_{sol} = (\Phi\rho)_{CS_2} + (\Phi\rho)_{et} \quad (6)$$

Results and Discussion

The viscosity data are given in table (I).

Equation (4) was used in analysing the data,an unweighted nonlinear least squares fit yielded B=0.73±0.08, and D=1.9±0.16.The relative viscosities are shown in figure (1) along with eq.(4) using the above values of the coefficients.As can be seen the agreement is very good,however the coefficients 0.73 and 1.9 are in significant disagreement with the values of 2.5 and 4.32-14.1 predicted from hard sphere models[5].Using Simha's expression and the molecular dimensions of ethanol one obtains the value B=2.53 for the coefficient of the linear term[3],this is not in any better agreement with 0.73 than the hard sphere value of 2.5.It is interesting to note that the values B=0.73,D=1.9 are much

smaller than the values B=3.07 and D=4.6 obtained for aqueous solutions of ethanol[3].

The disagreement between the theory and the experiment is perhaps not surprising due to the fact that we are dealing with molecules rather than hard spheres much larger than the solvent molecules.

In conclusion Einstein-Simha equation,eq.(4),describes the behavior of relative viscosity of ethanol solutions in carbon disulfide rather well,but the coefficients are significantly different than the hard sphere model coefficients.

REFERENCES

1. R. A. Robinson and R. H. Stokes, Electrolyte Solutions, second edition, Butterworths, London, (1959).

2. R. H. Stokes, Viscosity of Electrolytes and Related Properties, Pergamon Press, Oxford, (1965).

3. T. T. Herskovits and T. M. Kelly, J. Phys. Chem. 77, 381 (1973).

4. A. Einstein, Ann. Phys. 19, 289 (1906) and 34, 591 (1911).

5. E. Guth and R. Simha, Kolloid-Z. 74, 147, 266 (1936); (b)- E. Guth and O. Gold, Phys. Rev. 53, 322 (1938); (c)- R. H. Ewart, Advan. Colloid. Sci. 2, 197 (1946); (d)- H. Eilers, Kolloid-Z, M. 97, 313 (1941); (e)- J. M. Peterson and M. Fixman, J. Chem. Phys. 39, 2516 (1963); (f)- D. G. Thomas, J. Colloid Sci. 20, 267 (1965).

6. D. Eagland and G. Pilling, J. Phys. Chem. 76, 1902 (1972).

7. R. Simha, J. Phys. Chem. 44, 25 (1940).

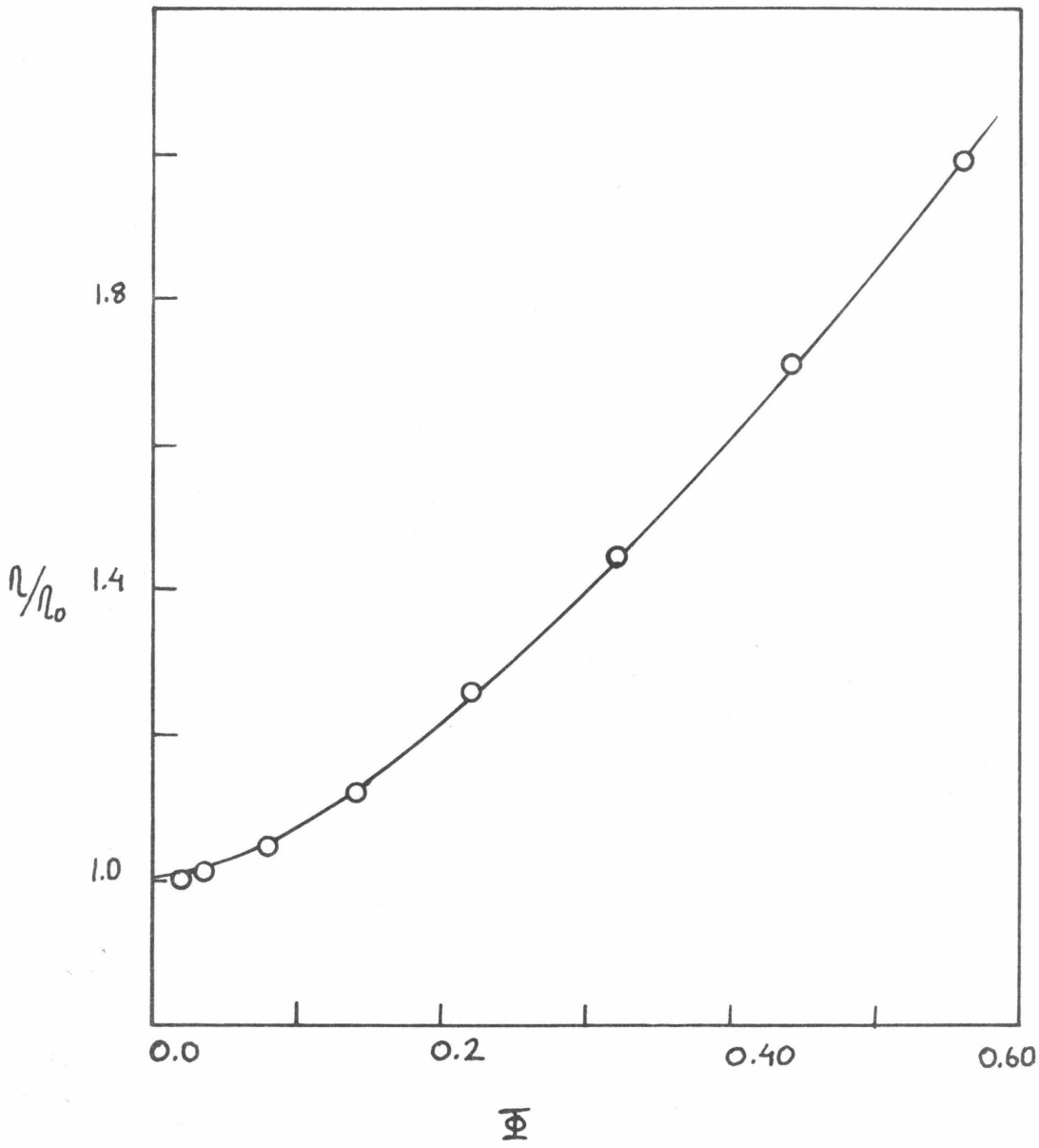

Figure 1. Relative viscosity, η/η_0, versus volume fraction of ethanol Φ. The solid line is given by $\eta/\eta_0 = 1 + 0.73\Phi + 1.9\Phi^2$.

TABLE I

Viscosity Data of Ethanol Solutions in Carbon Disulfide

Volume fraction of ethanol	η (cps)	η/η_0
0.02	0.3614	1.0003
0.04	0.3648	1.0097
0.08	0.3771	1.0437
0.14	0.4045	1.1196
0.22	0.4545	1.2579
0.32	0.5234	1.4488
0.44	0.6167	1.7068
0.56	0.7183	1.9880